EGG-RAAM-11145

Investigation of the Coolability of a Continuous Mass of Relocated Debris to a Water-filled Lower Plenum

J. L. Rempe

J. R. Wolf

S. A. Chavez

K. G. Condie

D. L. Hagrman

W. J. Carmack

Published September 1994

EG&G Idaho, Inc.

Idaho Falls, Idaho 83401

Contents

List of Figures

Tables

Investigation of the Coolability of a Continuous Mass of Relocated Debris to a Water-filled Lower Plenum

Summary

This report documents work performed to support the development of an analytical and experimental program to investigate the coolability of a continuous mass of debris that relocates to a water-filled lower plenum. Major aspects of this work are summarized below.

Program Objective

The objective of this program is to provide an adequate data base for developing and validating a model to predict the coolability of a continuous mass of debris relocating to a water-filled lower plenum. The model must address higher pressure scenarios, such as the TMI-2 accident, and lower pressure scenarios, which recent calculations indicate are more likely for most operating LWR plants. The model must also address a range of possible debris compositions.

Evidence Supporting Debris Coolability

Several sources of data indicate that a continuous mass of debris that relocates to a water-filled lower plenum will cool at rates more rapid than currently predicted by severe accident analysis codes. Data and analyses from the TMI-2 Vessel Investigation Program, lava flows in Iceland, and the FRAG-4 test investigating corium interactions with limestone concrete suggest that other mechanisms, beyond conduction through the crust that forms on upper and lower surfaces of the melt and radiation and convection heat losses from the upper crust surface in contact with the coolant, are present that enhance heat transfer from the debris to the coolant.

Data suggest several mechanisms may be responsible for debris cooling. In Section 1, three possible solidified debris configurations are postulated that would decrease the conduction heat transfer path through the debris and increase the heat transfer surface area between the debris and the coolant. Table S1 summarizes the data discussed in Section 2 supporting the hypothesis that each of these mechanisms is possible. However, it should be noted that none of these data sources conclusively indicate that the presence of a particular debris configuration is associated with enhanced debris cooling. Furthermore, the current data are not sufficient to rule out the presence of another, yet to be identified, cooling mechanism.

Table S1: Summary of evidence discussed in Section 2

	Debris Cracking	Debris-to-Vessel Gaps	Concave Upper Surface
Evidence	TMI-2 Solidified Lava FRAG-4 Test CCM Fuel Damage Tests (PBF, MP2, etc.)	TMI-2 FAI Tests	WETCOR

Overview of Program Required to Resolve Debris Cooling Questions

Figure S1 illustrates the three elements proposed to accomplish this program's objective. Each element includes obtaining data by flooding with water. The major results obtained from each element are listed on the right side of Figure S1.

Figure S1. Key elements of proposed debris coolability program

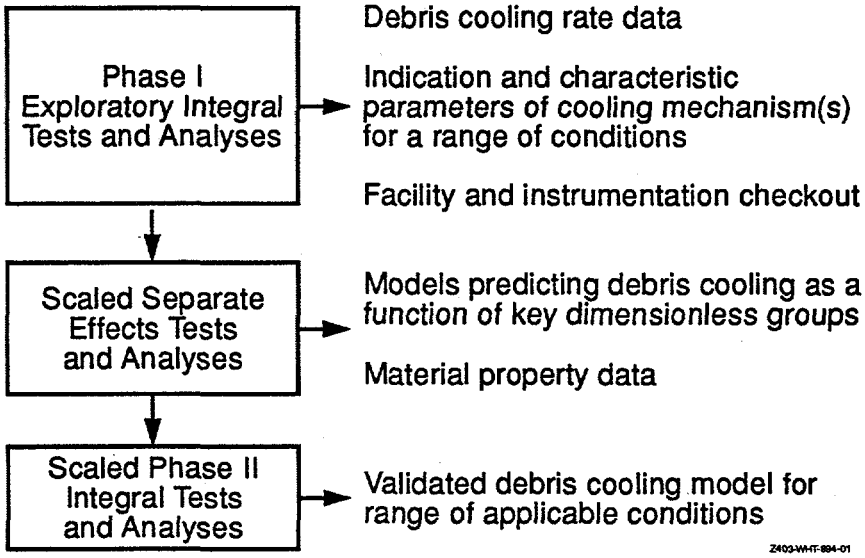

The first element, identified as Phase I Exploratory Integral Tests and Analyses, is primarily performed to quantify what additional cooling occurs and identify the mechanism(s) responsible for this cooling. As discussed above, there is little evidence for determining which, if any, of the postulated mechanisms are responsible for enhanced cooling. Hence, it is proposed that the first tests in this program be exploratory "integral" tests that will simulate debris cooling conditions expected during a severe accident. Data will be obtained from Phase I tests to verify that additional debris cooling occurs, to identify the mechanism(s) responsible for this cooling, to quantify the magnitude of cooling associated with the identified cooling mechanism(s), and to quantify characteristic geometries associated with the identified cooling mechanism(s) for a range of accident conditions.

The second element, Scaled Separate Effects Tests and Analyses, is performed to obtain detailed data required for developing models for each of the cooling mechanisms observed in Phase I tests. Separate effects test design parameters will be specified by performing scaling analyses for each of the mechanisms identified in Phase I. Hence, this element includes a task to obtain material property data required for scaling analyses and model development. Separate effects tests will be scaled so that the entire range of possible LWR accident conditions in which enhanced debris cooling is possible can be considered (i.e., both high and low pressure regimes can be evaluated). If more than one cooling mechanism is identified in Phase I tests, interactions between models developed for each mechanism will be assessed using Phase I data.

The third element, Scaled Phase II Integral Tests and Analyses, is performed to validate the models developed from the first two elements of this program. Although these tests will be per-

formed in a facility whose design specifications will be based on results from detailed scaling analyses, it is envisioned that the Phase II test facility will be larger in size and able to withstand higher pressures than the Phase I test facility. Furthermore, it is envisioned that more detailed measurements will be obtained from the Phase II tests. For example, in the Phase I tests, data will be obtained so that energy transfer rates can be estimated for determining time-dependent debris cooling rates; whereas in the Phase II tests, instrumentation will be added to ensure that data can be obtained to estimate time-dependent crust thickness, crust temperatures, and melt temperatures at various locations within the debris.

Insights and Recommendations from Scoping Calculations

If the mechanisms responsible for debris cooling were known, tests would be scaled considering both thermal and stress conditions. However, it is not currently known what mechanisms cause enhanced debris cooling, and several postulated cooling mechanisms yield different stress and thermal scaling relationships. Therefore, scoping calculations based on thermal-hydraulic data from the TMI-2 accident were used to gain insights for conducting Phase I tests. This decision allows the debris in the tests to experience thermal conditions equivalent to the TMI-2 thermal conditions, the best source of data for identifying what mechanisms are responsible for debris cooling. However, these tests may not be properly scaled to simulate the stress states experienced by the TMI-2 debris. Therefore, calculations were also performed to gain insights about parameters for the Phase I tests required to simulate TMI-2 debris stress states.

Results from these scoping calculations and from thermal equilibrium calculations yielded the insights summarized in Table S2. These insights suggest that tests should be conducted in a large scale facility that is able to withstand high pressures. However, debris cooling questions are of interest in both high and low pressure accident scenarios. In fact, recent analyses supporting the direct containment heating resolution issue suggest that without operator intervention, high pressure accidents in CE and Westinghouse plants are unlikely. In addition, improvements in operator training since the TMI-2 accident have decreased the likelihood for operator intervention to lead to high pressure scenarios (see Section 1). This information, in conjunction with cost considerations, have yielded the three element approach discussed above. Namely, that exploratory integral tests, Phase I tests, be conducted adopting all of the Table S2 recommendations except the suggestion for facility pressure; separate effects tests be conducted to obtain data necessary for model development for a range of possible severe accident conditions; and larger scale integral tests, Phase II tests, be conducted to validate models for the range of possible severe accident conditions.

Experimental Test Program

As discussed above, data will be obtained in each of the three major elements of this program, the Phase I Integral Tests, the Separate Effects Tests, and the Phase II Integral Tests. As discussed above, the tests required for completing the last two elements are dependent on Phase I Test results. Hence, preliminary design efforts have concentrated on Phase I tests. Information is provided in this report about the test facility design, the proposed test matrix, simulant debris fabrication, and Phase I test instrumentation requirements.

Table S2: Summary of recommendations for Phase I Tests

Test Parameter	Recommendation
Configuration	The quenching crucible radius should be 0.3 m, assuming that a scaled TMI-2 mass of 20 kg is sufficient.
	The nominal ratio of the debris height to the debris upper surface area radius should be approximately 0.32.
	The nominal ratio of the debris height to the quenching crucible radius should be approximately 0.2.
Melt Composition	Nominal debris compositions should consist of 78% wt.% UO_2; 17 wt.% ZrO_2, and small amounts (<1.5 wt.%) of iron, chromium, and nickel oxides.
Initial Melt Temperature	Debris decay heat may be omitted from the tests if initial pool superheats are greater than 185 K above the melt liquidus.
Estimated Initial Debris Heat Transfer Conditions	Nominal values for the initial upward heat fluxes from the debris should range from 0.4 to 1.2 MW/m^2.
	In order to perform sensitivity tests simulating equivalent stress states to values predicted for the TMI-2 debris, initial upward heat fluxes as high as 2.2 MW/m^2 should be tested.
	Nominal values for the initial downward heat fluxes should be less than one tenth the magnitude of the upward heat fluxes.
	The debris should initially cool at approximately 0.1 K/s (quench rate will be verified by examining debris microstructure after initial Phase I tests).
Test Facility Pressure	In order to match initial crust growth rates with values expected during initial stages after melt relocation during the TMI-2 accident (between 0.4 and 9 mm/s), tests should be conducted at pressures of 5 MPa or higher.
Melt Pot Material Composition	Tests may be conducted by heating the debris in a tungsten melt pot.
Initial Test Atmosphere	Air should be removed from the vessel to minimize oxidation of the tungsten melt pot.

A diagram depicting the Phase I test facility is shown in Figure S2. In general, these tests will be conducted by first purging the vessel with an inert gas and then melting simulant debris in the tungsten melt pot. Once the debris is heated to the desired amount of superheat, it will be poured into a prewetted stainless steel clad carbon steel crucible and quench water will be injected on top of the melt. Design parameters for key facility components are summarized in Table S3.

Figure S2. Block diagram for Phase I test facility

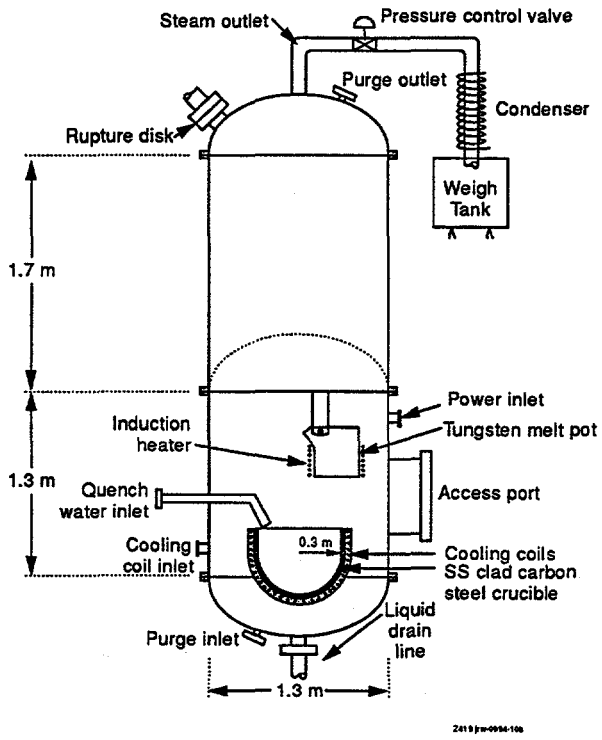

Table S3: Design parameters for key Phase I test components

Pressure Vessel	
Material Composition	Stainless steel
Inner Diameter, m	1.3
Height (excluding heads), m	1.3/3 (variable height using flanged sections)
Design Pressure, MPa	1.4
Operating Pressure, MPa	1.0
Melt Pot	
Material	Tungsten
Heating Method	Induction
Quenching Crucible	
Material	Carbon steel clad with Stainless Steel[a]
Inner diameter, m	0.6

a. First test, subsequent tests may use crucibles with Inconel cladding and/or penetrations to simulate other lower head geometries.

It is proposed that prototypic simulant debris be used in all Phase I tests. The use of this material is proposed for several reasons. First, the costs associated with handling radioactive material will be reduced because the simulant debris, which contains depleted uranium, has not been irradiated. Second, the use of this less-expensive simulant material allows a range of debris compositions to be tested. Initial Phase I tests will use debris similar in composition to the material found in the TMI-2 vessel. However, other melt compositions, ranging from melt with no metal oxides to melt with unoxidized metallic components, will be evaluated so that a range of accident debris conditions can be considered.

Table S3 lists the seven series of tests planned for Phase I. Each series varies a parameter that may impact the occurrence and characteristic parameters associated with postulated debris cooling mechanisms. The Series 1 tests investigate the impact of the presence of an initial wetted surface and on cooling water addition on debris cooling. The Series 2 tests investigate the effects of pressure and coolant subcooling on debris cooling. Series 3 tests investigate the impact of the initial cooling water height on cooling. Series 4 tests will assess the impact of debris height on cooling. Melt mass (and associated height) will be varied in these tests to determine their effect on characteristic parameters associated with debris cooling mechanisms, such as crack length, crack density, and gap size. The Series 5 tests investigate the impact of melt composition on debris cooling. Because scoping analyses indicate that material properties play an important role in postulated debris cooling mechanisms, a range of melt compositions will be tested to quantify variations in characteristic cooling mechanism parameters (crack size, crack length, gap size, etc.) and in the relative importance of various cooling mechanisms. The Series 6 tests will include penetrations in the quenching crucible. These tests are included to assess the potential for penetrations in the melt to enhance debris coolability. The Series 7 tests are included to evaluate the effects of varying the melt's initial superheat. Post-test examinations will be performed on debris from all of the above tests to identify any differences in composition, porosity, and grain size between the test debris and the TMI-2 debris. The test matrix shown in Table S3 is preliminary, and some modifications to this matrix may occur as results from initial tests are obtained.

Measurements will be performed during and after Phase I tests to obtain required data. Sufficient data must be obtained during the tests to determine when the debris is sufficiently superheated for testing and verify that the debris loses heat more rapidly than possible by conduction through the debris (i.e., comparisons must show that Phase I test debris temperatures are decreasing more rapidly than temperatures predicted by current severe accident code models). Post-test measurements will be performed to compare test debris microstructure (i.e., the composition, uniformity, porosity, and grain-size) with the microstructure of the TMI-2 debris and to identify the presence of, and characteristic dimensions associated with, configurations responsible for enhanced debris cooling.

In general, measurements required for completing the objectives of the Phase I experiments will be made using standard state of the art instrumentation that has been applied successfully in previous INEL experimental programs. Little, if any, instrumentation development is needed. During melting, the debris temperature will be directly measured using two methods: melt wires and two-color optical pyrometers. Ultrasonic thermometers and hafnium sheathed tungsten/rhenium sheathed thermocouples will be used to measure the debris temperature during quenching. Temperatures for the quench water, crucible cooling gas, steam condenser inlet/outlet, and vessel drain effluent will be measured using stainless steel sheathed type k thermocouple. Steam temperatures in the vessel will be measured using a standard, commercially available, shielded temperature probe. Vessel pressure will be measured using fast reacting piezoelectric or strain gauge pressure transducers. Heat losses from the vessel will be measured using heat flux

sensors. Crucible coolant flowrates will be measured using appropriate mass flow meters. Any liquid levels in the vessel will be measured by differential pressure cells. Experimental measurements will be recorded on existing INEL data acquisition systems.

Table S4: Proposed test matrix for Phase I

Test ID	Description	Maximum Pressure, MPa	Initial Water Height, m	Quench Water Temperature, K	Melt Mass, kg	Melt Composition
1/1	Scaled TMI-2 melt mass and composition; low pressure, varying introduction of initial water and quench water	1.0	No initial water	90 K subcooled	20	78 wt% UO_2; 17 wt% ZrO_2; < 5 wt% metal oxides
1/2			0.05	No water addition		
1/3			0.05	90 K subcooled		
2/1	Scaled TMI-2 melt mass and composition; varying pressure and quench water subcooling	0.5	0.05	90 K subcooled	20	78 wt% UO_2; 17 wt% ZrO_2; < 5 wt% metal oxides
2/2		1.0	0.05	50 K subcooled		
3/1	Scaled TMI-2 melt mass and composition; varying height of initial water	1.0	0.03	90 K subcooled	20	78 wt% UO_2; 17 wt% ZrO_2; < 5 wt% metal oxides
3/2			0.10			
4/1	Scaled TMI-2 melt composition; varying melt mass	1.0	0.04	90 K subcooled	8	78 wt% UO_2; 17 wt% ZrO_2; < 5 wt% metal oxides
4/2			0.07		40	
4/3			0.09		75	
5/1	Scaled TMI-2 melt mass; varying melt composition	1.0	0.05	90 K subcooled	20	80 wt% UO_2; 20 wt% ZrO_2
5/2						Mixed oxide with metal
6	Scaled TMI-2 melt mass and composition; maximum pressure; various penetrations	1.0	0.05	90 K subcooled	20	78 wt% UO_2; 17 wt% ZrO_2; < 5 wt% metal oxides
7	Scaled TMI-2 melt mass and composition; maximum pressure; varying melt initial superheat	1.0	0.05	90 K subcooled	20	78 wt% UO_2; 17 wt% ZrO_2; < 5 wt% metal oxides

Nomenclature

Lower Case

a	=	radius of debris upper surface; may be further designated with the subscript, *m*, for molten debris, or *s*, for solid debris (m)
c_{p_d}	=	debris specific heat capacity; may be further designated with the subscript, *s*, for solid (J/kg-K)
c_{p_w}	=	coolant specific heat (J/kg-K)
g	=	acceleration due to gravity (9.8 m/s^2)
g	=	shape factor (dimensionless)
h	=	heat transfer coefficient; may be further designated with the subscript, *b* for convective heat transfer from the bottom surface of a molten pool, *c* for convective heat transfer, *crust* for effective heat transfer through a crust, *fb* for film boiling heat transfer, *sfb* for subcooled film boiling heat transfer, *r* for radiation heat transfer, *r+sfb* for combined radiation and subcooled film boiling, *u* for convective heat transfer from the upper surface of a molten pool, or *v* for combined convective and radiative heat transfer from the vessel (W/m^{2}K)
h_f	=	enthalpy of liquid coolant draining from the vessel (J/kg)
h_{fg}	=	coolant heat of vaporization (J/kg)
h_{in}	=	enthalpy of coolant entering the vessel (J/kg)
h_p	=	molten pool height (m)
h_{out}	=	enthalpy of coolant exiting the vessel (J/kg)
h_{sat}	=	coolant enthalpy at saturated conditions (J/kg)
h_{steam}	=	enthalpy of steam exiting the vessel, J/kg
k_d	=	debris thermal conductivity; may be further designated with the subscript, *s*, for solid debris, or *m* for molten debris (W/mK)
k_g	=	thermal conductivity for vapor coolant (W/mK)
m	=	Weibull constant (dimensionless)
$\dot{m}$	=	coolant mass flow through a crack (kg/s)
$\dot{m}_{drain}$	=	flowrate of fluid draining from the vessel (kg/s)
$\dot{m}_{in}$	=	mass flow rate of coolant entering the vessel (kg/s)
$\dot{m}_n$	=	coolant flowrate through a channel in the crucible (kg/s)
$\dot{m}_{steam}$	=	flowrate of steam exiting the vessel (kg/s)
$\dot{m}_{out}$	=	mass flow rate of coolant exiting the vessel (kg/s)
n_{crack}	=	number of cracks

n_d	=	total number of n cooling channels in the crucible
q_{sink}	=	energy lost to coolant (W)
q''	=	debris heat flux; may be further designated by the subscript, *b* for heat fluxes from the bottom surface of a molten pool, *fb* for film boiling heat fluxes, fb_{sub} for subcooled film boiling heat fluxes, *r* for radiation heat fluxes, or *u* for heat fluxes from the upper surface of a molten pool (W/m^2)
q'''_{crust}	=	volumetric heat generation rate due to decay heat (W/m^3)
r	=	plate radius (m)
r_{in}	=	inner radius of cusped region postulated to form in solidified debris (m)
s	=	radius of a spherical pore (m)
t	=	time (s)
t_{gap}	=	debris-to-vessel gap thickness (m)
Δt_h	=	debris heating time (s)
Δt_q	=	debris quench time (s)
u	=	specific internal energy; may be further designated with the subscript, *d* for debris, d_s for solid debris, *g* for coolant vapor, *l* for coolant liquid, *c* for coolant, 1 for an initial state, or 2 for an endstate (J/kg)
x	=	RCS quality; may be further designated with the subscript, 1 for an initial state, or 2 for an endstate
z	=	debris height (m)
z_{crack}	=	crack length (m)

<u>Upper Case</u>

A	=	surface area; may be further designated with the subscript, *b*, for debris downward surface area, *crack* for crack surface area, *crust*, for average crust cross-sectional area, *d*, for lower crust surface area, *u* for upper crust surface area, u_m for upper surface area of molten debris, u_s for upper surface area of solid debris, or *v* for vessel outer surface area (m^2)
C	=	constant ($MPa\text{-}m^{1/2}$)
D_e	=	crack effective diameter (m)
E	=	elastic modulus (MPa)
$\Delta\dot{E}_a$	=	vessel energy loss rate (W)
$\Delta\dot{E}_c$	=	crucible energy removal rate (W)
$\Delta\dot{E}_s$	=	test facility structural energy storage term (W)
L_f	=	latent heat of fusion, may be further designated by the subscript, *d* for debris (J)

M_c = coolant mass in the RCS or test vessel; may be further designated with the subscript, 1 for an initial state, or 2 for an endstate (kg)

M_d = debris mass; may be further designated with the subscript, *m* for molten relocated debris, *s* for solidified debris, *rel* for total mass of relocated debris, *tot* for total relocated debris, 1 for an initial state, or 2 for an endstate (kg)

M_{mp} = melt pot mass (kg)

$\overline{Nu}$ = average Nusselt number; may be further designated by the subscript, *b* for downward heat transfer or *u* for upward heat transfer

ΔP = pressure differential across the crust (MPa)

$\dot{Q}_{decay}$ = debris decay heat (W)

$\dot{Q}_{ves}$ = vessel heat losses (W)

R = vessel radius (m)

R_t = thermal stress resistance, steady state temperature change required for failure (K)

R_{fail} = risk of failure (dimensionless)

Ra = steady-state Rayleigh number (dimensionless)

Ra' = transient Rayleigh number (dimensionless)

Re = Reynolds number (dimensionless)

T_{atm} = atmospheric temperature outside the vessel (K)

T_{bulk} = bulk coolant temperature (K)

Q_h = power input from heaters (W)

T_a = average temperature of gas or steam contained in the vessel (K)

T_d = debris temperature; may be further designated by the subscript, *avg* for average crust temperature, *int* for crust/coolant interface temperature, *p* for peak pool temperature, *s* for surface temperature, *sol* for melt solidification temperature, 1 for initial state, or 2 for endstate (K)

T_{sat} = coolant saturation temperature (K)

T_v = vessel temperature (K)

ΔT_m = difference between peak melt temperature and average crust temperature (K)

ΔT_{w_n} = temperature change of coolant traveling through a crucible cooling channel (K)

U_u = overall crust to coolant heat transfer coefficient (W/m^2K)

$V_{coolant}$ = reactor coolant system volume (m^3)

V = debris volume; may be further designated by the subscript, *m* for molten state or *s* for solid state (m^3)

Greek

α_d	=	thermal coefficient of expansion (1/K)
α	=	debris thermal diffusivity (m^2/s)
β_d	=	debris volumetric coefficient of thermal expansion (K^{-1})
δ_{crust}	=	crust thickness (m)
ε	=	strain, may be further designated by the subscript, *creep* for creep strain, *elastic* for elastic strain, *plastic* for plastic strain, *thermal* for thermal strain, or *total* for total strain.
ε_c	=	coolant emissivity
ε_{d_s}	=	crust emissivity
ε_{eff}	=	effective emissivity
ε_v	=	vessel emissivity
$\Delta\varepsilon_{total}$	=	total strain
μ_g	=	viscosity for vapor coolant (Pa-s)
ν_d	=	debris kinematic viscosity (m^2/s)
ν_g	=	coolant specific volume for saturated vapor; may be further designated with the subscript, 1 for the initial state, or 2 for the endstate (m^3/kg)
ν_l	=	coolant specific volume for saturated liquid; may be further designated with the subscript, 1 for the initial state, or 2 for the endstate (m^3/kg)
ν_P	=	Poisson's ratio (dimensionless)
ρ_c	=	coolant density; may be further designated by the subscript, *g* for vapor, or *f* for liquid (kg/m^3)
ρ_d	=	debris density; may be further designated by the subscript *m* for molten debris or *s* for solidified debris (kg/m^3)
σ_{SB}	=	Stefan Boltzmann constant (5.672×10^{-8} W/m^2K^4)
σ_c	=	surface tension for liquid coolant (N/m)
σ_f	=	fracture strength (MPa)
σ_p	=	the stress at the center of the plate from pressure (MPa)
σ_s	=	in-plane stress on the surface due to thermal expansion or contraction (MPa)

1. Introduction

This document has been prepared to support the design of an experimental and analytical test program to investigate the coolability of a non-fragmented mass of melt relocating to a water-filled lower plenum. These debris coolability questions were raised during the recently completed margin-to-failure analysis that was performed as part of the OECD-sponsored TMI-2 Vessel Investigation Project (VIP).[1] Results from the TMI-2 VIP analysis and other evidence suggest that additional cooling mechanisms, not considered in current severe accident analysis codes, are present when melt relocates to form a continuous solid or partially molten phase in a water-filled lower plenum.

Results from prototypical debris and representative debris/water volume experiments give conflicting results about the fraction of debris that will fragment as material relocates to a water-filled lower plenum.[2,3] However, data indicate that even if a major portion of the debris becomes fragmented into a non-coolable particulate debris bed, the debris will become molten and evolve into a continuous configuration. Hence, it is important to accurately model the manner in which a continuous debris configuration is cooled for a range of accident scenarios; not only the higher pressure conditions present in the TMI-2 vessel during the accident, but also the low pressure scenarios which recent analyses indicate may be more likely to occur in most PWR vessel designs.[4,5]

Although there are insufficient data to identify what mechanisms are responsible for this cooling, several mechanisms have been postulated based on the limited evidence supporting the presence of this cooling. Preliminary evaluation indicates that three possible debris configurations associated with the volume reduction that occurs during light water reactor debris solidification may significantly enhance debris-to-coolant heat transfer.

An experimental program is proposed to obtain data for identifying the mechanisms responsible for this cooling and to develop a model for predicting the cooling associated with these mechanisms. The proposed experimental program will use non-irradiated simulant debris composed of prototypical material. Although a range of debris compositions will be investigated, the first tests will be performed using simulant debris similar in composition to debris removed from the TMI-2 vessel. The simulant debris will be inductively heated in a tungsten melt pot and then poured into a quenching crucible with a prewetted surface. Quench water will be introduced into the crucible to cool the debris in integral tests. Examinations will be performed to confirm that the simulant debris used in integral tests is similar to debris removed from the TMI-2 vessel. Where necessary, material property tests will be performed to obtain thermal and structural properties needed to design separate effects tests and develop debris coolability models.

Three types of tests will be performed in this program. First, an initial set of exploratory integral tests, Phase I tests, will be performed to verify that the debris cools at rates that are faster than by rates possible by conduction through crusts that form on upper and lower surfaces of the debris, to identify the mechanism(s) responsible for this cooling, and to quantify characteristic parameters associated with these mechanisms. Separate effects tests will be performed to obtain detailed data necessary for developing models for each of the mechanisms identified in the Phase I tests. Interactions between mechanisms will be evaluated using Phase I data. Finally, larger-scale, confirmatory integral tests, Phase II tests, will be performed to validate debris cooling models developed in this program.

This report documents work performed to support this proposed program. In the remainder of this section, the cooling mechanisms currently considered in SCDAP/RELAP5 are reviewed,

mechanisms postulated to enhance debris cooling are described, and an overview of information that can be found in remaining sections of this document is provided.

1.1 Debris Cooling Mechanisms Modeled in SCDAP/RELAP5

Prior to discussing postulated debris cooling mechanisms that should be considered in severe accident analysis code models, it is useful to review the mechanisms for which sufficient data exist to support their inclusion in codes, such as SCDAP/RELAP5.[6] For scenarios in which a continuous mass of molten material relocates to a water-filled lower plenum, there are sufficient data to warrant modeling the mechanisms shown in Figure 1. When the molten material relocates to a water-filled lower plenum, a crust will form on lower surfaces of the debris in contact with the vessel and on upper surfaces of the debris in contact with the coolant. Heat will be transferred via convection from interior portions of the pool to the crust. Heat is transferred through upper and lower crusts via conduction. From the upper surface of the melt, heat will be initially be lost to the coolant via boiling and radiation and later via convection. As discussed in Reference 1, there are sufficient data to warrant increasing the debris upper surface area because of roughness associated with relocating melt solidifying. Downward heat losses will occur via conduction. In addition, sufficient data exist to model a small gap between the debris and the vessel that is associated with the surface roughness of solidified debris. Convection and radiation heat losses from the vessel to the containment are also included.

The currently modeled mechanisms are limited because of the surface area in contact with the coolant. Hence, heat must be transported via conduction through the crust. As discussed in Section 2, several sources of data indicate that additional heat losses occur when a continuous mass of debris relocates to a water-filled lower plenum. The objective of this research program is to obtain sufficient data to develop and validate models for predicting this additional cooling not currently considered in severe accident analysis codes.

Figure 1. Heat transfer mechanisms modeled in SCDAP/RELAP that impact debris cooling

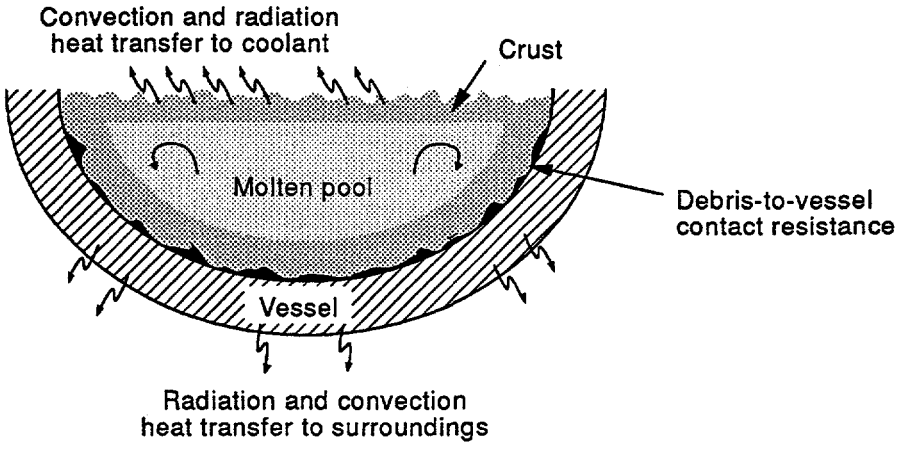

1.2 Possible Cooling Mechanisms

As will be discussed in this report, results from scoping calculations indicate that a significant volume reduction occurs during solidification of oxidized debris. Although there are insufficient data to determine how this material will solidify during a severe accident, it is postulated that this volume reduction may result in any of a combination of the solidified debris configurations shown in Figure 2: interconnected debris cracks, multiple gaps forming between the debris and the vessel, and increased upper debris surface area. These possible configurations are being considered because of limited evidence from the TMI-2 examinations, solidified lava in Iceland, melt/water interaction tests, fuel damage tests, and core/concrete interaction tests (see Section 2). It is recognized that other, unknown, mechanisms may also contribute to debris cooling. Therefore, the experimental test program described in this document has been developed in a manner so that additional mechanisms may be considered after initial tests are performed. However, initial tests and scoping calculations to support these tests concentrate on the three mechanisms identified in Figure 2. Although detailed data are not available to indicate which of these mechanisms cause enhanced debris cooling, data discussed in Section 2 indicate that debris may solidify into these configurations.

Figure 2. Possible solidified debris configurations.

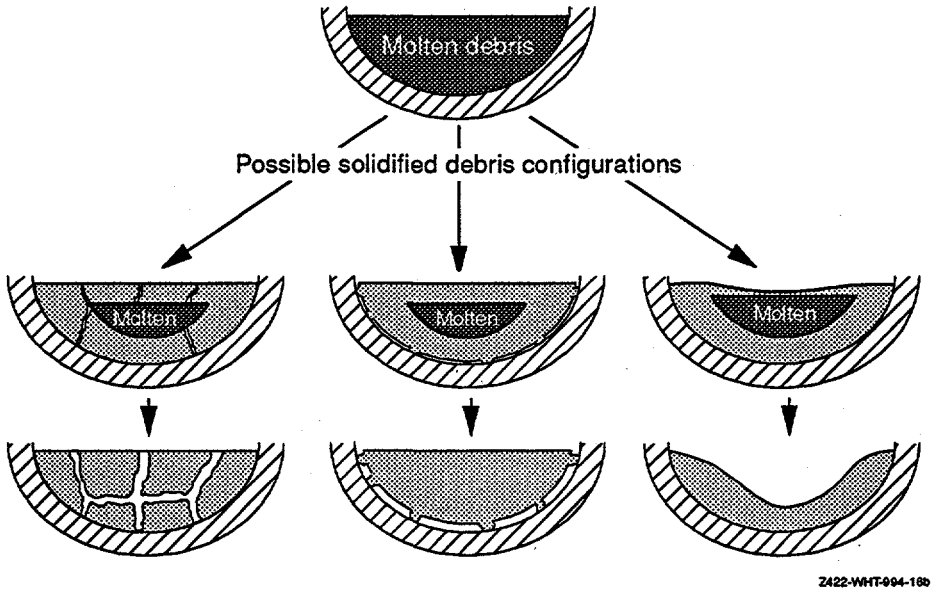

In each of these cases, the heat conduction path through the crust is reduced and the area available for convection and radiation heat losses is increased. For enhanced debris cooling via interconnected cracks, it is postulated that these channels or cracks within the debris allow the infusion of water to cool the debris near the channels. Enhanced debris cooling via gaps or channels is postulated to occur if coolant is able to travel through a series of interconnected gaps that form between the debris crust and the lower head. If the upper surface of the debris becomes concave due to the volume reduction associated with debris solidifying along the debris/vessel interface, the additional surface area for heat transfer on the top of the debris is postulated to result in another form of additional debris cooling, not currently considered in severe accident models.

1.3 Report Contents

Remaining sections of this report document work performed to support an analytical and experimental test program to investigate the coolability of debris relocating to a water-filled lower plenum. Section 2 of this report discusses evidence supporting the existence of enhanced debris cooling. Although the materials and scales investigated in Molten Core Concrete Interaction (MCCI) experiments significantly differ from parameters applicable to in-vessel debris coolability issues, information obtained from these ex-vessel debris coolability experiments and supporting analyses are summarized in Section 2 to resolve questions about the applicability of this data to in-vessel debris coolability questions. Models envisioned for predicting enhanced debris cooling from the currently postulated cooling mechanisms are also described in Section 2. An overview of the program being proposed to address debris cooling questions is found in Section 3. Because of uncertainties related to what mechanisms are responsible for debris cooling, it is proposed that exploratory tests be conducted in the first phase of this program. Section 4 describes scoping calculations estimating test conditions needed to cause the test debris to experience thermal conditions similar to conditions that the TMI-2 debris experienced. The test facility design and specific tests envisioned for the exploratory tests that will be conducted in the first phase of this program are outlined in Section 5.

2. Background

This section summarizes background information pertaining to the coolability of a continuous mass of relocated debris in a water-filled lower plenum. Evidence supporting the thesis that this material is cooled at rates that are as much as three to four times greater than that possible by conduction through the material is summarized in Section 2.1. Section 2.2 documents results from experiments being performed to investigate the coolability of debris material that interacts with concrete after it is expelled from the vessel. Although evidence discussed in this section indicates that there are insufficient data for predicting in-vessel debris coolability, models envisioned for predicting this phenomena are discussed in Section 2.3. Conclusions from information reviewed in this section are summarized in Section 2.4.

2.1 Summary of Evidence Indicating Enhanced Cooling

Experimental evidence indicates that additional cooling mechanisms, beyond conduction, are present when melt relocates to form a continuous solid or partially molten phase in a water-filled lower plenum. In this section, information from the TMI-2 Vessel Investigation Project, molten lava flows, and severe accident fuel damage tests is reviewed that support the hypothesis that some cooling mechanism supplements simple conduction in oxidic materials.

2.1.1 TMI-2 Vessel Investigation Project

Results from the recently completed OECD-sponsored Three Mile Island Unit 2 (TMI-2) Vessel Investigation Project (VIP) suggest that conduction through solidified debris was not the only debris cooling mechanism present in the reactor vessel.[1] Calculations were performed to investigate the vessel thermal and structural response to the heat load from relocated debris.[7] Initially, input was based on metallurgical examinations of specimens from the hard layer of relocated debris found next to the lower head. These examinations indicated that the material relocated in a molten state and remained relatively hot for several hours (3 to 72 hours).[8] Although only 6.5 kg of the 6,800 kg in this continuous layer were examined, results from all

specimens supported this conclusion. The calculated thermal and structural response results were compared to data from metallurgical examinations of vessel steel and known events.

Metallurgical examinations of the vessel steel indicate that relatively high vessel temperatures (~1400 K) occurred in an elliptically-shaped localized region (1.0 m x 0.8 m) of the vessel for approximately 30 minutes and that this "hot spot" was rapidly cooled (~10 to 100 K/min).[9] Data also indicate that vessel locations outside this hot spot remained relatively cool throughout the accident, because the ferritic-to-austenitic steel transition (occurring at 1000 K) was not observed. The calculated vessel thermal response, based on debris examination data, did not coincide with this metallurgical data, primarily due to lack of a cooling mechanism capable of causing this rapid quench. Furthermore, because the vessel was not cooled, calculations based on the debris data predicted that it would fail, contrary to known events.

Thus, additional scoping calculations were performed to investigate the potential for debris cooling to have occurred after relocation to the lower head. TMI-2 debris sample data were not sufficient to determine the exact mechanisms that caused the debris to cool within this time period. However, videos taken during defueling efforts of the TMI-2 vessel indicated that surface cracks were present on the hard layer of debris adjacent to the lower head and that gaps were present between the instrument nozzles and the debris surrounding the instrument nozzles. The presence of these cracks and gaps led to two postulated forms of cooling that could produce the required cooling: a "slow" cooling mode in which it is assumed that water slowly removes heat as it travels through channels or "cracks" within the debris; and a "rapid" cooling mode, in which it is assumed that coolant rapidly removes heat as it travels through channels or "gaps" between the vessel and the debris. Analysis results indicate that coolant traveling through a relatively insignificant volume of channels within the debris (i.e., less than 1% of the debris volume) and that coolant traveling through a debris-to-vessel gap of minimal thickness (i.e., as small as 1 mm) could provide the required amount of cooling.

2.1.2 Lava Flows in Iceland

Evidence obtained by watering a molten lava flow suggests that the process of water penetration into hot rock is an important cooling mechanism.[10] During the Heimaey eruption in Iceland in 1973, water was pumped onto the molten lava in an attempt to impede the flow and divert it away from the town. A stream of water, applied at 100 kg per second, spread over some 7,000 m^2 of lava engulfing the lava in steam. Drill holes revealed that after two weeks of watering, the solidification of the lava had progressed to a depth of ~12 m, leaving the solidified lava at the temperature of saturated steam (373 K). Temperature logs for these holes indicate that the transition layer, where the temperature rose from 373 to 1,323 K, was only a fraction of a meter thick indicating a very high temperature gradient in this layer. Excavation of lava after the eruption revealed that the structure of water-cooled lava was greatly different from the structure of locations where no water had been applied during solidification. The water-cooled rock was intensely fractured and broken into pieces commonly 10-20 cm across. Beneath the fractured region lay a thin layer of solid, uncracked rock, through which heat was transported via conduction. It was postulated that the first cracks which appeared above this layer were narrow and filled with superheated steam, but the bulk of the rock above had shrunk by cooling and developed cracks wide enough to admit percolation of a mixture of water and saturated steam. Results from simple heat transfer calculations suggest that coolant penetrating these cracks provided more cooling than what would have been observed from conduction alone.[11] However, there are notable differences between the lava and debris, such as the presence of decay heat in relocated debris, which must be considered before this information can be applied to in-vessel debris coolability issues.

2.1.3 Debris Endstate in Corium-Coolant Mixing (CCM) Tests

Several experiments have been performed to investigate quenching of molten core debris poured into a preexisting pool of water. Reference 12 reports results from the six Corium - Coolant Mixing (CCM) tests performed at Argonne National Laboratory to investigate melt/water interactions. In these tests, approximately 4 to 12 kg of corium (60 wt% UO_2, 16 wt% ZrO_2, 24 wt% Stainless Steel) were drained into varying depths and masses of water. Although these tests were performed to investigate fragmentation of the corium jet pouring through water and associated quenching of the debris particulates that form, some of their results for non-fragmented and reagglomerated debris are also of interest. For example, the cross-sectional view of the debris bed at the base of the interaction vessel shown below in Figure 3 indicates that there was significant cracking in the non-fragmented $(U,Zr)O_2$ debris. Furthermore, a gap appears to have formed between loose steel particles near the interaction vessel base and the overlying layer of oxide material. Discussions with ANL[13] indicate that in this test, the heavier steel relocated next to the vessel base and a gap formed because of differences in density between the solidified steel and $(U,Zr)O_2$. It is also interesting to note that the top surface is very rough. This roughness is due to the loose manner in which particulates have reagglomerated.

Figure 3. Cross-sectional view of debris bed on interaction vessel base from CCM-2 (debris shown in photograph is approximately 5 cm across).

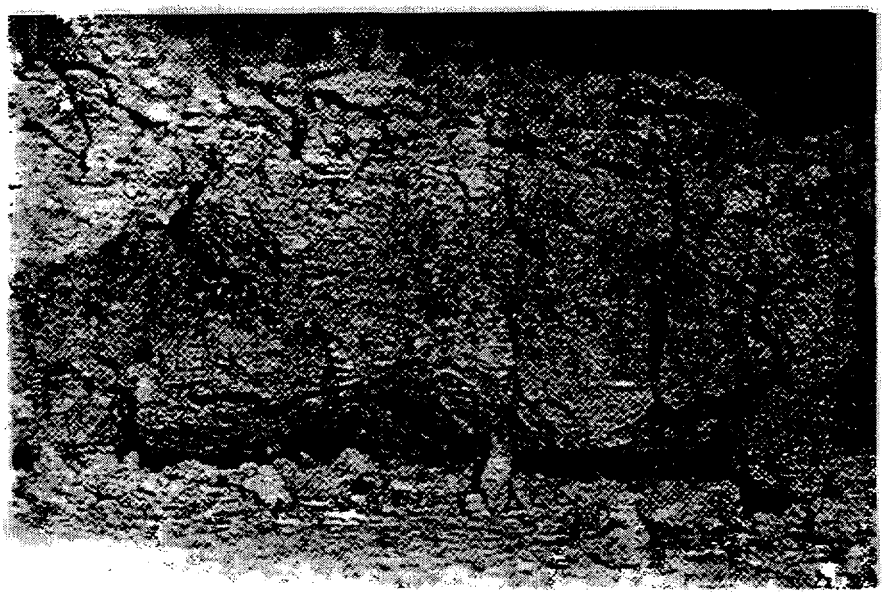

2.1.4 Zircaloy Oxidation

The lower-temperature (573 K) oxidation behavior of zircaloy offers circumstantial support for the idea that the cracking of surface layers increases transport across an oxide crust in LWR core materials as well as in lava flows. For zircaloy at reactor operating temperatures, the oxide impedes the transport of oxygen to the metal inside the oxide layer and the oxidation rate is initially proportional to the cube root of time. After the protective oxide reaches a transition thickness, the rate becomes a linear function of time. This change has been attributed to cracking of the

oxide layer when it reaches the transition thickness. Post-transition rates can be related to pre-transition rates by assuming the growth and cracking of an intact inner layer is out of phase in differing surface locations and assuming the fractured outer oxide layer does not impede the transport of oxygen to the metal under the oxide.[14]

Oxides formed on zircaloy differ from the crust formed on a slurry that relocates into a cooler environment in at least one way that should cause more cracking in the slurry's crust. The zircaloy oxide tends to expand as it is formed so that the oxide is under compression due to its attachment to a substrate that has not oxidized. In the case of a relocation of previously oxidized slurry into a cooler environment, the solid crust forms because the surface temperature is decreased. As the outer layers of the crust cool, they would tend to contract and thus be in tension as long as they adhere to or contain hotter inner layers. The tensile stress in a ceramic surface layer that is cooling and contracting is far more conducive to cracking than the stress state in a ceramic surface layer that is expanding against a constraint. In at least one of the Power Burst Facility Severe Fuel Damage tests, circumferential cracking attributed to cooling of previously molten bundle material was observed during post-irradiation examinations.[15]

2.2 Summary of Lessons Learned from Experiments Investigating Molten Core Concrete Interactions

Several melt coolability experiments have been performed to investigate the coolability of corium melt during molten core concrete interaction (MCCI) stages of a postulated LWR severe accident. Key aspects associated with a sampling of these experiments are summarized in Table 1. Although these tests have provided useful information for understanding ex-vessel MCCI melt behavior, their applicability to predict in-vessel debris coolability phenomena is limited because of differences in the material composition and scaling parameters. However, these data were reviewed to clarify why these data are not directly applicable to in-vessel debris coolability questions.

2.2.1 FRAG Tests

Results from experiments reported by Tarbell[16] suggest that water ingression via debris cracking and interconnected voids may occur under certain conditions. In the FRAG tests, 3-mm diameter mild steel spheres were inductively heated to form 45 kg of debris that was allowed to penetrate sidewards and downwards into a concrete cavity initially 0.2 m in diameter. Both limestone and basaltic concrete crucibles were tested. In two of the four FRAG tests, FRAG-3 and FRAG-4, water was added to the melt at the time that melt/concrete interactions were initiated. In the FRAG-3 test with limestone concrete, a stable crust was observed to form that was an effective heat transfer barrier. This crust prevented any water ingress and the concrete erosion rate was not impacted by the introduction of water. In contrast, in the FRAG-4 test with basaltic concrete, the crust that formed on the upper surface of the melt allowed water to penetrate through the debris via interconnected void areas and through cracks induced by thermal stresses. Although the scaling parameters and melt composition are considerably different than that expected for in-vessel debris cooling conditions, it is interesting to note that crust formation in this MCCI test did not preclude water ingression. Furthermore, it is interesting to note that debris quenching was possible via water ingress through the cracks and interconnected voids that formed in this debris (i.e. counter-current flows did not preclude debris quenching).

Table 1: Summary of MCCI Experiments

Test/Location	Objective	Procedure	Melt Composition and Weight	Crucible Description and Size	Comments
FRAG/SNL	To examine phenomena associated with long-term interaction of fragmented, solid core debris with concrete	FRAG-3: Water present at start of test; core/concrete interaction not initiated until water inflow terminated and debris bed dryout occurred. Water also added at time core/concrete interaction initiated.	mild steel; ~45 kg; Melt inductively heated (power input < 0.9 W/g).	FRAG-3: limestone concrete; inner diameter 21.6 cm.	FRAG-3: Stable crust formation was an effective heat transfer barrier that prevented water ingress;
		FRAG-4: Water added at time core/concrete interaction initiated.		FRAG-4: Basaltic concrete; inner diameter 22.8 cm.	FRAG-4: crust formation was not an effective heat transfer barrier; water penetrated through interconnected void areas and cracks induced by thermal stresses.
SWISS/SNL	To examine effects of an overlying water pool on high temperature melt/concrete interactions.	SWISS-1: Water introduced at ~ 35 min. after melt contacted the concrete (after 12 cm of concrete had eroded).	Stainless Steel Type 304; 46 kg; Molten steel inductively heated (power input of 1.3 to 1.7 W/g).	21.6 cm diameter disk of concrete contained in a MgO annulus and a limestone/common sand concrete base.	Stable crust formation observed in both tests without water ingression through cracks.
		SWISS-2: Water introduced at ~ 2 min. after the melt contacted concrete (before any significant erosion of concrete occurred).			
WETCOR	To ascertain if melt-coolant interactions were unstable for extended periods during the initial interaction period.	Test designed to extend the time for unstable melt-coolant interaction and promote bulk quenching process. Heat melt until 2 cm of concrete has ablated, then add water. Power was on during the interaction period.	80 wt% Al_2O_3 - 15 wt% CaO - 4 wt% SiO_2 - 1 wt% Fe_2O_3 34 kg;	MgO annulus lined with heated tungsten (to minimize heat flux limiting crusts). Limestone/common sand concrete base. 32 cm diameter.	Upward heat transfer initially at 1.5 MW/m^2. However, only 1-2 minutes of vigorous melt-water instability observed before stable crust formation occurred. Glassy crust solidified in a concave fashion with "blowholes" in the surface that allowed gas release.

Table 1: Summary of MCCI Experiments

Test/Location	Objective	Procedure	Melt Composition and Weight	Crucible Description and Size	Comments
MACE	To obtain information on the quenching behavior of prototypical oxide melt under MCCI conditions	Melt heated to simulate decay heat using direct electrical heating. Water introduced into the cavity through weirs at top of test section (In M0, water was added prior to upper crust formation. In M1 and M1b, water was added at 15 minutes after corium/concrete interactions initiated).	M0: 77 wt% UO_2, 16 wt% ZrO_2, 5 wt% Zr, 4.4 wt% SiO_2, and 4 wt% CaO; 100 kg.	M0: Limestone/-Sand concrete basemat (30 cm x 30 cm bottom area)	M0: A stable upper crust formed above a voided region.
			M1 and M1b: 77 wt% UO_2, 16 wt% ZrO_2, 3 wt% Zr, 3 wt% SiO_2, and 3 wt% CaO; 430 kg.	M1 and M1b: Limestone/Sand concrete basemat (50 cm x 50 cm bottom area)	M1 and M1b: In M1, sintered powders at top of charge failed to melt, and water was prevented from contacting the melt by the preexisting crust. In M1b, initial melt/water contact achieved and after a period of several minutes stable upper crust formation observed.

2.2.2 SWISS Tests

Similar results were obtained from later tests using melt masses, composition, and crucible sizes similar to the FRAG test with a limestone/common sand concrete base crucible.[17] In the Sustained Water Interactions with Stainless Steel (SWISS) tests, 46 kg of stainless steel were inductively heated in a 0.21 m crucible with a limestone/common sand concrete base. In the SWISS-1 test, water was introduced at approximately 35 minutes after melt had eroded approximately 12 cm of the concrete. In the SWISS-2 tests, water was introduced at approximately 2 minutes after the melt had contacted the concrete with little concrete erosion. A stable upper crust was observed to form in both of these tests. This stable crust did not crack, and significant water ingression into the melt was not observed. However, it should be noted that several references[11,17, and 18] (including individuals who performed the SWISS tests) caution against applying results from these tests to MCCI conditions because of the small scale and the absence of an appreciable fraction of oxidized melt in the SWISS tests. Therefore, data from these tests are also not applicable to in-vessel debris coolability conditions.

2.2.3 WETCOR Tests

The WETCOR tests were performed at Sandia National Laboratory (SNL) to investigate debris coolability by overlying water pools.[19] Previous investigations suggest that during MCCI, there is an initial time period during melt-coolant interactions where instabilities occur that allow very high rates of heat transfer, promote relatively rapid bulk freezing, and limit interactions with the concrete basemat. These tests were designed and executed in a manner to extend this time period for unstable melt-coolant interactions. In these tests, a 34 kg charge material of Al_2O_3, CaO, SiO_2, and Fe_2O_3 was melted in a crucible with tungsten-lined sidewalls and a limestone/common sand basemat. The tungsten sidewalls were heated in order to reduce crust formation and heat losses associated with this crust formation.

In these tests, there was an initial period of vigorous melt-water interactions which lasted for 1 to 2 minutes. Then, a relatively stable crust-water geometry occurred with substantially reduced rates of energy transfer to the overlying water. These rates of energy transfer were insufficient to quench the melt or to discontinue the pre-established melt/concrete ablation process. Post-test examinations revealed that the crust that formed on the upper surface was concave and appeared to be made up of thousands of connected black bubbles or spheres. Gas was released from the crust surface via numerous "blowholes," approximately 1 to 2 mm in diameter. Because these experiments were small scale and considered melt with concrete components, they are also not applicable to in-vessel debris coolability conditions.

2.2.4 MACE Tests

A series of MCCI experiments is currently being performed at Argonne National Laboratory (ANL). The latest tests performed in the ANL investigation are referred to as the Melt Attack and Coolability Experiments (MACE) Program tests.[18, 20, and 21] The experiments investigate the interaction of a 70% oxidized PWR corium melt with a limestone/common sand concrete basemat in the presence of a water overlayer at nominally atmospheric pressure. The corium contained UO_2, ZrO_2, Zr, CaO, and SiO_2. The addition of major limestone/common sand concrete constituents, CaO and SiO_2, at the beginning of the tests was based upon results from earlier tests indicating that concrete components are rapidly added to the melt during MCCI.

Results from the M0 and M1b tests suggest a two stage heat extraction process occurs between the melt and the overlying layer of water. First, bulk cooling of the melt resulting from vigorous agitation (due to MCCI-related gas sparging) extracts sufficient heat to solidify (or create a slurry in) much of the melt. Second, there is a stage of interfacial heat transfer which is characterized by crust formation at the melt/water interface. This crust, which appears to be impermeable to downward water flow, grows and limits heat extraction. However, analyses in support of these experiments indicate that oxidic debris crusts are unstable at larger, reactor-scale, conditions.[22] Analyses suggest that crusts in a cavity with a radius larger than 1.3 m will break up under the combined forces of water weight, thermal (membrane and bending) stresses, and the agitation associated with MCCI gas release.

Material property data obtained from debris removed from the MACE M0 and M1 tests emphasize the impact that the concrete components have on the melt's behavior. For example, Reference 22 indicates that for temperatures between approximately 1000 and 2000 K,[a] the Modulus of Elasticity for UO_2 is a factor of 1500 greater than that for debris from the MACE tests and that the thermal coefficient of expansion for UO_2 is nearly a factor of two greater than debris from the MACE tests. The much larger Modulus of Elasticity and thermal coefficient of expansion for UO_2 indicate that for a given temperature difference, UO_2 will experience much higher thermal stresses, and thus be more susceptible to cracking, than the MACE debris. These large differences in material properties illustrate why most MCCI data are not applicable to in-vessel debris coolability issues. Furthermore, the MACE experience suggests the importance of identifying key mechanisms causing the phenomena of interest and obtaining material property data affecting these mechanisms prior to performing expensive, large-scale, debris coolability tests.

2.3 Proposed Models for Predicting Enhanced Heat Transfer

Although the mechanisms responsible for debris cooling are not known, it is useful to perform scoping calculations to estimate possible increases in cooling that may occur with various postulated cooling mechanisms. These calculations are also useful for illustrating the types of models envisioned for predicting enhanced cooling due to various postulated cooling mechanisms. For these calculations, a debris mass and composition similar to that found in the hard layer of material on the lower head of the TMI-2 vessel were considered. In addition, some calculations considered other debris compositions to illustrate the impact of debris composition on debris cooling. Other input parameters for these calculations, such as coolant temperatures and RCS pressures, were also based upon data from the TMI-2 accident.

2.3.1 Volume Reduction during Debris Solidification and Cooling

As illustrated in Figure 4, data for a range of postulated severe accident debris compositions indicate that their density increases as the melt solidifies and cools to the coolant temperature.[14] Hence, the volume of material decreases during melt solidification and cooling. To estimate the change in volume that occurs when melt solidifies and cools to the coolant temperature (600 K), the following equation was applied

$$\textit{Fractional decrease in debris volume} = \frac{V_m - V_s}{V_m} = \frac{M_{d_s}}{M_{d_{tot}}}\left(1 - \frac{\rho_{d_m}}{\rho_{d_s}}\right) \quad (1)$$

a. Although Reference 22 does not explicitly state for which temperatures these material properties were obtained, it applies these properties over this temperature range.

where

V_m = Debris volume in molten state, m^3
V_s = Debris volume in solid state (at 600 K), m^3
M_{d_s} = Mass of solidified debris (at 600 K), kg
$M_{d_{tot}}$ = Total mass of relocated debris, kg
ρ_{d_m} = Density of molten debris (evaluated at $T_{liquidus}$), kg/m^3
ρ_{d_s} = Density of solidified debris (evaluated at 600 K), kg/m^3

Using a 10,000 kg mass of relocated debris (the maximum estimate for the hard continuous layer of debris found in the TMI-2 vessel), Equation 1 was applied to a debris composition similar to the composition of the TMI-2 debris assuming chemical reactions or phases unique to mixtures during heating and cooling are negligible. For comparison purposes, highly metallic debris and pure UO_2 debris were also considered (see Figure 4). Results, illustrated in Figure 5, indicate that the volume reduction that occurs during melt solidification and cooling may be as high as 23% (assuming a pure UO_2 composition). Note that density behavior (see Figure 4)[14] indicates that the most substantial reduction in density per change in temperature occurs during melt solidification although additional volume reduction occurs during cooling from the melt liquidus to 600 K.

Figure 4. Temperature-dependent density behavior for possible debris compositions

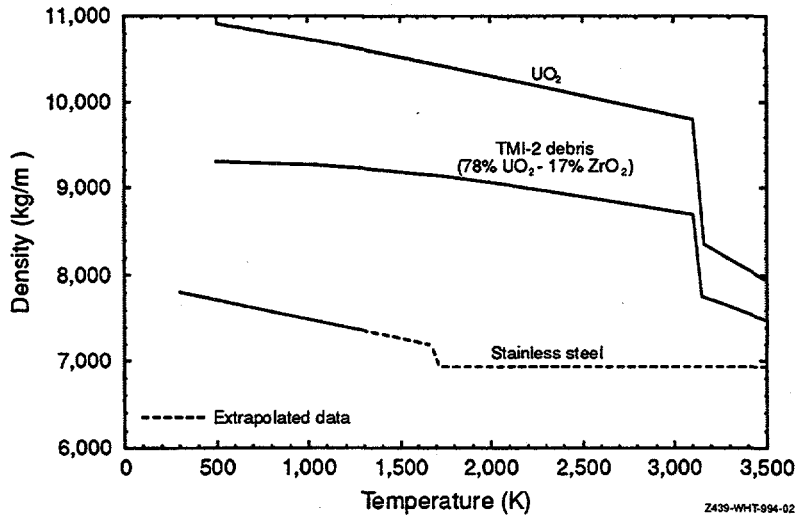

Figure 5 also illustrates that the volume reduction associated with solidification and cooling is dependent upon material composition. Considerably less volume reduction is predicted if the material is metallic (a maximum of 10% is predicted for stainless steel), rather than ceramic (a maximum of 23% is predicted for UO_2). In this section, subsequent calculations will assume a debris composition found in the TMI-2 lower head, a 78% UO_2-17% ZrO_2 weight fraction compound. For this composition, a volume reduction of 16% is predicted when all of the melt solidifies.

Figure 5. Volume reduction estimate for possible debris configurations.

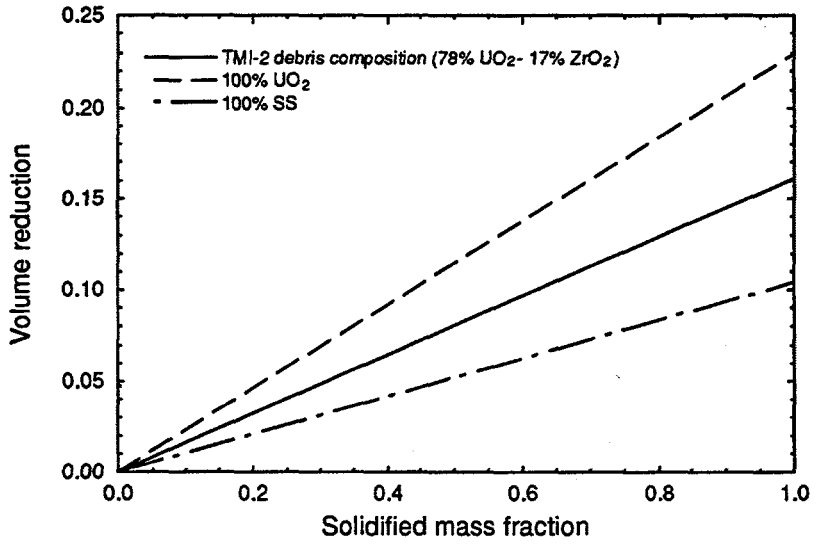

2.3.2 Cooling by Water Ingress into Cracks

Results in Section 2.3.1 indicate that the volume of ceramic debris will decrease (by as much as 23%) during solidification. One postulated debris cooling mechanism is that the debris solidifies to form cracks and that coolant ingresses into these cracks and cools the debris. As discussed in Sections 2.1 and 2.2, evidence from several experiments, the TMI-2 accident, and solidified lava support that cracks occur as debris solidifies. Furthermore, evidence from the FRAG-4 test and the TMI-2 accident suggest that these cracks may enhance debris cooling. In this section, an approach similar to that used in Reference 7 was applied to estimate the amount of heat that could be removed via coolant traveling through cracks within a 10,000 kg bed of 78% UO_2-17% ZrO_2 weight fraction debris. Although it is envisioned that a model similar to the one discussed in this section is applicable to debris cooling via coolant traveling through cracks, it should be noted that at this time there are currently no data to validate the use of this model. Furthermore, the lack of data for estimating geometrical and heat transfer parameters in this model results in considerable uncertainty. However, upper and lower bound estimates for many of these parameters are assumed so that order-of-magnitude estimates for cooling can be obtained.

For these calculations, "through cracks" were assumed to exist in the debris. Hence, coolant would be able to flow through the cracks with negligible countercurrent flow or chemical reaction effects. Although it is expected that cracks would form in a rectangular geometry, an effective diameter approach was used to model the cracks (see Figure 6). No quantitative data are available to characterize crack dimensions. Therefore, these scoping calculations assume values based on TMI-2 video examinations. Although quantitative dimensions could not be obtained from these videos, these cracks appeared to be at least 0.5 cm by 6 cm, which corresponds to an effective diameter, D_e, of 1 cm. A minimum height for a "through crack" within the debris, z_{crack}, was estimated as approximately twice the average height of the debris bed or the maximum debris bed height (0.45 m for the 10,000 kg debris bed considered in these calculations). For the volume

reduction predicted during solidification for the 10,000 kg of this debris, approximately 4,500 cracks with a 1 cm effective diameter and 0.45 m length are possible.

Figure 6. Geometry assumed for estimating heat losses associated with coolant traveling through debris cracks

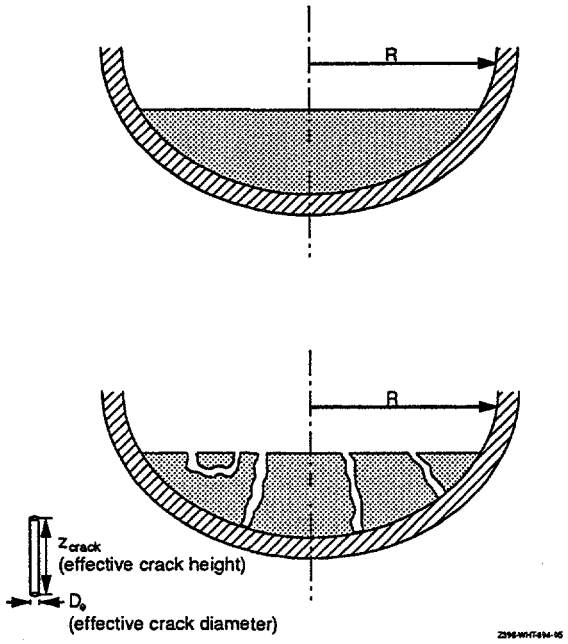

For these scoping calculations, a conservative approach was adopted in which the coolant was assumed to remain liquid. This is conservative because additional heat would be removed if subcooled or saturated boiling heat transfer were considered. The coolant inlet temperature was assumed as 400 K, based upon cold leg temperatures measured during the TMI-2 event during relocation.[23] A saturated coolant exit temperature was assumed, with the actual value dependent upon the RCS pressure considered (calculations considered 3 to 15 MPa RCS pressures). The energy lost to the coolant, q_{sink}, as it is transferred from its initial subcooled state to its final saturated state was estimated using

$$q_{sink} = n_{crack}\dot{m}\,(h_{sat} - h_{in}) \tag{2}$$

where

n_{crack} = number of cracks
$\dot{m}$ = coolant mass flow through a crack, kg/s
h_{in} = coolant inlet enthalpy, J/kg
h_{sat} = coolant enthalpy at saturated conditions, J/kg

Because it is not known how the heat flux will vary as a function of distance through the cracks, a constant heat flux was assumed. The energy transferred from the debris to the coolant, q_{sink}, was estimated using

$$q_{sink} = n_{crack}h_c A_{crack}(T_{d_s} - T_{bulk}) \tag{3}$$

where

h_c = convective heat transfer coefficient, W/m^{2}K
T_{d_s} = debris surface temperature, K
T_{bulk} = bulk coolant temperature, K
A_{crack} = surface area of a crack with effective diameter, D_e, and length, z_{crack}, m^2
= $\pi D_e z_{crack}$

Although a range of possible debris surface temperatures are possible, calculations assumed a 1700 K debris surface temperature. The bulk coolant temperature was assumed as the average of the saturation exit temperature and a 400 K inlet temperature (the minimum cold leg temperature measured prior to melt relocation during the TMI-2 accident). The convective heat transfer coefficient, h_c, is dependent upon the mass and heat transfer conditions. Because there are currently insufficient data to select an appropriate heat transfer correlation, a range of correlations were evaluated. Although it is expected that natural convection will dominate heat transfer, correlations for both natural and forced convection were considered. These correlations are listed in Table 2 with the range of conditions for which they are applicable.

Table 2: Results for estimating heat transfer via coolant traveling in debris cracks.

Correlation	Basis	Assumptions	Range	Heat transfer coefficient (W/m^{2}K)	Heat removal rate per crack (kW)
Elenbass[24] & Dyer[25]	Experimental and theoretical	Natural convection through an isothermal cylinder	$Ra < 10^4$	230-260	4.1-4.7
Rohsenow[26]	Experimental and theoretical	Natural convection through an isothermal channel	$Ra < 10^4$ 4:1 side ratio	1600-1800	29.-32.
Todreas & Kazimi[27]	Theoretical	Fully developed laminar flow under forced convection through a cylinder with a constant heat flux	$Re < 2300$	240-290	4.3-5.2
Todreas & Kazimi[27]	Theoretical	Fully developed laminar flow under forced convection through a rectangular channel with a constant heat flux	$Re < 2300$ 8:1 side ratio	370-440	6.7-7.9
Collier[28]	Experimental	Laminar flow under forced convection modified to include natural convection effects	$Re < 2000$ $z_{crack}/D_e > 50$	270-21,000	4.9-38.
Dittus-Boelter[29]	Experimental	Turbulent flow under forced convection	$Re > 2300$	3800-110,000	68.-2000.

Each of these heat transfer correlations was combined with the energy conservation equations to solve for the amount of energy, q_{sink}, that could be removed as a function of the number of cracks within the debris. Results, summarized in Table 2, indicate that a wide range of values for the heat transfer coefficient and corresponding heat removal per crack are possible. Higher values are predicted with forced turbulent convective flow correlations, and smaller values are

predicted with natural convection and laminar flow correlations. Upper and lower bound estimates for heat removal are plotted in Figure 7 as a function of the number of cracks within the debris bed. Although the estimated cooling is linearly proportional to the crack number, results are plotted on a semilog graph because estimates vary by several orders of magnitude. For the 10,000 kg mass of debris considered in this paper, a maximum of 4500 1 cm diameter and 0.45 m long cracks are possible. This number and size of cracks would increase the heat transfer surface area between the coolant and the debris by a factor of 13. Based upon results in Figure 7, it is estimated that an additional 15 to 8400 MW could be removed from the debris via these cracks.

Figure 7. Debris cooling as a function of crack number.

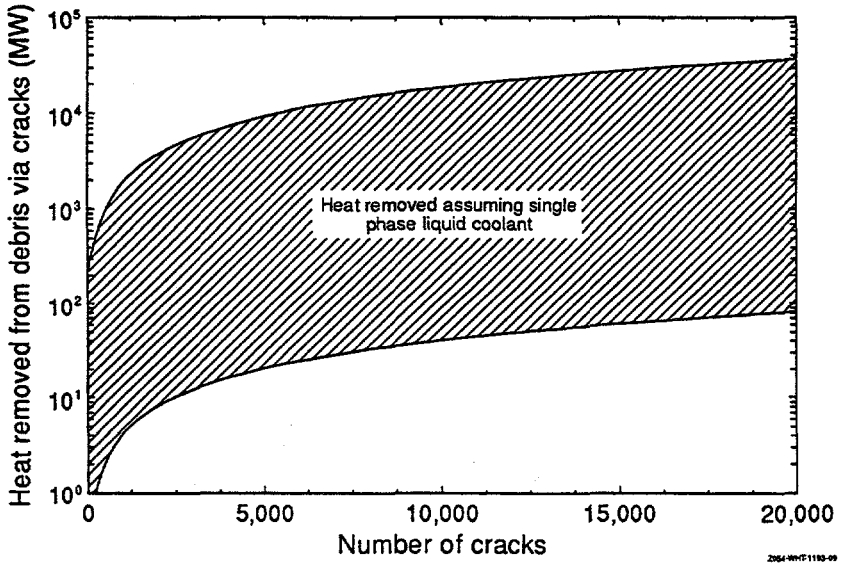

2.3.3 Cooling by Debris-to-Vessel Gaps

A second postulated cooling mechanism is via coolant traveling through gaps that form between the vessel and the solidified debris. As discussed in Section 2.1, gaps between instrument tube nozzles and debris surrounding these nozzles suggest that gaps may occur between relocated debris and the vessel.[a] In this section, an approach similar to that used in Reference 7 was applied to estimate the amount of heat that could be removed via coolant traveling through gaps forming between the vessel and the 10,000 kg bed of 78% UO_2-17% ZrO_2 weight fraction debris. Although it is envisioned that a model similar to the one discussed in this section is applicable to debris cooling via coolant traveling through debris-to-vessel gaps, it should be noted that at this time there are currently no data to validate the use of this model. Furthermore, the lack of data for estimating geometrical and heat transfer parameters in this model results in considerable uncertainty. However, upper and lower bound estimates for many of these parameters are assumed so that order-of-magnitude estimates for this cooling can be obtained.

The approach and many of the input parameters for these calculations are similar to what was used in the Section 2.3.2 calculations. For the volume reduction predicted during debris solidification, it is estimated that the maximum debris-to-vessel gap thickness, t_{gap}, would be 2.7 cm.

a. The potential for gaps to occur and result in reduced debris to vessel contact is also supported by results from small scale experiments performed at FAI.[30]

It was also assumed that the debris solidified to form a sufficient number of wide gaps that countercurrent flow considerations could be eliminated. Furthermore, it is assumed that the gaps can be treated as essentially one large gap, although it is recognized that the existence of this gap requires intermittent contact between the debris and the vessel. This gap may increase the heat transfer surface area between the debris and the coolant by as much as a factor of 2.1.

The conservative assumption that the coolant remained in a liquid state was also applied in these calculations. The coolant was assumed to enter this gap at 400 K and exit at the saturation temperature for the pressure assumed (calculations considered 3 to 15 MPa RCS pressures). The energy lost to the coolant with mass flow, $\dot{m}$, was estimated using

$$q_{sink} = \dot{m}\,(h_{sat} - h_{in}) \tag{4}$$

Assuming a constant heat flux along the bottom surface of the vessel, the energy transferred from the debris to the coolant was estimated using

$$q_{sink} = h_c A_b\,(T_{d_s} - T_{bulk}) \tag{5}$$

where A_b, the downward surface area of the debris with a maximum height, z_{crack}, in a vessel with radius, R (see Figure 8) is given by

$$A_b = 2\pi R z_{crack} \tag{6}$$

Figure 8. Geometry used to estimate maximum gap size associated with volume reduction.

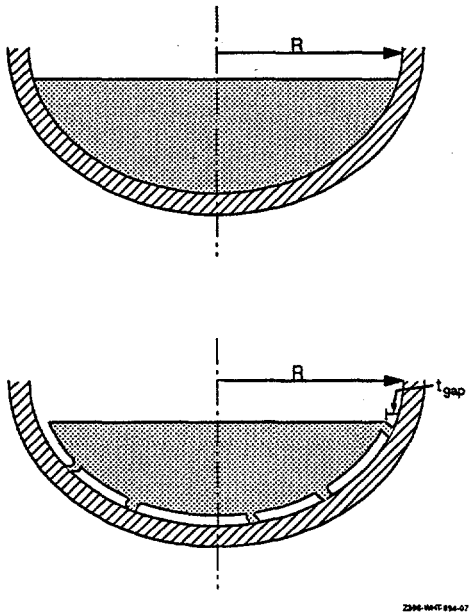

Although a large number of correlations for predicting heat transfer to a liquid are available, no correlations could be found that were directly applicable to the geometry in question. Hence, several single phase liquid heat transfer correlations for various geometries were compared to obtain an order-of-magnitude estimate for the heat transfer coefficient. Heat transfer correlations for flow between parallel plates in which natural convection heat transfer dominates

were considered most appropriate for these calculations. However, forced and natural convection correlations were considered for flow between parallel plates as well as for flow over a sphere and flow over vertical and horizontal surfaces. Correlations applied in these calculations are summarized in Table 3. Each of these heat transfer correlations was combined with the energy conservation equations to solve for the amount of energy, q_{sink}, that could be removed via coolant traveling through a debris-to-vessel gap. Results, summarized in Table 3, indicate that a wide range of values for the heat transfer coefficient and corresponding heat losses are possible. Upper and lower bound estimates for heat removal are plotted in Figure 9 as a function of the mass fraction of material solidified within the debris bed. For the 10,000 kg mass of debris considered in this paper, results in Figure 9 indicate that between 0.2 and 2.0 x 10^7 MW could be removed via coolant traveling through this gap.

Table 3: Results for estimating the heat transfer coefficients through a debris-to-vessel gap.

Correlation	Basis	Assumption	Range	Heat transfer coefficient (W/m^2K)	Maximum heat removal rate [a] (MW)
Rohsenow[26]	Experimental and theoretical	Natural convection through heated vertical parallel plates	$Ra < 10^5$	22,000-25,000	130-190
Kazimi and Todreas[27]	Theoretical	Laminar flow under forced convection between heated horizontal parallel plates	$Re < 2300$	43-51	0.26-0.38
Dittus-Boelter[29]	Experimental and theoretical	Turbulent flow under forced convection between heated horizontal plates	$Re > 2300$	60-2100	0.36-16.
Raithby and Hollands[32,33]	Experimental and theoretical	Natural convection over an isothermal sphere	$10 \le Ra \le 10^9$	2900-3800	18.-28.
Welty[31]	Experimental	Natural convection over a spherical surface	$10^4 < Ra < 10^9$	810-1000	4.9-7.4
Eckert and Jackson[34]	Experimental and theoretical	Natural convection over a heated vertical wall	$Ra < 10^9$	1000-1300	6.1-9.6
Eckert and Jackson[34]	Experimental	Natural convection over a heated vertical wall	$Ra > 10^9$	5700-7600	35.-56.
McAdams[31]	Experimental	Natural convection over a downward facing, heated, horizontal heated plate	$10^5 < Ra < 10^{10}$	490-630	3.0-4.7

a. Assuming all the mass solidifies.

Figure 9. Cooling associated with coolant traveling through a debris-to-vessel gap.

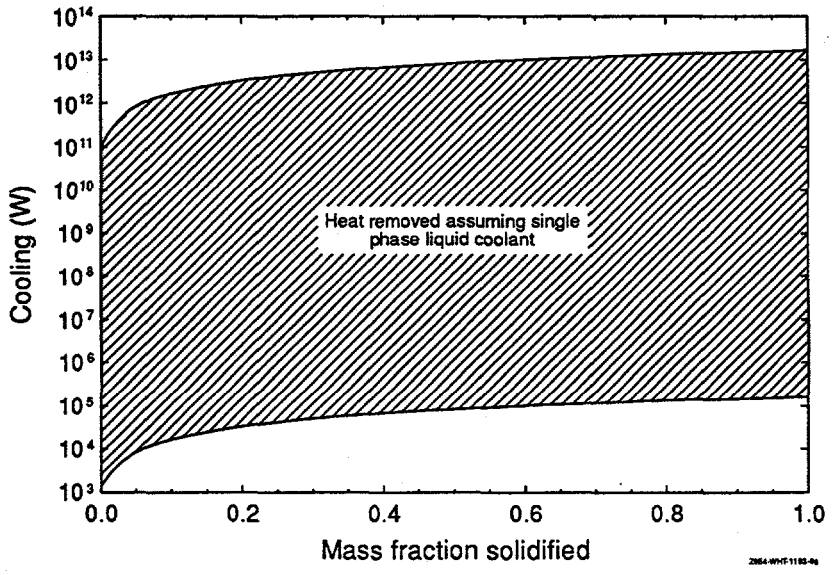

2.3.4 Cooling by Enhanced Area

The volume reduction that occurs during debris solidification may also affect the curvature of the debris bed's upper surface. The concave upper surface observed in the WETCOR experiments discussed in Section 2.2.3 suggest that this mechanism should be considered. Although it is recognized that this additional upper surface area cannot, by itself, explain the rapid cooling inferred from the TMI-2 accident, its presence will contribute to debris coolability. Scoping calculations were performed to estimate the maximum increase in debris bed upper surface that could occur during solidification of a 10,000 kg debris bed. In these calculations, the debris was assumed to solidify with a concave upper surface.[a] Although many configurations are possible, the debris was assumed to solidify in a manner that would leave a spherical "cusp" void in the center. This geometry was assumed to maximize the upper surface area of the solidified debris.

The volume associated with a debris bed of height, z, and upper surface radius, a, contained in a hemisphere with radius, R, can be estimated using

$$V = \frac{1}{3}\pi z^2 (3R - z) = \frac{1}{6}\pi z (3a^2 + z^2) \quad (7)$$

Using the geometry shown in Figure 10, the initial molten and final solidified upper surface area of the debris, A_{u_m}, and A_{u_s}, were then calculated using the following relationships

a. It should be noted that these calculations neglect the increased surface area associated with surface roughness occurring as relocating melt solidifies or an enhanced surface area associated with stretching and rupture of the solid crust in contact with the liquid. As discussed in Section 2.1.3, surface roughness has been observed in experiments with melt relocating through water. The latter postulated mechanism for increased surface area is based on observations of lava flows.

$$V_m - V_s = \frac{2}{3}\pi r_{in}^3 \tag{8}$$

$$A_{u_m} = \pi a_m^2 \tag{9}$$

$$A_{u_s} = \pi (a_m^2 - r_{in}^2) + 2\pi r_{in}^2 \tag{10}$$

Figure 10. Geometry assumed for estimating surface area increase during debris solidification

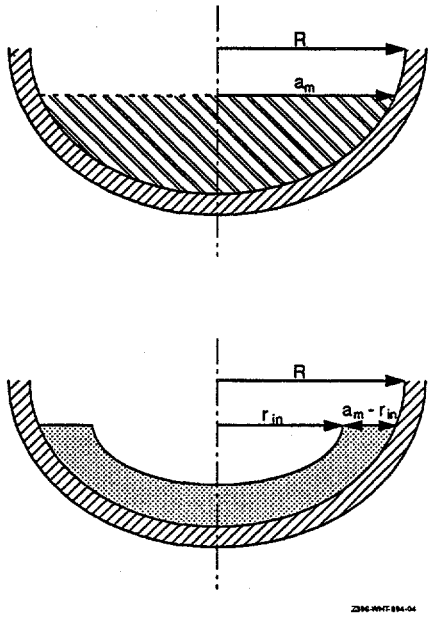

Using the above equations and assuming a 10,000 kg mass of debris, the upper surface area may increase by as much as 22%. Calculations performed in Reference 7 indicate that nucleate boiling heat transfer dominates heat loss from the upper surface of the debris to the coolant. Hence, the heat flux between the upper debris bed surface and the coolant is independent of the upper surface area. For the pressure and temperature ranges considered in Reference 7, nucleate boiling heat fluxes were estimated to range from 2.4×10^6 to 8.2×10^6 MW/m^2. Hence, the increase in surface area predicted for this 10,000 kg debris may increase heat losses by as much as 7×10^6 MW. Note that during an LWR severe accident, an even larger increase in surface area may occur if the upper surface of the relocated melt is rough as suggested by CCM test results discussed in Section 2.1.3 or if the crust undergoes stretching and ruptures as suggested by observations of lava flows.

2.4 Summary

There are limited, if any, data available to indicate how a continuous solid or partially molten phase of debris cools after relocating to a water-filled lower plenum. Information from the recently-completed TMI-2 VIP, lava flows in Iceland, and fuel damage tests suggest that additional cooling, beyond that possible via conduction, will occur when melt relocates to a water-filled lower plenum. Experimental data obtained from many tests investigating MCCI phenomena suggest that debris crusts that form are able to prevent water ingression. One exception was the

FRAG-4 test with basaltic concrete. In this test, water was able to penetrate through cracks within the crust that formed on the upper surface of the melt. Even in tests where the crust prevented water ingression, analyses suggest that the presence of concrete components in the debris and the small scale of these tests have promoted stable crust formation in these tests. Therefore, it is concluded that experimental test data are needed to identify and model the mechanisms responsible for debris cooling after relocation to a water-filled lower plenum.

Based on information discussed in this section, three solidified debris configurations that could lead to enhanced debris were postulated: interconnected debris cracks, gap formation between the debris and vessel, and increased upper debris surface area. Although there are not sufficient data to predict whether one or all three of these mechanisms occur during melt solidification during a severe accident, scoping calculations were performed to estimate the magnitude of cooling that is possible from these mechanisms. First, calculations were performed to estimate the amount of volume reduction that will occur for three debris compositions. Results indicate that the debris volume will decrease by as much as 23% during solidification. However, considerably less volume reduction is predicted if the material is metallic (a maximum of 10% is predicted for stainless steel), rather than ceramic (a maximum of 23% is predicted for UO_2). Although there is considerable uncertainty in selecting a model for predicting debris cooling, scoping calculations were performed to evaluate the magnitude of cooling possible for each debris configuration. Calculation results indicate that large amounts of additional cooling are possible via coolant traveling through cracks, coolant traveling through a debris-to-vessel gap, and from the additional upper surface area that may occur during solidification of a 10,000 kg debris bed. Order-of-magnitude estimates for the additional heat that could be removed as coolant travels through cracks within the debris range from 15 to 8400 MW. Estimates for heat removal due to coolant traveling through a debris to vessel gap range from 0.2 to 2×10^7 MW. Additional surface area that may occur during solidification of a stationary pool is estimated to increase heat removal by as much as 7×10^6 MW. Note that results from these calculations have considerable uncertainty, because of uncertainty in input values, such as the crack density, crack diameter, coolant temperature, coolant state, heat flux distribution as a function of location, and debris-to-coolant heat transfer coefficient. Furthermore, calculations to estimate possible cooling rates often invoked conservative assumptions, such as a liquid coolant endstate. Therefore, the upper values on these estimates may be several orders of magnitude too low. However, if the high end of the uncertainty band is correct for any of these three postulated cooling mechanisms, they will significantly contribute to debris cooling.

3. Overview of Proposed Program

This section outlines major elements and tasks that have been identified for completing this experimental and analytical program. This program has been developed in a manner consistent with recommendations from the task group for Scaling Methodology for Severe Accidents (SASM).[35] Furthermore, the structure of this program has been developed in a manner to easily accommodate changes. As noted within this section, the uncertainty associated with output from various steps may impact the manner in which subsequent steps are completed. For example, output from a certain task may indicate that subsequent steps are unnecessary or that additional tasks are required.

A high level overview of this program, in which key elements are identified, is found in Section 3.1. Major tasks required for program completion are identified in Section 3.2. Sections

3.3 through 3.5 provide more detailed descriptions of tasks associated with each program element. Required input and desired output for each task are also identified in Sections 3.3 through 3.5.

3.1 Key Program Elements

As discussed above, the objective of this program is to obtain a validated model that accurately predicts debris cooling. Figure 11 illustrates the three key elements proposed to accomplish this objective. Each element includes obtaining data and performing analyses. The major results obtained from each element are listed on the right side of Figure 11.

The first element, identified as Phase I Exploratory Integral Tests and Analyses, is primarily performed to quantify what additional cooling, beyond that possible by conduction through the debris, occurs and identify the mechanism or mechanisms responsible for this cooling. As discussed in Section 2, there is little evidence for determining which, if any, of the postulated mechanisms are responsible for the observed cooling. Hence, it is proposed that the first tests in this program be exploratory "integral" tests, i.e. tests simulating the debris cooling in a manner representative of that expected during severe accident conditions. Because recent calculations indicate that low pressure accidents are more likely for most operating reactors[4,5] and because of cost considerations, it is proposed that these tests be performed at lower pressures (< 1.4 MPa). Although analyses in Section 4 indicate that there may be some differences in debris cooling phenomena at high pressure, these smaller sized, low pressure, tests provide an inexpensive method identify which cooling mechanisms occur, the cooling associated with these mechanisms, and quantify characteristic parameters associated with these cooling mechanisms for a range of conditions.

Figure 11. Flow diagram illustrating key elements of proposed debris coolability program

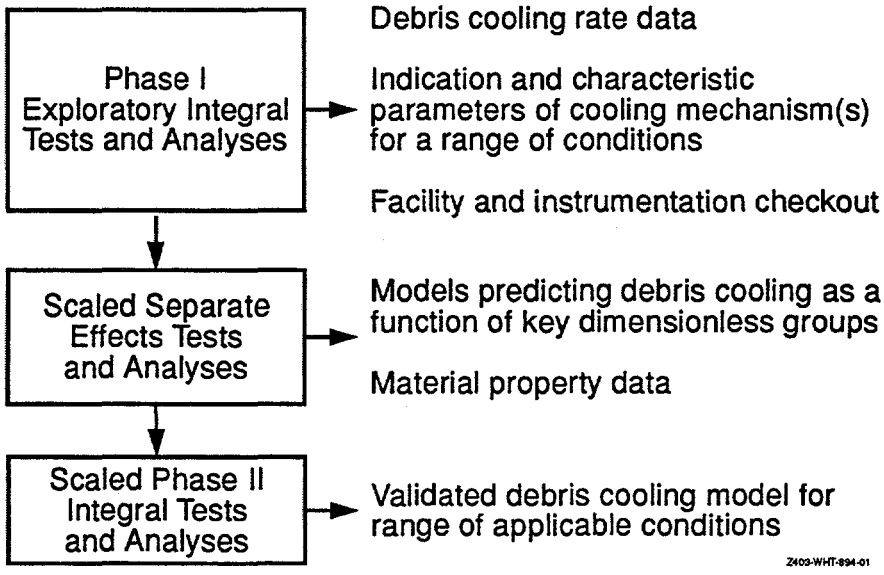

The second element, Scaled Separate Effects Tests and Analyses, is performed to obtain detailed data required for developing models for each of the cooling mechanisms observed in Phase I tests. Separate effects test design parameters will be specified by performing scaling anal-

yses for each of the mechanisms identified in Phase I. Furthermore, these scaled tests can be designed so that the entire range of possible LWR accident conditions in which enhanced debris cooling is possible can be considered (i.e., both high and low pressure regimes can be evaluated). If more than one cooling mechanism is identified in Phase I tests, interactions between models developed for each mechanism from the separate effects tests can be assessed using Phase I data.

The third element, Scaled Phase II Integral Tests and Analyses, is performed to validate the models developed from separate effects and Phase I test data. Although these tests will be performed in a facility whose design specifications will be based on results from a detailed scaling analyses, it is envisioned that the Phase II test facility will be larger in size and able to withstand higher pressures than the Phase I test facility. Furthermore, it is envisioned that more detailed measurements will be obtained from the Phase II tests. For example, in the Phase I tests, data will be obtained so that energy transfer rates can be estimated for determining time-dependent debris cooling rates; whereas in the Phase II tests, instrumentation will be added to insure that data can be obtained to estimate time-dependent crust thickness, crust temperatures, and melt temperatures.

It is proposed that simulant debris be used in all of the planned tests. The use of this material is proposed for several reasons. First, the costs associated with handling radioactive material will be reduced because the simulant debris, which contains depleted uranium, has not been irradiated. Second, the use of this less-expensive simulant material allows a range of debris compositions to be tested. Although it is planned to perform initial tests with debris similar in composition to the material found in the TMI-2 vessel, other compositions will be evaluated so that a range of accident conditions can be considered.

Figure 11 is success oriented. For example, it is assumed that debris cooling mechanisms will be observed in the lower pressure, Phase I tests and that no new mechanisms will be observed in the final, high pressure, Phase II tests. If any of these assumptions prove to be incorrect, new tasks, such as additional separate effects tests, must be added to this diagram.

3.2 Major Tasks for Program Completion

The flow diagram in Figure 12 illustrates major tasks that will be completed in this program. Like Figure 11, this diagram is also success oriented. Inputs and outputs for each task identified in Figure 12 are identified in subsequent flow diagrams in this section.

As shown in this Figure 12, there are three major tasks associated with Phase I: initial scoping analyses, Phase I exploratory integral tests, and simulant debris examinations. The first task is to perform scoping calculations to quantify the range of conditions in which additional debris cooling has been observed. As discussed in Section 2, there are insufficient data to identify what mechanism(s) are responsible for this cooling or to perform a complete scaling analyses for debris cooling tests. In such cases, it is recommended in the Severe Accident Scaling Methodology (SASM) program[35] that exploratory tests be performed to gain sufficient information to identify key scaling parameters. Scoping calculations will be used to specify the nominal values for these parameters in the Phase I exploratory tests. Results from the scoping analyses will also be used to demonstrate how phenomena not present in the proposed Phase I tests, such as the decay heat associated with fission products, impact the applicability of data to severe accident conditions. Key Phase I test parameters, such as debris cooling rates, debris mass, system pressure, will be varied to evaluate their effect on debris cooling. Although initial tests will be conducted using a debris similar in composition to the TMI-2 debris, subsequent tests will consider other composi-

tions. After completion of initial Phase I tests, post-test examinations will be conducted to verify that the debris microstructure is similar to the material found in the TMI-2 lower head. If the quench rates estimated in the scoping calculations do not produce debris microstructures similar to the TMI-2 debris, the quench rates in subsequent Phase I tests will be modified.

Figure 12. Flow diagram of major tasks for proposed program.

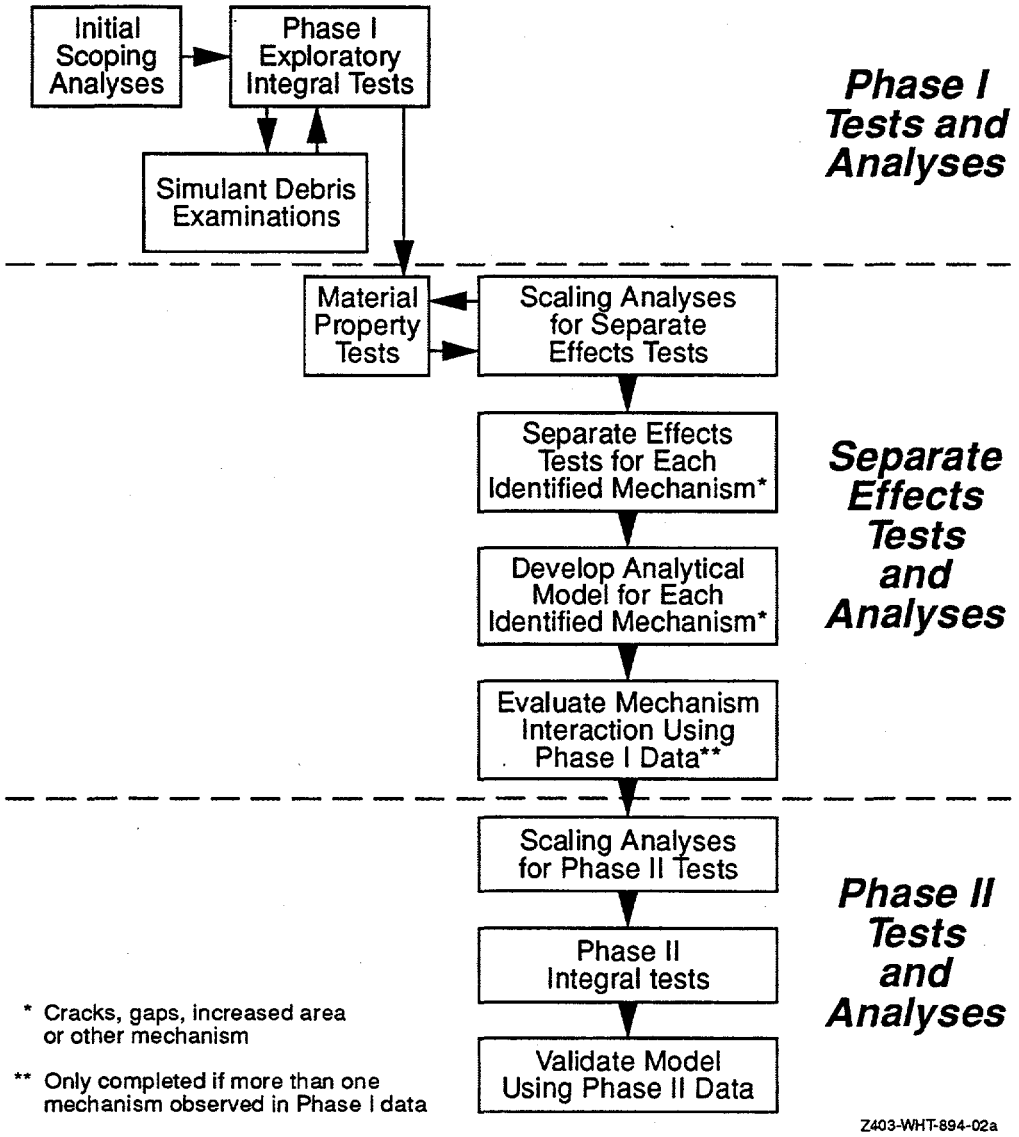

Because of cost constraints, the Phase I integral tests will not attempt to obtain all the data needed to develop models for predicting the cooling that may occur in debris for a range of postulated severe accident conditions. Rather, subsequent tasks will be undertaken so that models can be developed for predicting the cooling associated with mechanisms identified in the Phase I tests. As indicated in Figure 12, there are five tasks associated with completing the second element of the program, Separate Effects Tests and Analyses: material property tests, scaling analyses, sepa-

rate effects tests, model development, and evaluation of mechanism interactions. The first task is to obtain material properties, specific to the each of the cooling mechanisms identified in Phase I tests, that are needed for model development. As discussed in Section 5, most of this data will be obtained from the literature. However, it is anticipated that it will be necessary to obtain some structural properties that are not currently available for the simulant material. This data will be used in scaling analyses to obtain design parameters for the separate effects tests. For each identified mechanism, separate effects tests will be performed so that a model can be developed for predicting the cooling associated with this mechanism for the range of postulated severe accident conditions. For example, it is anticipated that for most postulated cooling mechanisms, correlations can be obtained to predict heat transfer as a function of key dimensionless groups, such as the Reynolds number, the Prandtl number, and the Rayleigh number. If more than one cooling mechanism is identified in the Phase I tests, interactions between cooling mechanisms will be quantified by comparing model predictions with Phase I integral test data.

In the last element of this program, Phase II Tests and Analyses, there are three tasks: scaling analyses, Phase II integral tests, and model validation. The Phase II tests will be scaled so that both low and high pressure conditions will be evaluated. Results from these tests will be used to validate models developed from the separate effects tests for the entire range of postulated accident conditions.

3.3 Tasks for Completing Phase I Tests

Figures 13 through 15 illustrate the relationship between results from the initial scoping analyses, the Phase I exploratory integral tests, and the simulant debris examinations. As discussed in Section 4, scoping analyses will be used to determine that cooling of the debris is prototypic by defining initial debris composition, mass, cooling rates, and temperatures. The primary objective of the Phase I integral tests is to determine if the debris cools at a rate greater than that possible by conduction. If it is demonstrated that the debris cools more rapidly than possible by conduction, Phase I test results will be used to determine which cooling mechanisms occur and to obtain characteristic parameters (crack length, crack density, gap size, etc.) associated with these cooling mechanisms. These characteristic parameters can then be used to define test conditions for subsequent separate effects tests. If more than one cooling mechanism is identified, Phase I tests data can be used to assess interactions between cooling mechanisms using the models developed from separate effects tests. A final objective of the Phase I tests is to verify that the facility and instrumentation function. Although less instrumentation is required for the Phase I tests than the Phase II tests, instrumentation required for Phase II tests will be tested in some of the Phase I tests. After each Phase I test is completed, the simulant debris will be examined to determine its composition, porosity, and grain size. In initial tests, these parameters will be compared with the TMI-2 specimens and subsequent test parameters, such as cooling rates, will be varied to insure that these tests produce material similar to specimens removed from the TMI-2 vessel.

Figure 13. Initial scoping studies flow diagram.

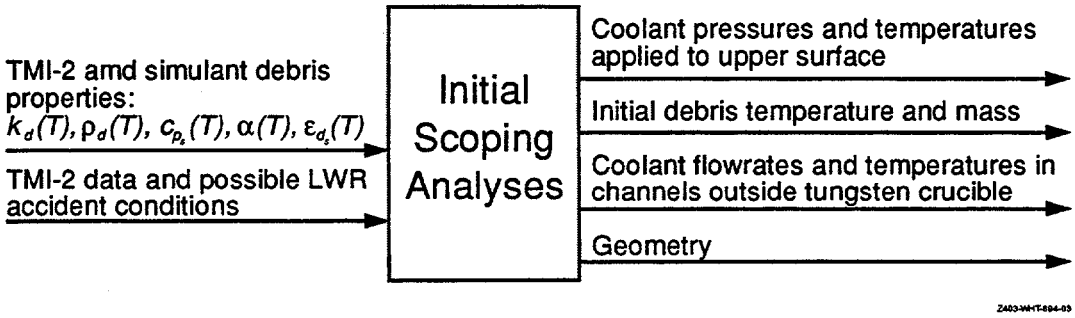

Figure 14. Phase I exploratory integral test flow diagram.

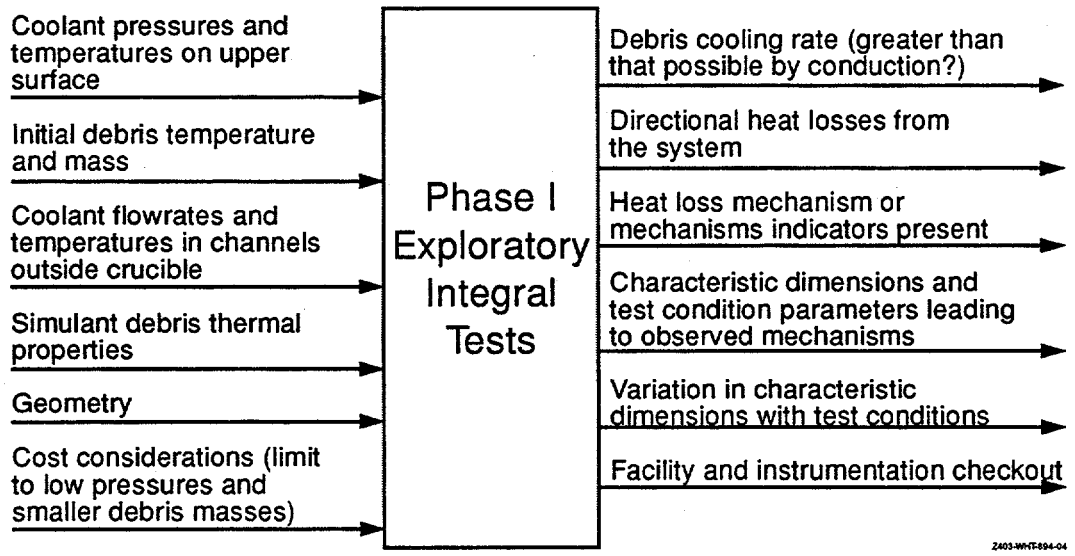

Figure 15. Flow diagram for verifying physical characteristics of debris from the Phase I integral tests.

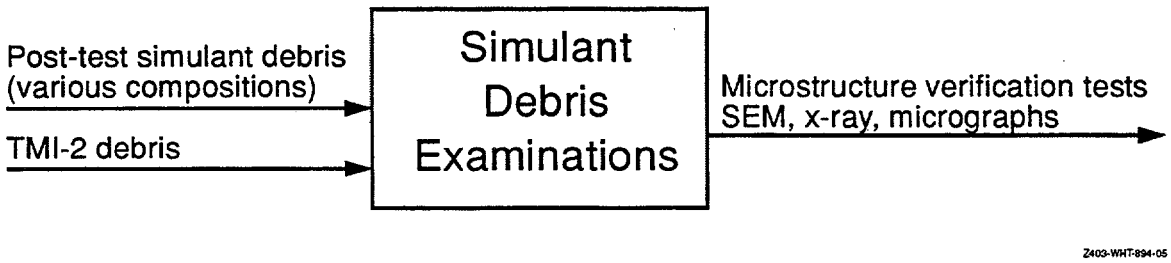

3.4 Tasks for Completing Separate Effects Tests and Model Development

Figures 16 through 20 illustrate the relationships between tasks for performing separate effects tests and developing models for predicting debris cooling. In general, the first step is to obtain material properties required to develop models for predicting a particular debris cooling mechanism identified in the Phase I tests. These material properties will primarily be obtained from the literature, although it is anticipated that tests will be required to obtain some structural properties. Second, a scaling analyses will be performed to identify key scaling parameters for designing the separate effects tests and the range of conditions to be evaluated. Third, the separate effects tests will be performed to obtain data indicating the relationship between the debris cooling rate and key test parameters. Note that these separate effects tests will typically be less expensive than the Phase I integral tests. Hence, some tests may be performed at high pressure. This data is then used in the fourth step to develop a model predicting debris cooling for the mechanism investigated. Once models are obtained for each of the mechanisms identified in the Phase I tests, interactions between various cooling mechanisms must be considered. As illustrated in Figure 20, this task will be completed by comparing model predictions with Phase I integral test data.

Figure 16. Flow diagram for additional material property tests.

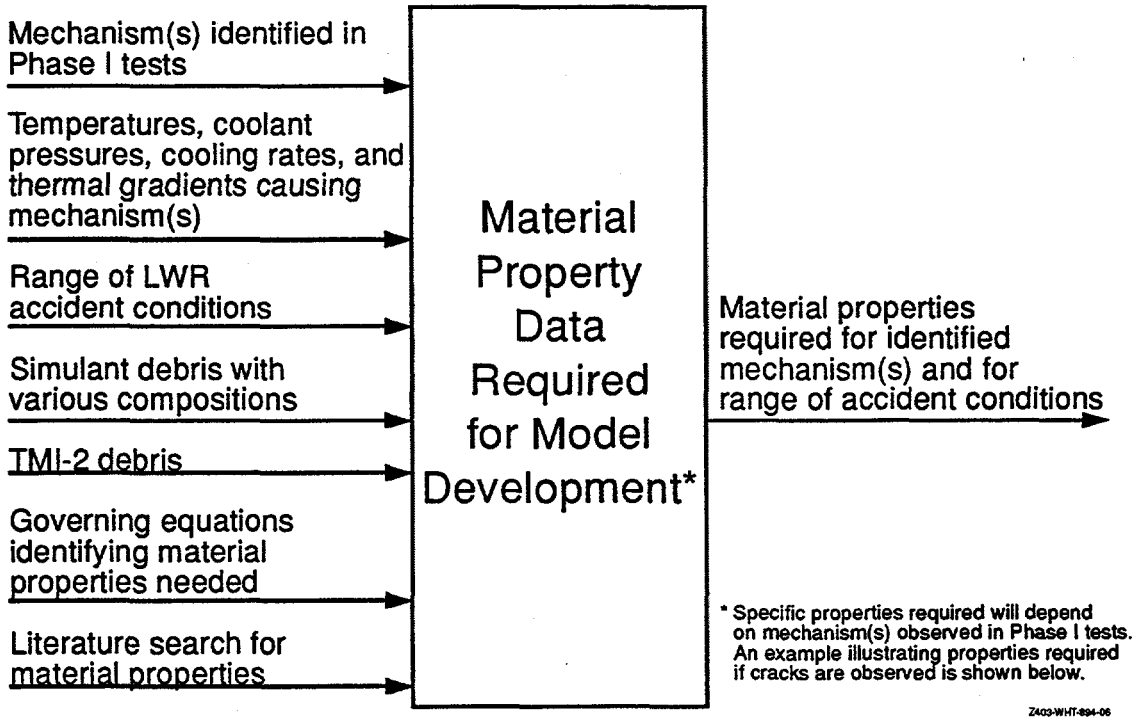

Figure 17. Scaling analyses flow diagram for separate effects tests.

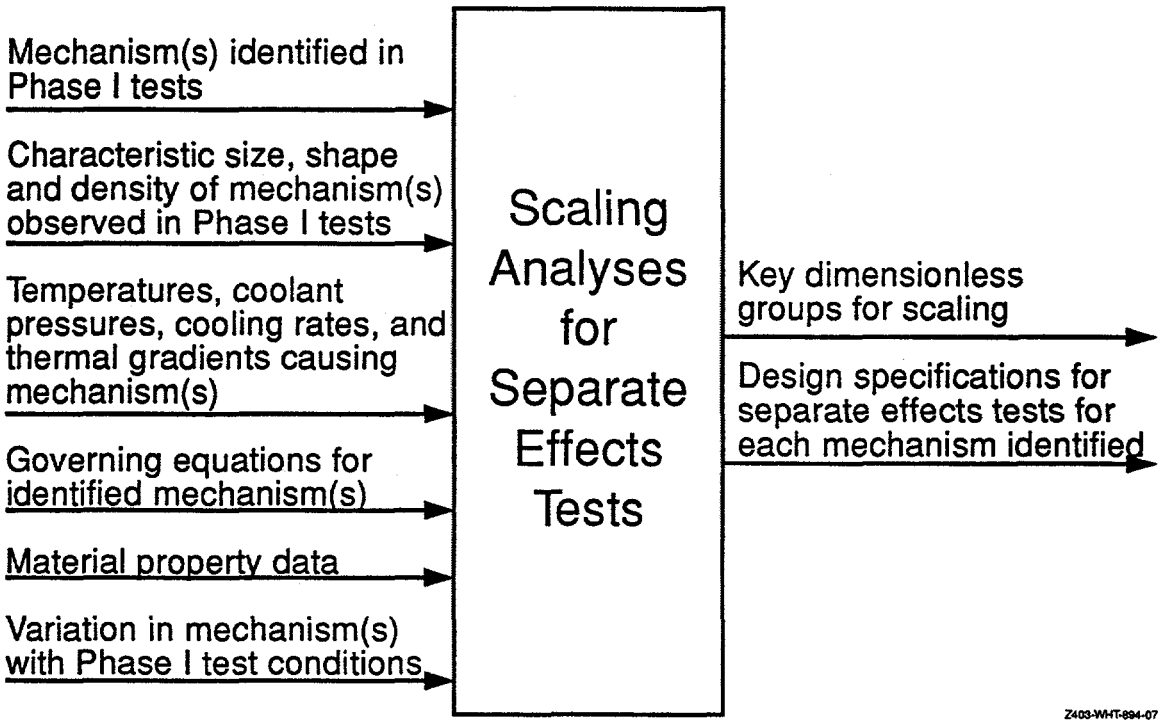

Figure 18. Flow diagram for separate effects tests.

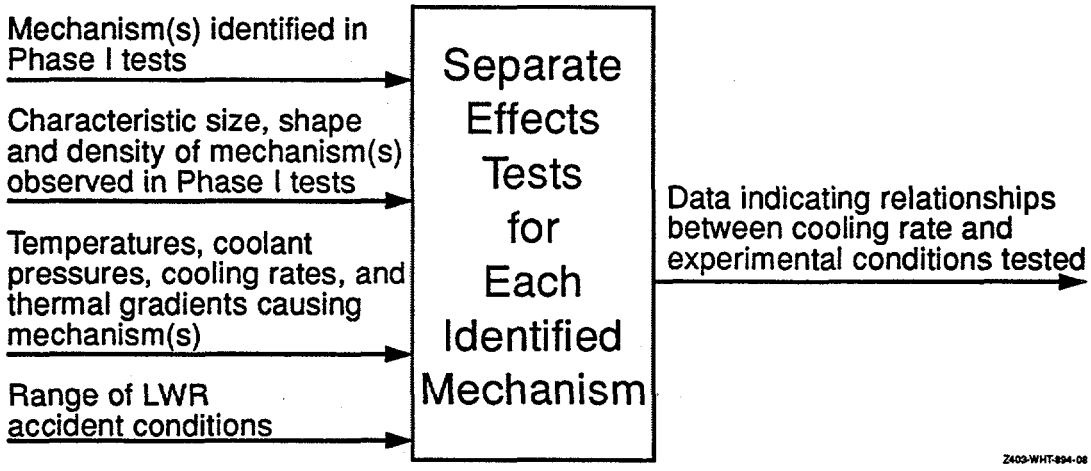

Figure 19. Flow diagram for developing models using data from separate effects tests

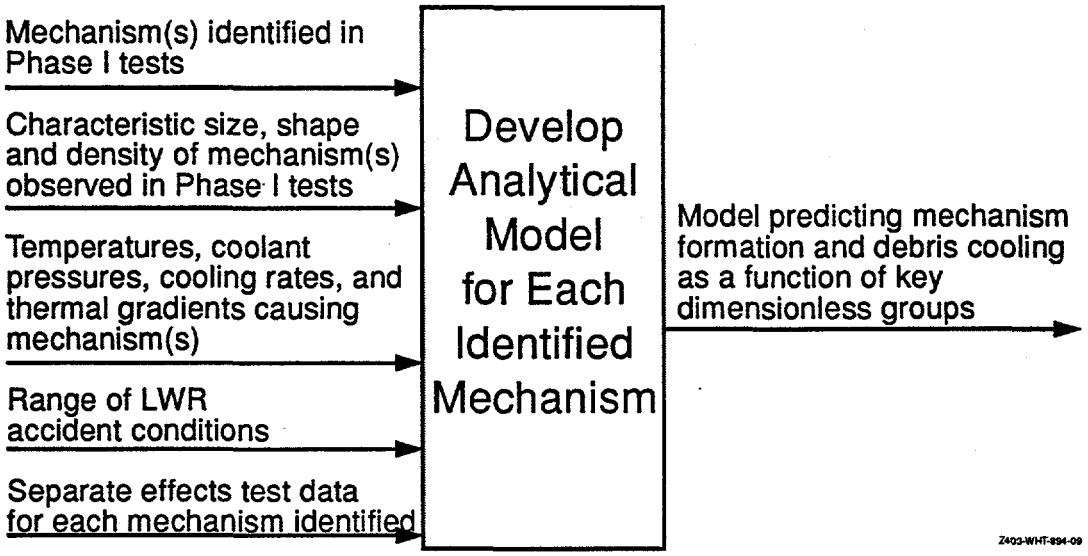

Figure 20. Flow diagram for evaluating mechanism interactions

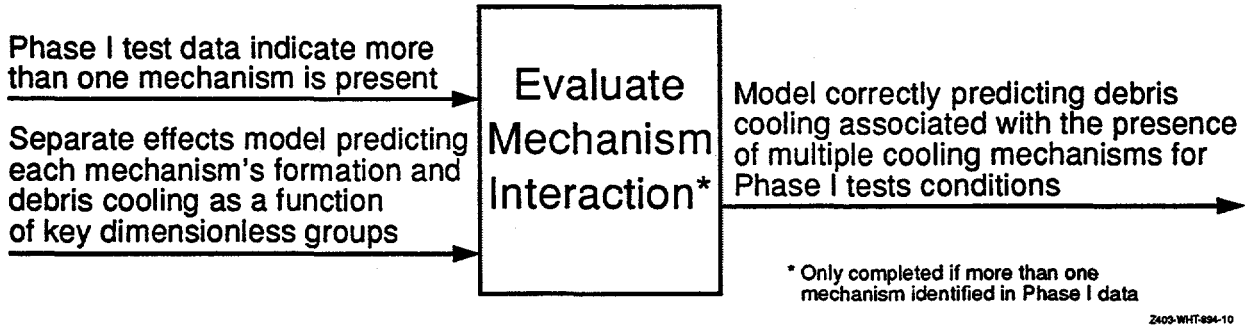

To illustrate the procedure that would be used to develop a model with separate effects test data, consider a case in which Phase I integral test data indicate that cracks form in the debris and that significant cooling occurs because of coolant traveling through these cracks. For this case, the general procedure illustrated in Figure 21 would be completed. This procedure is more complicated than that envisioned for other postulated mechanisms because separate effects tests are required to obtain data for crack growth and for crack cooling.

Figure 21. Example illustrating tasks required for separate effects testing and model development if cracking is identified in Phase I tests

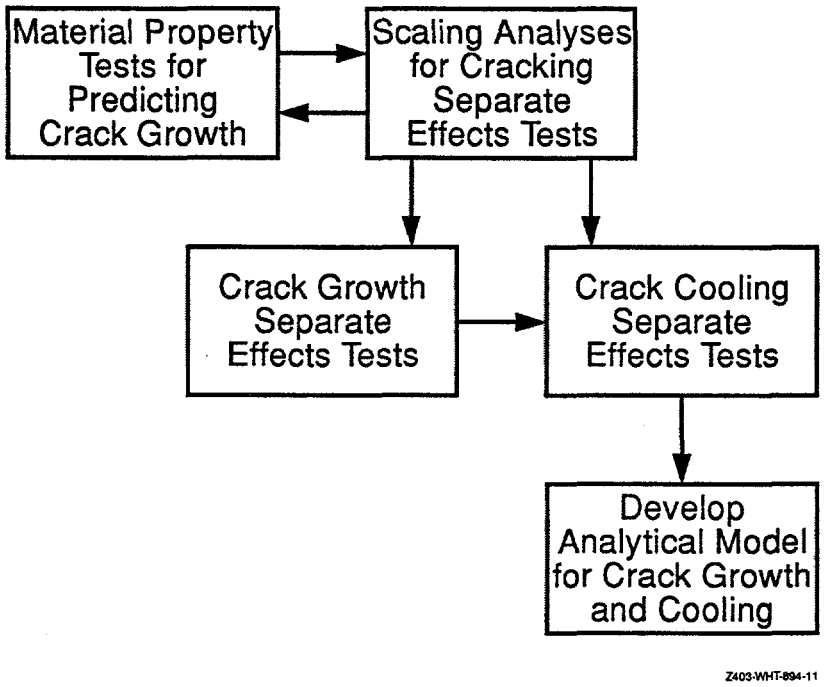

Specific input and output from each of the tasks shown in Figure 21 are shown in Figures 22 through 26. As indicated in these figures, material property data are needed to develop models for predicting crack growth and cooling. Although many of these properties can be obtained from the literature, preliminary review indicates that structural data are inadequate to predict crack growth for debris compositions similar to the TMI-2 debris. This data will be used in analyses to determine key scaling parameters to predict crack growth and cooling for the range of conditions expected during LWR accident conditions. Results from these calculations will be used to select design parameters for separate effect tests. Separate effect test data will be sufficient to develop models for predicting crack growth and cooling. For example, the model will be able to predict heat losses associated with a crack in the debris as a function of dimensionless groups, such as Rayleigh and Prandtl number.

Figure 22. Flow diagram for obtaining material properties for predicting crack growth

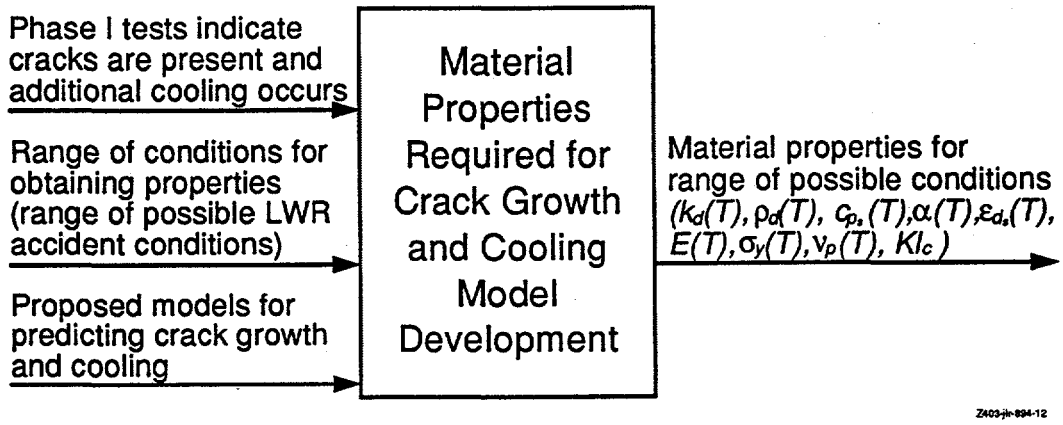

Figure 23. Flow diagram for performing scaling analyses for predicting crack growth and cooling

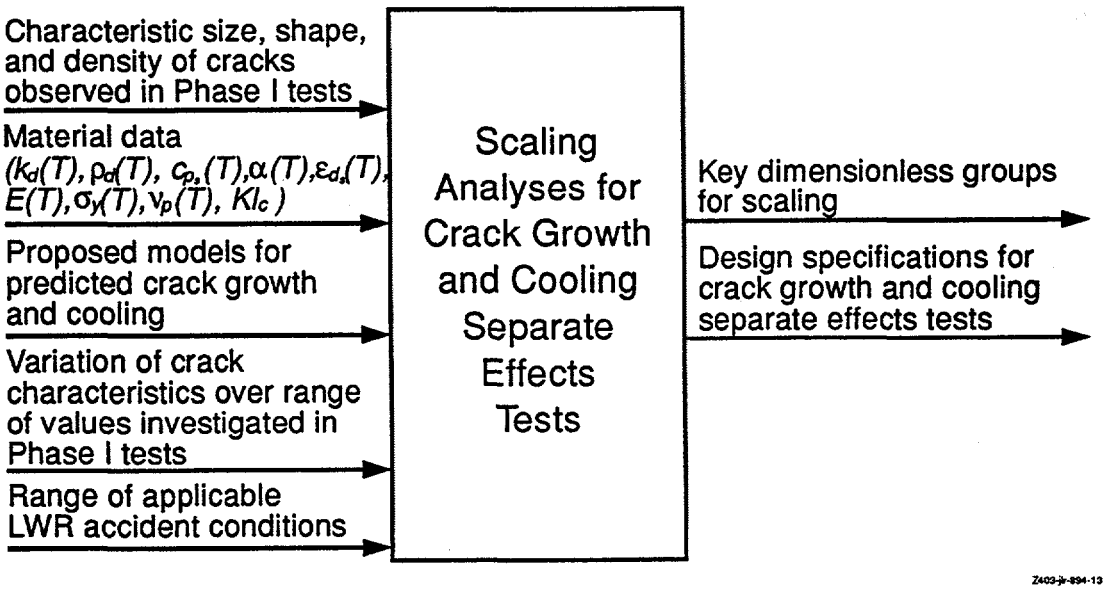

Figure 24. Flow diagram for performing crack growth separate effects tests

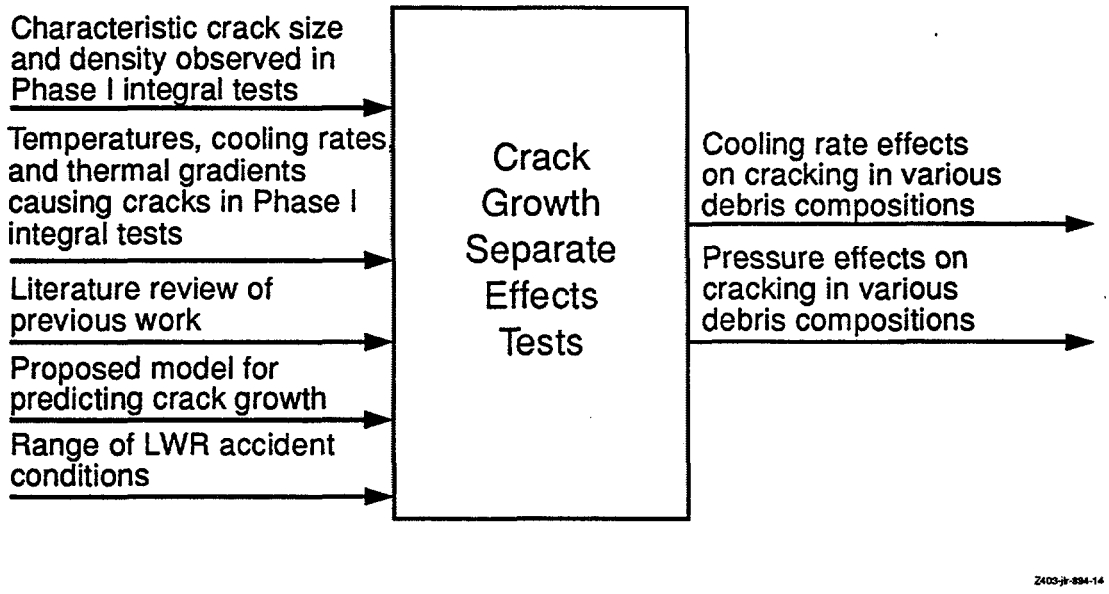

Figure 25. Separate effects tests flow diagram for investigating crack cooling.

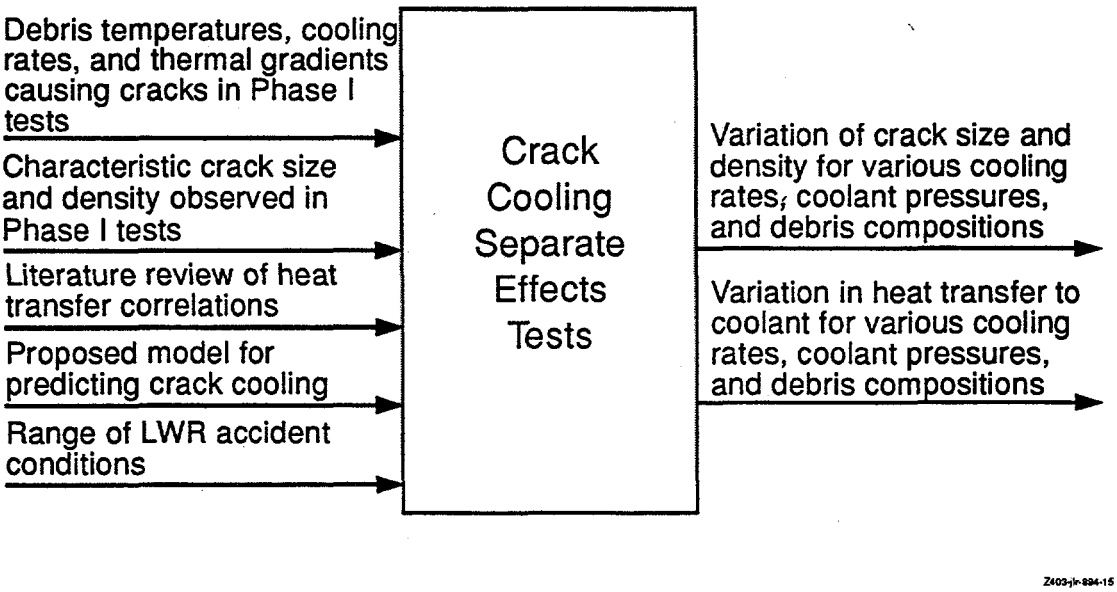

Figure 26. Flow diagram for developing model to predict crack growth and cooling.

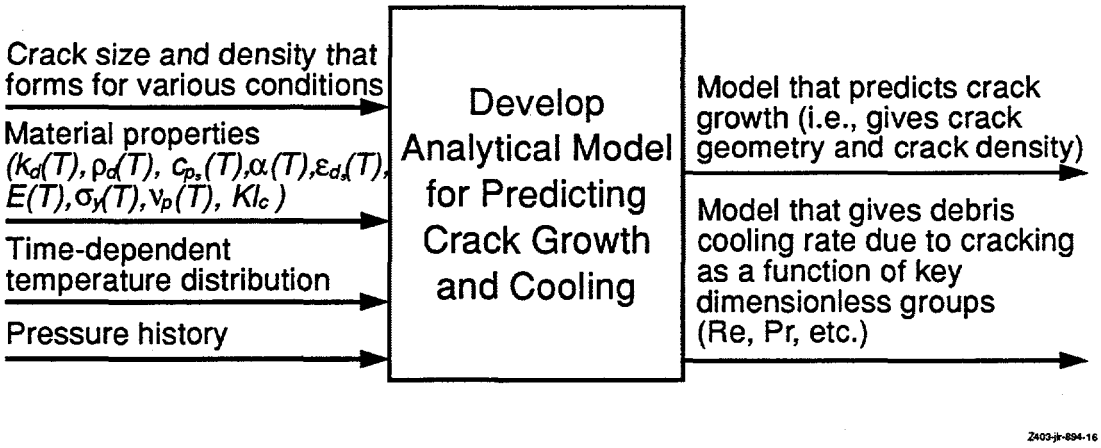

3.5 Steps for Completing Phase II Tests and Model Validation

The last element in this program is to perform larger scale, Phase II integral tests and validate the debris cooling model. Figures 27 through 29 illustrate the relationship between tasks required for this element of this program. As illustrated in Figure 27, newly-developed models for predicting debris cooling will be used to define conditions for the Phase II tests. Scoping analyses results reported in Section 4 suggest that the Phase II integral tests will be much larger in scale and constructed so that a range of pressures (both low and high pressures), quench rates, and coolant temperatures will be evaluated. As illustrated in Figure 29, results from these final tests will be compared with model predictions to obtain a validated model that predicts debris cooling.

Figure 27. Flow diagram for Phase II integral test scaling analyses.

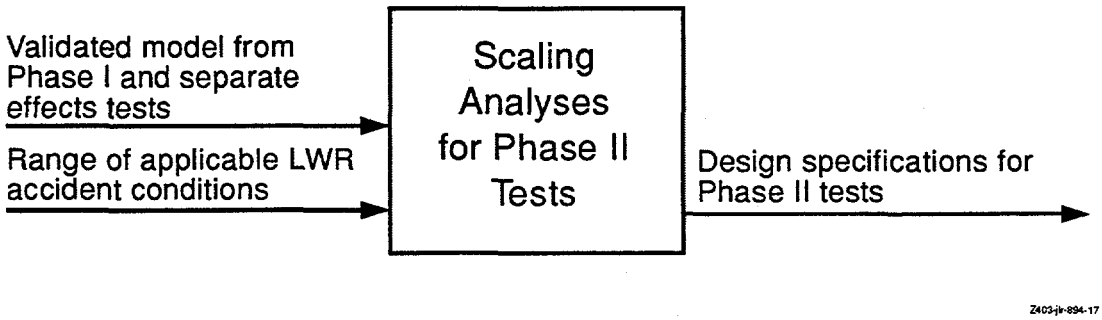

Figure 28. Phase II Integral Tests flow diagram

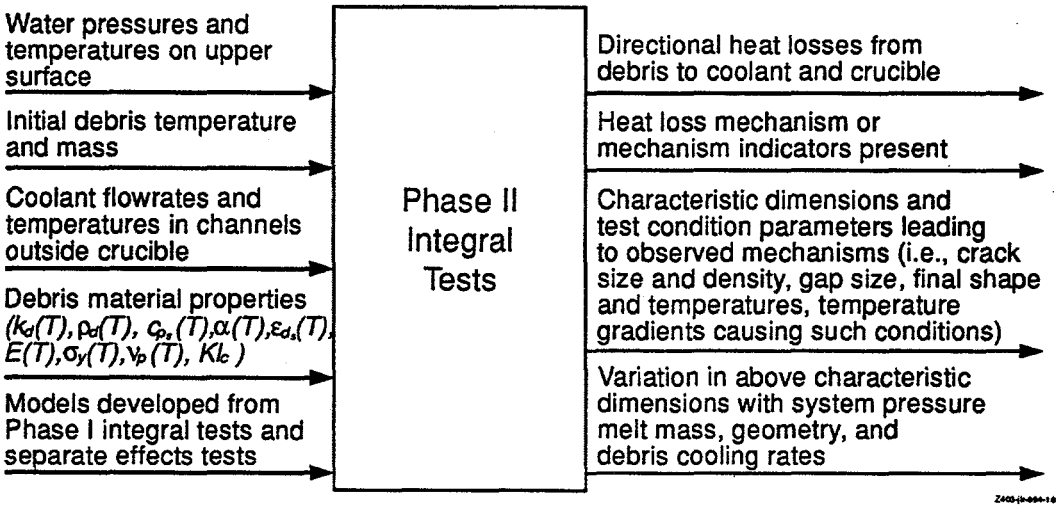

Figure 29. Flow diagram for validating model using Phase II data

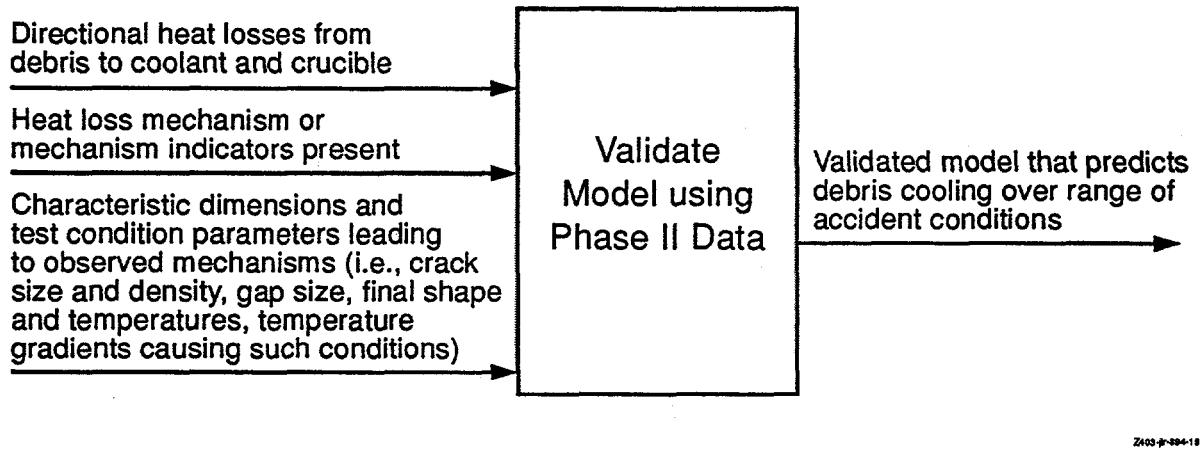

4. Initial Scoping Analyses

If the mechanism(s) responsible for debris cooling were known, scaling analyses should be performed to select test facility design parameters. In previous sections of this document, several possible enhanced cooling mechanisms are hypothesized. It is not known which of these mechanisms (if any) is active, and analyses reported in this section indicate that the different mechanisms yield different stress and thermal relationships. Thus, exploratory tests (Phase I tests) are proposed to identify the mechanisms responsible for debris cooling. Fortunately, thermal-hydraulic conditions of the coolant, and in some cases, the temperature history of the vessel are often well-quantified for the TMI-2 accident conditions. Thus, scoping calculations were performed

using thermal-hydraulic data from the TMI-2 accident to gain insights about conditions that would allow the test debris to experience thermal conditions equivalent to the TMI-2 thermal conditions. Results from these scoping calculations are reported in Section 4.1. Scoping calculations investigating the stress conditions experienced by the debris are discussed in Section 4.2. Calculations were also performed to assess chemical reactions that may occur in the proposed tests. Results from these calculations are reported in Section 4.3. Section 4.4 summarizes results from these scoping calculations and recommendations for the Phase I tests.

4.1 Scoping Analyses for Simulating Thermal Conditions

Analyses were performed to quantify various thermal conditions that resulted in the enhanced debris cooling rates inferred from TMI-2 data. Analyses considered three different control volumes: the RCS vessel, the debris that relocated onto the vessel lower head, and the crust that formed on the upper surface of the relocated debris. For each type of analysis, scoping calculations were performed to obtain order of magnitude estimates for parameters in the governing equations. Results from these scoping calculations indicate the relative importance of several factors affecting debris cooling during a severe accident. By identifying what parameters play a significant role in debris coolability, scaling relationships and test facility design simplifications could be suggested.

Based on these analyses, several key parameters were deemed important for designing a test facility: debris cooling rates, upward heat fluxes, directional heat flux ratio, debris height to test facility ratio, debris upper surface radius to test facility ratio, initial crust growth rate, and crust initial temperature gradients. Values for these parameters are quantified in this section.

4.1.1 Analyses Input from TMI-2 Data

All of the thermal analyses require input parameters based on data measured during the TMI-2 accident or obtained from subsequent examinations of material removed from the TMI-2 vessel. Because many of these parameters are used in several of these analyses, all of the model inputs are discussed in this section. Figure 30 summarizes various instrumentation data available from the TMI-2 accident that were used to quantify many of the input parameters for these calculations. There is considerable uncertainty associated with some of these input parameters. Upper and lower bound estimates for inputs are provided below to indicate the magnitude of uncertainty associated with each input. These upper and lower bound estimates were used in sensitivity calculations for the analyses reported in this section.

Time until Debris Cooled

As discussed in Reference 1, analyses performed in the TMI-2 Vessel Investigation Project suggest that the vessel cooled prior to the time that it was repressurized or vessel failure would have occurred. Hence, an upper bound for the time period for debris cooling is the repressurization time, approximately 320 minutes after reactor trip (see Figure 30). Examination of steel samples removed from the TMI-2 vessel suggest that peak temperatures were sustained for approximately 30 minutes. This 30 minute time period after melt relocation was used as a lower bound time period for debris cooling (i.e., as a lower bound, it was assumed that the debris cooled at 250 minutes after reactor trip).

Figure 30. Various instrumentation data during the TMI-2 accident

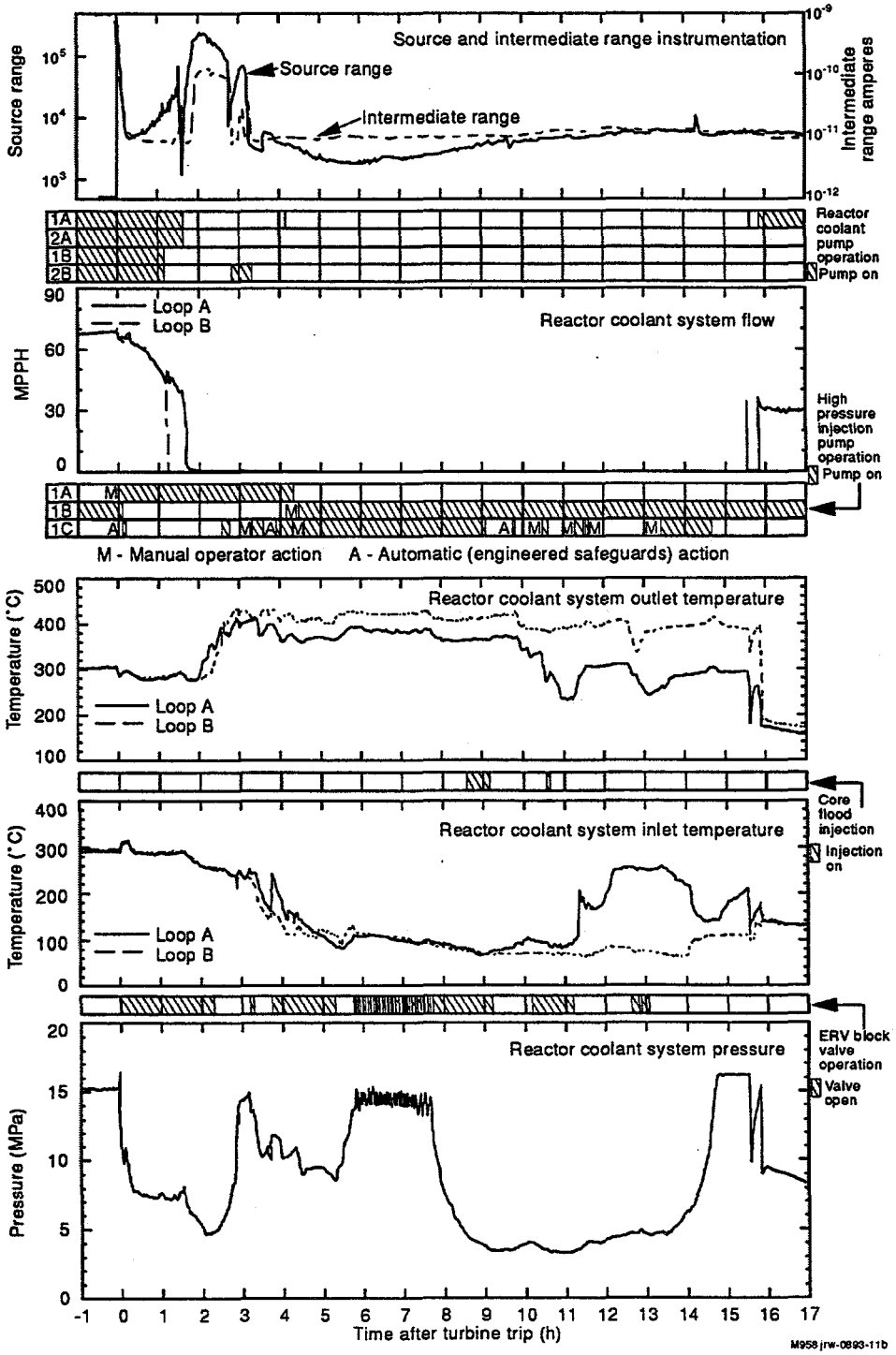

Coolant Entering the Vessel

During the time period of interest, coolant entered the Reactor Coolant System (RCS) via the high pressure injection (HPI) and the makeup system. Makeup coolant is provided to the RCS through the reactor coolant pump seals and via the normal makeup line. During an accident in which the RCS pressure drops below 11.4 MPa or the reactor building pressure exceeds 0.2 MPa, high pressure water is injected from the borated water storage tank into the RCS via the HPI pumps. Although makeup and HPI flow rates were not recorded during the accident, Anderson [38] estimated these flow rates based on knowledge of the HPI system and analyses of the accident's progression. Recommended makeup and HPI flow rates are plotted in Figure 31. Anderson acknowledges that there is considerable uncertainty in makeup and HPI flow rate estimates, and suggests that uncertainties may cause flowrates to vary by ±25%.[38]

Figure 31. Combined high pressure injection and makeup flow into the RCS

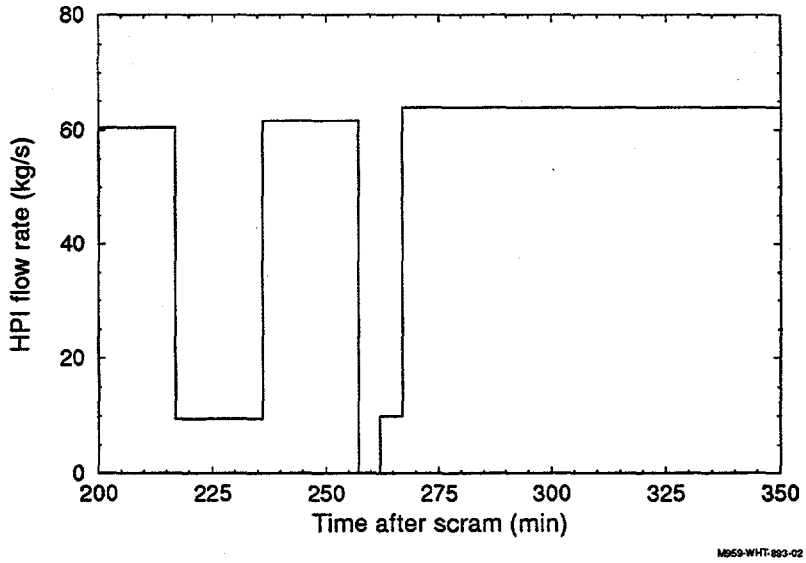

Coolant Exiting the Vessel

During the time period of interest, coolant exited the system via the normal coolant letdown system and via the pilot operated relief valve (PORV), which failed in a stuck-open position. Although neither of these flow rates were measured during the transient, data for other plant parameters were used to estimate these flow rates.

RCS pump seal flow entering the RCS necessitates a continuous letdown flow of reactor coolant to maintain the desired coolant inventory balance. Letdown flow is also required for removal of impurities and boric acid from the reactor coolant. The letdown mass flow rate was estimated by performing an energy balance on the letdown coolers using the measured A-loop cold leg temperature as the primary side inlet temperature. The resulting flow rate is plotted in Figure 32. Sensitivity studies indicate that the uncertainty in the letdown flow is ±1.2 kg/s.

Figure 32. Letdown flow rate of coolant.

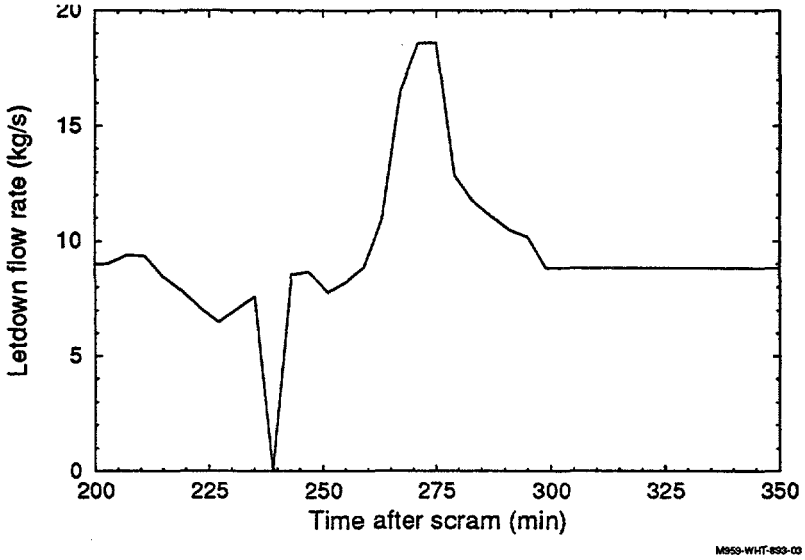

The pressurizer PORV in TMI-2 opened at its setpoint of 15.6 MPa a few seconds after initiation of the accident and failed in the stuck-open position. After the PORV opened, flow through the PORV depended on the status of the block valve situated upstream of the PORV. Although the flow rate out the PORV was not measured, it has been estimated based on knowledge of measured plant parameters, such as the RCS pressure history, the status of the block valve (which is situated upstream of the PORV), and the pressurizer liquid level. Kuan and Tolman calculated the discharge flow out the PORV assuming that the flow rate is proportional to the square root of the primary system pressure. For the time period of interest, they assumed that the system was filled with saturated liquid and estimated the void fraction of the steam exiting through the PORV. Nomura estimated the PORV flow rate using the homogenous equilibrium critical flow model for higher qualities (i.e., $0.02 < x \leq 1$), the Henry-Fauske model for saturated liquid (i.e., $x = 0$), and a curve fit between the two models at low quality ($0 < x < 0.02$). The quality out the PORV orifice was based on the measured pressurizer liquid level and the Wilson bubble rise model. Figure 33 compares the flow rates estimated by Nomura and Kuan. For most of the time period of interest (220 to 320 minutes after reactor scram), the Nomura estimates are higher than the Kuan estimates. Both Kuan and Nomura estimate that their calculated PORV flow rates have an uncertainty of ±20%.

RCS Thermal Properties

RCS thermal properties, such as internal energy, were obtained from Keenan, based on the system pressure and coolant temperature measurements for the time period of interest. The system pressure history, shown in Figure 30, is a composite pressure curve that was based on several sources of plant data. The maximum calculated uncertainty for points on this composite pressure curve is estimated to be ±0.2 MPa. No plant data are available to quantify the quality of the coolant in the system at either 220 or 320 minutes. Therefore, a large range of possible initial and final coolant qualities is considered in analyses reported in this section.

Figure 33. Pilot-operated relief valve flow rate.

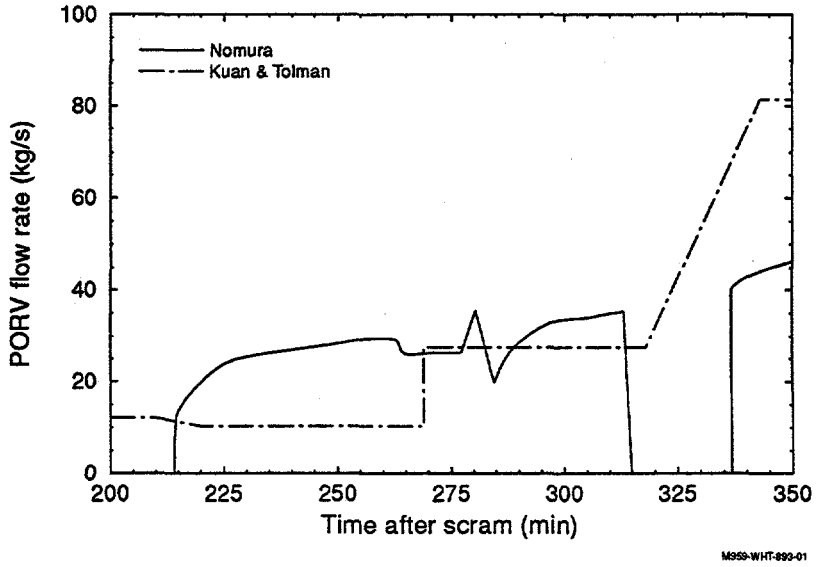

Debris Decay Heat

The decay power in the debris is related to the amount of fission products retained in the core material. During the TMI-2 accident, significant release of volatile fission products occurred. For example, in the lower plenum, it is estimated that only 3% of the iodine and 13% of the cesium were retained.[44] The reductions in total core decay power as a result of volatile fission product release for the TMI-2 fuel inventory were estimated by Schnitzler.[45] For the time periods of interest, results indicate that the decay power can be reduced by as much as 40%. Using a decay power curve, the power of the TMI-2 core at 224 minutes was estimated as approximately 25 MWt. However, if the reduction resulting from volatile fission product release is included, this number can be as low as 18 MWt. Sensitivity studies were performed to assess the impact of debris decay heat in each of the analyses performed.

Results from examinations of the hard layer of material found next to the vessel lower head, the "companion samples" were used to quantify the volumetric heat generation rate associated with decay heat for this material.[46] These examinations indicated that the nominal heat generation rate for this material was 1.0 MW/m^3 with an uncertainty of ±20%.

RCS Coolant Volume

References indicate that the volume of coolant in the RCS, including the pressurizer volume, is between 327 and 334 m^3.[37,47]

Vessel Heat Losses

Heat is transferred from the vessel via natural convection and radiation. As discussed in Reference 47, previous analyses indicate that this heat transfer coefficient may range from 1 to 100 W/m^2K. The value for this coefficient is dependent on parameters such as vessel and containment temperatures, which vary during the transient.

Melt Composition and Peak Temperature

Analyses of samples removed from the TMI-2 vessel suggest that the debris removed from the hard layer of material found on the lower head was 78 wt% UO_2 and 17 wt% ZrO_2. The remaining 5% consisted primarily of stainless steel and Inconel that were probably melted during relocation. Examinations indicate that the peak melt temperature ranged from 0 to 250 K above its liquidus temperature of 2873 K at the time of relocation.

Debris Mass and Volume

At the time that the accident occurred in the TMI-2 reactor, there was approximately 93,000 kg of UO_2 and 19,100 kg of ZrO_2 in the reactor vessel. Information in Reference 1 suggests that the mass of hard layer of $(U,Zr)O_2$ material found next to the TMI-2 vessel weighed approximately 10,000 kg. Density data (see Reference 14) and geometrical relationships were then used to estimate that the debris volume was approximately 1.2 m^3, the average height was 0.42 m, and the debris upper surface area radius was 1.3 m.

4.1.2 Analysis of Debris and Coolant in TMI-2 Vessel

In this analysis, volume, mass, and energy conservation equations were applied to debris and coolant in the TMI-2 vessel to determine the change in debris internal energy and associated debris cooling rate between the time when a major relocation of debris occurred in the TMI-2 vessel (220 minutes after reactor trip) and the time when evidence suggest that the debris experienced additional cooling beyond that considered in severe accident models (see Section 1.1). Figure 34 illustrates the control volume assumed for applying these conservation equations to the TMI-2 vessel. Results from this analysis demonstrate that the debris experienced significant cooling during the time period of interest. Although useful for estimating upper and lower bounds for debris cooling rates, this method was not used to derive specific test design parameters because uncertainties in key parameters were too large.

Figure 34. Control volume for calculations to estimate debris cooling rate

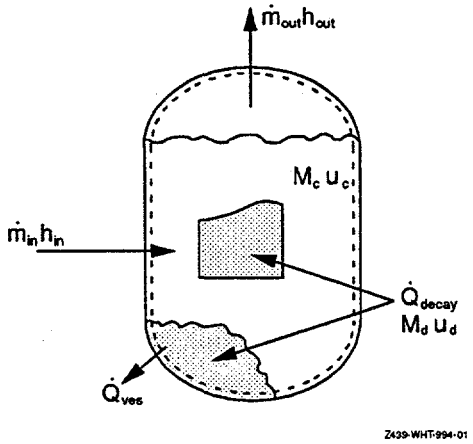

Conservation of volume in the vessel at the beginning and end states (designated by the subscripts, 1 and 2, respectively) yields

$$V_{coolant} = M_{c1}[(1-x_1)\nu_{l1} + x_1\nu_{g1}] \tag{11}$$

$$V_{coolant} = M_{c2}[(1-x_2)\nu_{l2} + x_2\nu_{g2}] \tag{12}$$

where

$V_{coolant}$	=	Reactor coolant system volume (m^3)
M_c	=	Coolant mass in the RCS (kg)
x	=	RCS quality
ν_l	=	Saturated liquid specific volume (m^3/kg)
ν_g	=	Saturated vapor specific volume (m^3/kg)

Conservation of mass in the vessel yields

$$M_{c1} + \int_1^2 \sum \dot{m}_{in}\,dt = M_{c2} + \int_1^2 \sum \dot{m}_{out}\,dt \tag{13}$$

where

$\dot{m}_{in}$	=	mass flow rate of coolant entering the vessel (kg/s)
$\dot{m}_{out}$	=	mass flow rate of coolant exiting the vessel (kg/s)

Sources of coolant entering the vessel during this time period include normal RCS makeup and high pressure injection from the emergency core cooling system. Sources of coolant exiting the vessel during this time period include normal RCS letdown and coolant flowing out the open PORV.

Finally, conservation of energy in the vessel was applied:

$$\int_1^2 \dot{m}_{in}h_{in}\,dt + M_{c1}[(1-x_1)u_{l1} + x_1u_{g1}] + \int_1^2 \dot{Q}_{decay}\,dt + M_{dtot}u_{d1}$$
$$= M_{c2}[(1-x_2)u_{l2} + x_2u_{g2}] + \int_1^2 \dot{m}_{out}h_{out}\,dt + M_{dtot}u_{d2} + \int_1^2 \dot{Q}_{ves}\,dt \tag{14}$$

where

$\dot{Q}_{decay}$	=	debris decay heat (W)
$\dot{Q}_{ves}$	=	vessel heat losses (W)
M_{dtot}	=	total debris mass in the vessel (kg)
h_{in}	=	enthalpy of coolant entering the vessel (J/kg)
h_{out}	=	enthalpy of coolant exiting the vessel (J/kg)
u_d	=	debris internal energy (J/kg)
u_l	=	liquid coolant internal energy (J/kg)
u_g	=	vapor coolant internal energy (J/kg)

The above energy equation is applied during the time period after relocation. Hence, energy from zircaloy oxidation is neglected because most oxidation is predicted to occur during earlier stages of the transient. The main RCS pumps did not run during this time period; thus, the primary source of heat loss from the system is associated with mass exiting the system. Any additional heat transferred to upper plenum structures in the vessel via natural circulation was neglected.

The above equations were solved to obtain the change in debris internal energy, $M_{dtot}(u_{d2} - u_{d1})$, as a function of other parameters in the system. Upper and lower bound estimates for various input parameters were evaluated, and results are summarized in Table 4. Because of simplifying assumptions used in these calculations, values in this table should only be viewed as order-of-magnitude estimates.

Results in Table 4 are useful for understanding the relative impact of input parameter uncertainties on the heat loss from the debris. Both upper and lower bounds for inputs were considered in these sensitivity studies. The most variation in cooling rate predictions is observed for cases in which the heat loss parameters from the vessel to the containment are varied (Cases 10 and 11). For example, debris cooling rate estimates are reduced to 6 K/s if it assumed that the vessel has a nearly adiabatic outer surface and cooling rates may increase to 110 K/s if high heat transfer rates are assumed for the vessel outer surface. Little variation is seen for the other sensitivities investigated.

The magnitudes for debris energy losses in Table 4 are greater than 10^5 MJ for all the cases evaluated, suggesting that significant debris cooling occurred during the time periods considered. Two possible debris cooling rates are shown in the lower two rows of Table 4. Possible maximum cooling rates in Table 4 were calculated assuming that only the melt that relocates to the lower head cools. Possible minimum cooling rates were calculated assuming that all of the UO_2 and ZrO_2 in the vessel cools. Results from both the maximum and minimum cooling rate calculations indicate that the predicted debris energy loss rates are sufficient to solidify the debris and cool it at rates that range from 6 to 110 K/s (assuming only 10,000 kg of debris cools) or from 0.4 to 9.8 K/s (assuming that 112,000 kg of debris cools). Because the mass of debris experiencing this cooling during the first 30 to 100 minutes after relocation is not well known, this analysis was not directly used to specify Phase I test design parameters. However, the cooling rates predicted from this analyses provides insight into subsequent analyses from which test design parameters were derived.

Table 4: TMI-2 Energy balance results

	Base Case	Coolant Volume		Coolant Inlet Flowrate		Coolant Exit Flowrate	
	1	2	3	4	5	6	7
Decay Heat, MW	Base (20)	Base	Base	Base	Base	Base	Base
Energy added, MJ	1.2×10^5	1.2×10^5	1.2×10^5	1.2×10^5	1.2×10^5	1.2×10^5	1.2×10^5
Coolant Volume, m^3	Base	327	334	Base	Base	Base	Base
Coolant entering	Base	Base	Base	25% reduced	25% increased	Base	Base
Energy added by coolant entering, MJ	5.3×10^4	5.3×10^4	5.3×10^4	4.0×10^4	6.7×10^4	5.3×10^4	5.3×10^4
Coolant exiting	Base	Base	Base	Base	Base	20% reduced	20% increased
Energy lost by coolant exiting, J	2.2×10^5	2.2×10^5	2.2×10^5	2.2×10^5	2.2×10^5	1.7×10^5	2.6×10^5
Vessel losses	Median	Median	Median	Median	Median	Median	Median
Energy removed, MJ	1.4×10^6	1.4×10^6	1.4×10^6	1.4×10^6	1.4×10^6	1.4×10^6	1.4×10^6
Initial quality	0.10	0.10	0.10	0.02	0.48	0.18	0.06
End quality	0.00	0.00	0.00	0.00	0.00	0.00	0.00
Debris cooling time, min.	100	100	100	100	100	100	100
Total heat in, MJ	1.7×10^5	1.7×10^5	1.7×10^5	1.6×10^5	1.9×10^5	1.7×10^5	1.7×10^5
Total heat out, MJ	1.6×10^6	1.6×10^6	1.6×10^6	1.6×10^6	1.6×10^6	1.6×10^6	1.6×10^6
Debris energy loss, MJ	1.6×10^6	1.6×10^6	1.6×10^6	1.5×10^6	1.7×10^6	1.6×10^6	1.6×10^6
Max. debris cooling, K/s[a]	45	45	45	42	47	45	45
Min. debris cooling, K/s[b]	3.9	3.9	3.9	3.6	4.1	3.9	3.9

a. Values estimated assuming that only the hard layer of debris that relocated to the lower head cools.
b. Values estimated assuming that all UO_2 and ZrO_2 in the fuel (93,000 kg UO_2 and 19,000 kg ZrO_2) undergoes equal cooling.

Table 8: TMI-2 energy balance results (continued)

	Decay Heat		Vessel Heat Losses		Final Coolant Quality	Cooling Time
	8	9	10	11	12	13
Decay heat, MW	25	18	Base	Base	Base	Base
Energy added, MJ	1.5×10^5	1.1×10^5	1.2×10^5	1.2×10^5	1.2×10^5	3.6×10^4
Coolant volume, m^3	Base	Base	Base	Base	Base	Base
Coolant entering	Base	Base	Base	Base	Base	Base
Energy added by coolant entering, MJ	5.3×10^4	5.3×10^4	5.3×10^4	5.3×10^4	5.3×10^4	1.1×10^4
Coolant exiting	Base	Base	Base	Base	Base	Base
Energy lost by coolant exiting, MJ	2.2×10^5	2.2×10^5	2.2×10^5	2.2×10^5	2.2×10^5	5.5×10^4
Vessel losses	Median	Median	Low	High	Median	Median
Energy removed, MJ	1.4×10^6	1.4×10^6	2.0×10^4	3.8×10^6	1.4×10^6	4.2×10^5
Initial quality	0.10	0.10	0.10	0.10	0.69	0.02
End quality	0.00	0.00	0.00	0.00	0.04	0.00
Debris cooling time, min.	100	100	100	100	100	30
Total heat in, MJ	2.0×10^5	1.6×10^5	1.7×10^5	1.7×10^5	1.7×10^5	4.7×10^4
Total heat out, MJ	1.6×10^6	1.6×10^6	2.4×10^5	4.0×10^6	1.6×10^6	4.8×10^5
Debris energy loss, MJ	1.6×10^6	1.6×10^6	2.1×10^5	4.0×10^6	1.6×10^6	4.7×10^5
Max. debris cooling, K/s[a]	44	45	6	110	44	44
Min. debris cooling, K/s[b]	3.9	3.9	0.4	9.8	3.9	3.9

a. Values estimated assuming that only the hard layer of debris that relocated to the lower head cools.
b. Values estimated assuming that all UO_2 and ZrO_2 in the fuel (93,000 kg UO_2 and 19,000 kg ZrO_2) undergoes equal cooling.

4.1.3 Heat Fluxes, Heat Flux Ratios, and Geometry

In this analysis, an energy conservation equation is applied to the material that relocated to form the hard layer of debris found next to the TMI-2 vessel lower head. Using the simplified geometries of the debris in the TMI-2 vessel and the test facility quench crucible shown in Figure 35, calculations were performed to estimate directional heat losses from the melt. Results are used to gain insights for the Phase I tests initial values for directional heat losses ratios, melt superheats, heat fluxes, and geometrical ratios. A relationship between the scaled debris masses and heat fluxes is also developed from this analysis.

Applying conservation of energy to the TMI-2 debris yields the following relationship

$$M_d \int_1^2 du_d = \int_1^2 (\dot{Q}_{decay} - q''_b A_b - q''_u A_u)\, dt \qquad (15)$$

where state 1 refers to the time that a major relocation of melt occurred in the accident, state 2 refers to a time period when significant debris cooling has occurred,

q'' = heat flux from the debris, W/m^2

A = surface area, m^2

M_d = mass of molten relocated debris, kg

and, the subscripts, u and b, refer to upward and downward directions.

Figure 35. Control volumes assumed for heat flux analyses.

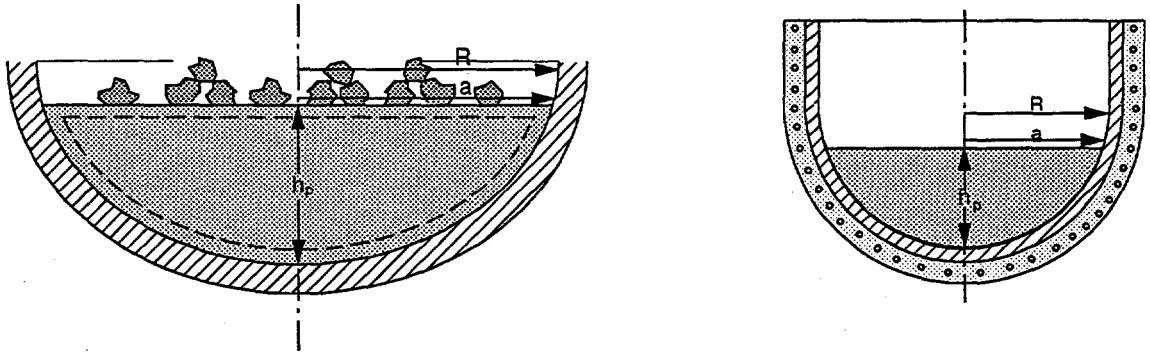

For initial time periods after melt relocation during the TMI-2 accident, the heat fluxes from the melt are estimated using transient natural convection heat transfer correlations. Because heat losses from convection are higher than those possible from conduction through a solid mass, these heat flux estimates also bound maximum heat losses possible via conduction. The following transient natural convection heat transfer correlations, which were obtained from the COPO tests, were applied to predict natural convection heat transfer coefficients[48,49]

$$\overline{Nu_u} = \frac{h_u R}{k_{d_m}} = 0.25 Ra'^{0.3038} \qquad (16)$$

$$\overline{Nu}_b = \frac{h_b R}{k_{d_m}} = 472 \left(\frac{h}{R}\right)^{0.3171} Ra'^{0.2195} \quad (17)$$

where the vessel radius, R, and pool height, h, are illustrated in Figure 35, the transient Rayleigh number, Ra', is given by

$$Ra' = \frac{g\beta_d R^3 \Delta T_m}{\alpha_d \nu_d} \quad (18)$$

and g = acceleration due to gravity (9.8 m/s^2)

β_d = debris volumetric coefficient of thermal expansion (K^{-1})

α_d = debris thermal diffusivity (m^2/s)

ν_d = debris kinematic viscosity (m^2/s)

k_{d_m} = debris thermal conductivity (W/mK)

ΔT_m = difference between peak melt temperature and average crust temperature (K)

h_u = convective heat transfer coefficient for pool losses on the top surface (W/m^{2}K)

h_b = convective heat transfer coefficient for pool losses on the bottom surface (W/m^{2}K)

Debris material properties and vessel geometrical parameters for these preliminary calculations were based on data in References 14 and 50. Data used to quantify other inputs to these equations are discussed in Section 4.1.1. Note that the heat transfer coefficient for upward heat losses is primarily dependent on pool superheat, ΔT_m, and pool thermal properties and is nearly independent of pool size; whereas the heat transfer coefficient for downward heat losses is dependent on pool superheat, pool thermal properties, and pool size ($R^{-0.6586}$).

The above relationships were used to estimate heat fluxes possible from the debris at the time of relocation. Results are summarized in Table 5 for cases assuming pool superheats of 100 and 250 K above the melt liquidus. Values in Table 5 are typically lower than debris cooling rates inferred from the analyses based on TMI-2 plant data in Section 4.1.2. Thus, results from these calculations indicate that some mechanism, beyond that possible via convection from the melt, led to higher heat losses from the debris during the TMI-2 accident. For example, cracking in crusts that form on the upper surface of the debris will increase surface area in contact with RCS water and associated heat losses.

Table 5 also contains ratios indicating the relative magnitudes of the heat input associated with decay heat, the heat losses upward, and the heat losses downward. It is recognized that these calculations underestimated heat losses from the debris for time periods after enhanced cooling mechanisms, such as cracking, occur. However, heat loss estimates should be valid for initial time periods, prior to the occurrence of any phenomena that enhance the contact area between the debris and the coolant. For these time periods, estimated upward heat losses are approximately a factor of 10 greater than the estimated downward heat losses.

Preliminary evaluation indicates that experiments will be considerably simpler if they can be performed without simulating debris decay heat. Values in Table 5 indicate heat loss magni-

tudes are between approximately 2 to 6 times as large as the decay heat in the melt. Subsequent calculations indicate that the heat input associated with decay heat becomes less than 25% of the heat losses if the melt is initially superheated by 185 K. Hence, results from this analysis suggest that decay heat effects can be neglected in the integral tests if the melt temperature is superheated more than 185 K above its liquidus.

Table 5: TMI-2 heat flux analysis results

Parameter	100 K Pool Superheat	250 K Pool Superheat
Ra'	3.2×10^{12}	7.9×10^{12}
Nu_u	1570	2070
Nu_b	155	190
q''_u, MW/m^2	0.36	1.1
q''_b, MW/m^2	0.035	0.11
q''_b/q''_u	0.099	0.092
Decay energy to total heat loss ratio	0.53	0.16
Downward to upward heat loss ratio	0.11	0.10
Debris cooling rate, K/s	0.2	1.0

When Equation (15) is applied to the integral tests, there will be no debris decay heat. Hence, this equation becomes

$$M_d \int_1^2 du_d = \int_1^2 (-q''_b A_b - q''_u A_u)\, dt \tag{19}$$

As discussed above, results for the TMI-2 analyses suggest that decay heat can be omitted from tests without significantly impacting test results if tests are performed with the melt superheated to at least 185 K above the melt liquidus temperature.

The term in Equation (19) corresponding to the change in debris internal energy can be simplified by recognizing that the latent heat of fusion, L_{f_d}, is constant and that the change in debris specific heat, c_{p_d}, is much smaller than the change in debris temperature, T_d, as shown below

$$M_d \int_1^2 du_d = M_d d(c_{p_d} T_d + L_{f_d}) \approx M_d c_{p_d} dT_d \tag{20}$$

Comparing the relationships obtained from Equations (15), (19), and (20)

$$\frac{M_d c_{p_d} \left.\frac{dT_d}{dt}\right|_{exp}}{M_d c_{p_d} \left.\frac{dT_d}{dt}\right|_{TMI}} = \frac{(-q''_b A_b - q''_u A_u)|_{exp}}{(-q''_b A_b - q''_u A_u)|_{TMI}} = \frac{\left. q''_u a^2 \left(\frac{q''_b}{q''_u} \left(1 + \left(\frac{h_p}{a} \right)^2 \right) + 1 \right) \right|_{exp}}{\left. q''_u a^2 \left(\frac{q''_b}{q''_u} \left(1 + \left(\frac{h_p}{a} \right)^2 \right) + 1 \right) \right|_{TMI}} \quad (21)$$

Equations (16) and (18) indicate that upward heat fluxes will be similar if pools contain similar materials heated to similar temperatures. Although it is possible to vary peak pool temperature, the desire to avoid simulating debris decay heat in these tests suggest that peak pool temperatures should be at least 185 K above the melt liquidus. Furthermore, analyses indicate that this upward heat flux dominates heat losses from the pool.

Information in Section 4.1.1 indicate that the ratio of the TMI-2 debris height to the debris upper surface radius is approximately 0.32. Equations (17) and (18) indicate that downward heat fluxes and associated energy losses are dependent on vessel radius, the ratio of the melt height to the vessel radius, melt material properties, and melt superheat. However, results in Table 5 indicate that downward heat losses are only about one tenth the size of the upward heat losses for a pool similar in geometry to the configuration estimated for the melt that relocated to the TMI-2 lower head. Therefore, if debris in the Phase I tests experiences upward heat fluxes similar to the TMI-2 estimated upward heat fluxes, has similar geometrical parameter ratios, and has similar thermal properties, the above expression simplifies to

$$\left.\frac{M_d \frac{dT_d}{dt}}{a^2}\right|_{exp} = \left.\frac{M_d \frac{dT_d}{dt}}{a^2}\right|_{TMI} \quad (22)$$

Equation (22) can be used to define the possible debris cooling rates, masses, and test facility radii for these tests. As indicated in Table 6, several possible parameter combinations can be used in these tests. In selecting the combination of conditions for the facility's design, preliminary evaluation indicates that the debris mass should be minimized in order to minimize test costs. Hence, it is recommended that scaled masses for initial tests should be approximately 20 kg, which corresponds to a debris upper surface radius of 0.16 m and initial debris cooling rates of 0.13 K/s. However, other test masses will be investigated to assess the effects of geometry ratios on debris cooling.

Table 6: Possible parameter combinations for initial integral tests

Facility radius, m	Debris height, m	Debris upper surface radius, m	Debris Mass, kg	Initial Debris Cooling Rate, K/s
0.2	0.04	0.12	8	0.10
0.3	0.05	0.16	20	0.13
0.4	0.08	0.24	60	0.18
0.5	0.10	0.30	120	0.23
0.6	0.11	0.35	200	0.27
0.8	0.15	0.47	480	0.36
1.0	0.19	0.59	940	0.45
2.2[a]	0.42	1.30	10000	1.0

a. Size of TMI-2 vessel, debris height, mass, etc.

4.1.4 Initial Crust Growth Rate and Temperature Response

To gain insight about the initial crust growth rate and temperature gradients that occurred at the upper debris/coolant interface during the TMI-2 accident, an energy balance was applied to the crust geometry illustrated in Figure 36. As discussed in this section, results from this energy balance were also used to quantify the impact of thermal-hydraulic conditions and decay heat on crust growth.

Figure 36. Crust geometry analyzed to quantify crust growth rate and temperature behavior

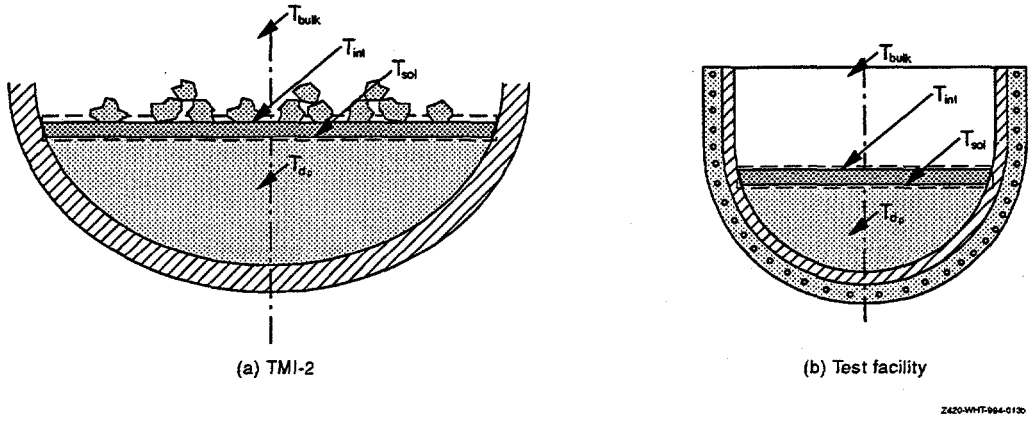

The methodology used to perform this analysis is similar to that used in the TMI-2 margin-to-failure analyses[50] and in the CORCON/MOD3 computer code.[51] Using a lumped parameter approach, an energy balance was applied to the control volume corresponding to the layer of crust on top of the debris shown in Figure 36

$$\frac{d}{dt}(\rho_{d_s} u_{d_s} A_{crust} \delta_{crust}) = U_u A_u (T_{d_{sol}} - T_{bulk}) - h_u A_d (T_{d_p} - T_{d_{sol}}) - q'''_{crust} A_{crust} \delta_{crust} \quad (23)$$

where

u_{d_s} = Crust internal energy (J/kg)
δ_{crust} = Crust thickness (m)
U_u = Overall crust to coolant heat transfer coefficient (W/m^2K)
h_u = Pool to crust heat transfer coefficient (W/m^2K)
T_{d_p} = Peak pool temperature (K)
$T_{d_{sol}}$ = Melt solidification temperature (K)
T_{bulk} = Bulk coolant temperature (K)
A_{crust} = Average crust cross-sectional area (m^2)
A_u = Upper crust surface area (m^2)
A_d = Lower crust surface area (m^2)
q'''_{crust} = Volumetric heat generation rate due to decay heat (W/m^3)

Because this analysis is only being applied to initial stages of crust formation, the following simplifying assumptions were invoked

- The crust thickness, δ_{crust}, is small.
- All crust cross-sectional areas are equal (i.e., $A_{crust} = A_u = A_d$).
- Film boiling and radiation heat transfer dominate upward heat losses from the crust.

For small crust thicknesses (i.e. $\delta_{crust} < 0.02$ m), analyses indicate that the crust growth rate term is significantly larger than other terms that occur when the first term of Equation (23) is expanded. Hence, the first term of Equation (23) simplifies to

$$\frac{d(\rho_{crust} u_{d_s} A_{crust} \delta_{crust})}{dt} = \rho_{d_s} A_{crust} (L_{f_d} + c_{p_{d_s}} T_d) \frac{d\delta_{crust}}{dt} \tag{24}$$

where L_{f_d}, represents the latent heat of fusion for the melt. Equation (24) and the assumption of equal areas allows Equation (23) to be rewritten in terms of the crust growth rate as shown below

$$\frac{d\delta_{crust}}{dt} = \frac{U_u (T_{d_{sol}} - T_{bulk}) - h_u (T_{d_p} - T_{d_{sol}}) - q'''_{crust} \delta_{crust}}{\rho_{d_s} (L_{f_d} + c_{p_{d_s}} T_{crust})} \tag{25}$$

The overall debris to coolant heat transfer coefficient is quantified using the following relationship between the effective crust heat transfer coefficient, h_{crust}, and the combined radiation and subcooled film boiling heat transfer coefficient, h_{r+sfb}

$$\frac{1}{U_u} = \frac{1}{h_{crust}} + \frac{1}{h_{rsfb}} \tag{26}$$

In this equation, the effective crust heat transfer coefficient is evaluated using

$$h_{crust} = \frac{k_{d_s}}{\delta_{crust}}. \tag{27}$$

The combined radiation and subcooled film boiling heat transfer coefficient is evaluated using the following relationships from the CORCON code manual [51] and Collier [52]

$$h_{r+sfb} = h_{sfb} + 0.75 h_r \tag{28}$$

In Equation (28), the radiation heat transfer coefficient, h_r, is evaluated using

$$h_r = \sigma_{SB} \varepsilon_{eff} \frac{(T^4_{d_{int}} - T^4_{bulk})}{(T_{d_{int}} - T_{bulk})} \tag{29}$$

where

σ_{SB}	=	Stefan Boltzmann constant (5.672×10^{-8} W/m^{2}K^4)
ε_{eff}	=	Effective emissivity
T_{int}	=	Crust/coolant interface temperature (K)

The effective emissivity, which is a function of the crust emissivity, ε_{d_s}, and the coolant emissivity, ε_c, is evaluated using

$$\varepsilon_{eff} = \frac{1}{\frac{1}{\varepsilon_{d_s}} - \frac{1}{\varepsilon_c} - 1} \tag{30}$$

As shown below, the subcooled film boiling heat transfer coefficient in Equation (28) is a function of the coolant thermal properties and the saturated film boiling heat flux, q''_{fb}

$$h_{sfb} = \frac{q''_{sfb}}{T_{d_{int}} - T_{bulk}} \tag{31}$$

$$q''_{sfb} = q''_{fb}\left(1 + \frac{0.98\,(T_{sat} - T_{bulk})^4}{(T_{d_{int}} - T_{sat})^4}\right) \tag{32}$$

$$q''_{fb} = 0.425\left(\frac{g\,(\rho_f - \rho_g)\,\rho_g k_g^3 h_{fg}}{\mu_g\left[\frac{\sigma_c}{g\,(\rho_f - \rho_g)}\right]}\right)^{0.25} (T_{int} - T_{sat})^{0.75} \tag{33}$$

where

g	=	acceleration due to gravity (9.8 m/s^2)
σ_c	=	surface tension for liquid coolant (N/m)
k_g	=	thermal conductivity for vapor coolant (W/mK)
ρ_f	=	density for liquid coolant (kg/m^3)
ρ_g	=	density for vapor coolant (kg/m^3)
h_{fg}	=	coolant heat of vaporization (J/kg)
μ_g	=	viscosity for vapor coolant (Pa-s)
T_{sat}	=	coolant saturation temperature (K)

The pool to crust heat transfer coefficient is simply the upward heat transfer coefficient from a molten pool during transient stages of natural convection, or h_u in Equation (16), which is repeated below

$$h_u = 0.25\frac{k_d}{R}\left(\frac{g\beta_d R^3 \Delta T_m}{\alpha_d \nu}\right)^{0.3038} \tag{34}$$

As discussed in Section 4.1.3, this heat transfer coefficient is primarily dependent on pool thermal properties and superheat, ΔT_m, and is nearly independent of pool size.

The above relationships were combined in a FORTRAN model to obtain order-of-magnitude estimates for initial crust growth rates, crust thickness, crust interface temperature, and average crust temperature. In this model, crust/coolant interface temperature, $T_{d_{int}}$, and average crust temperature, $T_{d_{avg}}$, were updated assuming a linear temperature distribution through the crust

$$T_{d_{int}} = T_{d_{sol}} - \frac{q''_{r+sfb}\delta_{crust}}{k_{d_s}} \tag{35}$$

$$T_{d_{avg}} = T_{d_s} - \frac{q''_{r+sfb}\delta_{crust}}{2k_{d_s}} \tag{36}$$

Base case assumptions for these calculations corresponded to a bulk coolant temperature of 550 K, a pool superheat of 250 K, an RCS pressure of 14 MPa, and a volumetric heat generation rate of 1 MW/m^3. Sensitivity studies were performed for these assumptions, and results are summarized in Table 5. In all of the cases considered, the crust experiences rapid growth until it becomes sufficiently thick that its presence reduces heat losses to the coolant. As indicated in Table 5, crust thicknesses during this slow growth or "semi-equilibrium" period range from 0.53 to 1.1 cm. However, it should be noted that crust growth rates may be significantly higher once additional mechanisms, such as crust cracking, increase the crust heat transfer area and associated heat losses. Peak crust growth rates, which occur prior to the semi-equilibrium period, range from 0.043 to 0.9 cm/s. Crust/coolant interface temperatures at the beginning of the semi-equilibrium period range from 1900 to 2100 K. Model predictions for crust growth rate seem to be most sensitive to assumptions related to molten debris initial superheat. This result provides additional support that initial tests should contain melts heated to superheats similar to those estimated for the TMI-2 melt. Representative results from sensitivity studies for a range of parameters possible during the TMI-2 event are summarized in Table 7.

Table 7: TMI-2 crust analysis results

	Base Case 14 MPa 1.0 MW/m^3 ΔT_m = 250 K	Variation			
		8 MPa	1.2 MW/m^3	ΔT_m= 185K	T_{bulk} = 470 K
Peak crust growth rate, cm/s	3.7e-2	2.8e-2	3.7e-2	8.9e-1	4.3e-2
Semi-equilibrium crust thickness, cm	0.62	0.53	0.62	1.1	0.63
Semi-equilibrium crust/coolant interface temperature, K	2000.	2100	2000.	1900	2000.
Semi-equilibrium debris decay heat input per unit area, W/m^2	6.2e3	5.3e3	7.4e3	1.1e4	6.3e3
Semi-equilibrium heat flux to coolant, W/m^2	1.1e6	1.1e6	1.1e6	7.3e5	1.1e6
Heat flux from molten pool, W/m^2	1.1e6	1.1e6	1.1e6	7.2e5	1.1e6

Results in Table 5 also provide insight into what parameters have the most impact on crust growth. For example, decay heat input estimates are typically two orders of magnitude smaller than estimates for the heat transferred to the coolant and the heat transferred from the molten pool. These results also suggest that debris decay heat simulation is not needed in debris coolability tests.

Assuming that material properties are similar to the TMI-2 debris and that decay heat is negligible, Equation (25) indicates that the crust growth rate is a function of the following variables:

$$\frac{d\delta_{crust}}{dt} = f(U_u, T_{bulk}, T_{d_p}, h_u) \tag{37}$$

As discussed above, results suggest that Phase I integral tests use molten pools heated to similar temperatures above the melt liquidus. Thus, the melt to crust heat transfer coefficient will be similar because this coefficient is nearly independent of pool size. The crust growth rate is then reduced to being a function of the product of the overall heat transfer coefficient between the crust and the coolant and the temperature difference between the melt solidus and the coolant bulk temperature. Hence, the following relationship should be preserved in order to obtain similar crust growth rates

$$U_u (T_{d_{sol}} - T_{bulk})\Big|_{TMI} = U_u (T_{d_{sol}} - T_{bulk})\Big|_{exp} \tag{38}$$

Equations (26) through (33) indicate that the overall heat transfer coefficient is a function of the pool interface temperature, the coolant bulk temperature, and coolant thermal properties (coolant viscosity, thermal conductivity, saturation temperature, volumetric coefficient of thermal expansion, surface tension, etc.). Coolant saturation temperature and thermal properties will vary with pressure. Hence, the two remaining parameters that can be varied in these experiments to obtain similar heat losses to the coolant are system pressure and coolant bulk temperature. Several calculations were performed to identify possible test conditions to achieve the desired heat loss rate. Results, which are summarized in Table 8 indicate that results are more sensitive to changes in system pressure. In fact, Table 8 values indicate that it is not possible to achieve the desired heat transfer rates unless the tests are performed in a system that is pressurized to at least 5 MPa. Therefore, these analyses suggest that tests should be performed at 5 MPa in order to match crust growth rates predicted for TMI-2 debris. However, as discussed in Sections 1 and 3, the objective of this test program is to develop models that predict debris cooling for any scenario in which melt relocates to a water filled lower plenum. Because recent analyses indicate that lower pressure

accident are more likely in most operating LWRs and because of cost considerations, it is recommended that Phase I tests concentrate on lower pressure scenarios (see Section 5).

Table 8: Crust scaling analysis results

	Pressure and Bulk Coolant Temperature Assumed				
	0.1 MPa	0.1 MPa	0.1 MPa	1 MPa	5 MPa
	300 K	350 K	380 K	380 K	380 K
Peak crust growth rate, cm/s	6.6e-4	6.5e-4	6.5e-4	2.6e-3	1.7e-2
Semi-equilibrium crust thickness, cm	0.26	0.26	0.26	0.33	0.51
Semi-equilibrium crust/coolant interface temperature, K	2400	2400	2400	2300	2100
Semi-equilibrium heat flux to coolant, W/m^2	1.2e6	1.2e6	1.2e6	1.2e6	1.2e6
Heat flux from molten pool, W/m^2	1.2e6	1.2e6	1.2e6	1.2e6	1.2e6

4.2 Structural Scaling Analyses for Hypothesized Cooling Mechanisms

In order to perform a structural scaling analysis, the debris cooling mechanism(s) must be known or assumed. Because the actual cooling mechanisms are unknown and because calculations reported below indicate that different stress conditions occur for different mechanisms, it is not possible to design tests based on structural scaling relationships. Nevertheless, it is useful to assume a cooling mechanism and perform analyses to gain insights into the effects of experimental parameters. Furthermore, it is anticipated that separate effect tests may be based on relationships discussed below if these mechanisms are identified in Phase I tests.

In these analyses, the general procedure is to: (1) assume a mechanism, (2) identify the governing equation and a dimensionless, governing parameter (such as strain or normalized stress), (3) hold the governing parameter constant for the experiment and actual conditions, and (4) develop relationships between independent variables (such as temperature or geometry) using closed-form structural solutions.

4.2.1 Cracking

Two mechanisms to drive cracking in the top crust are considered: cracking due to thermal stress and cracking due to pressure stress. Within each of these two mechanisms, there are localized and bulk effects. Bulk thermal stresses result from the bulk temperature gradient through the crust thickness; whereas, localized thermal stresses arise from temperature gradients in a localized area around the crack tip. Bulk pressure stresses may result from fission gas release; whereas, localized pressure stresses on crack faces may arise from coolant expanding while inside the crack.

Localized effects, thermal or pressure, are too complex for the closed-form solutions needed in scaling analyses; therefore, structural scaling is based on bulk thermal and pressure

stresses. If the dominant physical phenomena are from localized effects, the experimental design based on these analyses may not scale properly. Scaling the experiment uses results from these analyses and, by necessity, engineering judgement.

Cracking due to Thermal Stresses

Two governing parameters are considered for use in scaling analyses for thermal stresses: (1) normalized surface stress, with no regard to flaw distribution, and (2) risk of failure, which accounts for surface stress and specimen size effects due to flaw distribution. Throughout the structural analyses, failure is assumed to occur when stress exceeds fracture strength. Crack healing likely occurs at high temperatures, but is very difficult to predict and is not considered.

Thermal stress analysis - equivalent normalized stress. Thermal stresses occur in a body when some or all of its parts are not free to expand or contract in response to changes in temperature. A body which is free to expand or contract simply does so when subjected to a temperature change, thus relieving thermal stresses. One way to induce thermal stress cracking in a molten debris bed is by quenching the outside layer. If the entire outer layer of an initially molten debris bed undergoes a significant temperature drop, and the temperature of the interior remains approximately constant, tensile stresses develop in the outer crust layer. Tensile thermal stresses, combined with reduced ductility at cooler temperatures, may lead to cracking. Alternatively, if the quench is slow and the debris bed is small, the entire debris bed cools and contracts without developing significant thermal stresses.

The governing equation for thermal stresses following quench are taken from elastic analysis of brittle solids.[53, 54, and 55] If the top (flat) surface of a hemispherical debris bed at an initial constant temperature is suddenly cooled on the surface, and well-constrained from bending, in-plane stresses at the surface take the form:

$$\sigma_s = \frac{E\alpha}{(1-\nu_P)}\left(T_{d_{avg}} - T_{d_{int}}\right) \tag{39}$$

where

σ_s = in-plane stress on the surface due to thermal expansion or contraction (MPa)
E = elastic modulus (MPa)
α = thermal coefficient of expansion (1/K)
ν_P = Poisson's ratio (dimensionless)
$T_{d_{avg}}$ = average crust temperature (K)
$T_{d_{int}}$ = crust/coolant interface temperature (K)

Normalizing by a fracture strength, σ_f, yields the following equation:

$$\frac{\sigma_s}{\sigma_f} = \left[\frac{E\alpha}{\sigma_f(1-\nu_P)}\left(T_{d_{avg}} - T_{d_{int}}\right)\right]_{TMI} = \left[\frac{E\alpha}{\sigma_f(1-\nu_P)}\left(T_{d_{avg}} - T_{d_{int}}\right)\right]_{exp} \tag{40}$$

Because thermal stresses rely on the condition of constraint, there are no dimensional parameters. Equation (40) indicates that even if debris material properties change between an actual accident

and the experiment, the normalized accident stress state can be reproduced in the experiment by adjusting the difference between the average and surface temperature.

Thermal stresses - porosity considerations. Equation (39) does not consider pores or surface cracks and only predicts stresses on the outer surface. An average porosity of 18% was measured for resolidified debris removed from the TMI-2 vessel.[46] With this much porosity, it seems reasonable to assume that porosity, rather than surface cracks, dominates the structural response of the crust.

Coble and Kingery[56] experimentally examined the effect of porosity on resistance to thermal stress in sintered alumina. Resistance to thermal stress was defined:

$$R_t = \sigma_f \frac{(1-\nu_P)}{E\alpha} \tag{41}$$

where

R_t = thermal stress resistance, is the steady state temperature change required for failure

σ_f = fracture strength (MPa)

In the Coble and Kingery experiments, resistance to thermal stress decreased with increasing porosity. Resistance to thermal fracture, with a constant rate of temperature change, also decreased with increasing porosity. The experiments yielded results with considerable scatter (average deviation +18%), typical of thermal stress testing. These results indicate that porosity should be kept constant between the TMI-2 condition and the experiment to failure for the same temperature conditions.

Tachibana et al.[57] measured the effect of pore size on fracture strength of UO_2 under Hertzian point loads. Results showed good agreement with fracture theory:[58]

$$\sigma_f = C\left(\frac{1}{s}\right)^{0.5} \tag{42}$$

where

σ_f = fracture strength (MPa)

C = constant (MPa-$m^{1/2}$)

s = radius of a spherical pore (m)

Equation (42) indicates that fracture strength decreases with increasing pore size. The constant, C, depends on fracture toughness, a material property. In theory, if the fracture toughnesses of the experimental and actual debris materials are different, the pores can be sized to give equivalent fracture strengths. Realistically, it would be best to test materials as similar as possible in pore size and density (and all other material properties for that matter) to incorporate other unidentified parameters which may affect cracking.

Thermal stress analysis - equivalent risk of failure. The above discussion considers pore size and density, but does not consider the size. Size is known to have a significant effect on fracture strength when initial flaw distribution dominates behavior.[59,60] The following analysis assumes that porosity creates a size effect in the fracture strength of the solidified debris; that is, smaller debris beds are expected to have higher fracture strengths because they are less likely to contain a fatal flaw (pore) than a large debris bed.

The risk of rupture for a structure (e.g., top crust) is defined in terms of fracture test specimen parameters:

$$R_{fail} = \left[\frac{g_{exp} V_{exp}}{g_f V_f}\right]\left[\frac{\sigma_{s_{exp}}}{\sigma_f}\right]^m ln\,(2) \tag{43}$$

where

R_{fail}	=	risk of failure (dimensionless)
g	=	shape factor (dimensionless)
V	=	crust volume (m^3)
σ_s	=	in-plane stress on the surface due to thermal expansion or contraction (MPa)
σ_f	=	average fracture strength of the test specimens (MPa)
m	=	Weibull constant (dimensionless)

and the subscripts, *exp*, and *f*, indicate experiment and fracture tests, respectively. The *ln* (2) results from the assumption that there is a 50% probability of failure at the average fracture strength. The experimental and fracture test specimen materials are assumed to be the same.

Equating the risk of failure for the experiment to the risk failure for the TMI-2 condition, assuming shapes of the experimental and TMI-2 top crusts are the same (equivalent shape factors), and assuming the TMI-2 and experimental debris are the same:

$$\frac{V_{TMI}}{V_{exp}} = \left[\frac{\sigma_{s_{exp}}}{\sigma_{s_{TMI}}}\right]^m \tag{44}$$

From Equation (39) and assuming a circular plate geometry for the crust:

$$\frac{(a^2\delta_{crust})_{TMI}}{(a^2\delta_{crust})_{exp}} = \left[\frac{(T_{d_{avg}} - T_{d_{int}})_{exp}}{(T_{d_{avg}} - T_{d_{int}})_{TMI}}\right]^m \tag{45}$$

where

a	=	crust radius (m)
δ_{crust}	=	crust thickness (m)

Obviously, even if crust thickness could be controlled, it would not be independent of the difference between surface and average crust temperatures. Purely for illustration, let us assume that the experimental crust volume is one-tenth the TMI-2 crust volume at the time of failure. m=7 is a typical value for the Weibull constant for ceramics. From Equation (44):

$$(T_{d_{avg}} - T_{d_{int}})_{exp} = 1.39\,(T_{d_{avg}} - T_{d_{int}})_{TMI} \tag{46}$$

The smaller volume crust requires a more severe quench to failure because it is less likely to contain a "fatal" pore. In Section 4.4, Equation (45) is used to define the range of parameters for sensitivity studies in the integral tests.

Intuitively, we know that if the quench is severe enough, the crust will crack. In fact, the entire experimental debris bed may shatter - which is not predicted by the above analyses. The above analysis assumes that crack size remains small relative to crust thickness, it does not account for crack blunting or healing, which may be more likely in the TMI-2 condition where bulk temperatures may stay higher for longer times, and it assumes that surface stresses govern cracking. In other words, there is a great deal of uncertainty in the analysis and some engineering judgement should be used to determine the best experimental procedure. Equations (40) and (44) can be used to identify the upper and lower bound conditions for crust cracking.

Cracking due to pressure stresses

This analysis quantifies pressure stresses in the solidified crust due to gas release from the molten pool or a change in system pressure. Governing equations lead to a relationship between TMI-2 and experimental parameters, however, quantitative scaling cannot be performed for the initial integral tests because they will not be designed to control pressure. This analysis is performed to gain insights into the role of pressure in crust failure, which can be used in later separate effects tests, if needed. It should be noted that a pressure differential (hence pressure stresses) can only exist if the crust is gas impermeable, which has not been established.

Pressure stress analysis - equivalent normalized stress. Gas releases or a sudden drop in system pressure may create a positive pressure differential after crust solidification, resulting in tensile stresses which could lead to cracking on the top crust surface. Modeling the top crust as a circular fixed plate of uniform temperature, the in-plane stress is:

$$\sigma_p = \frac{3}{8}\Delta P\,(1+\nu_P)\,\frac{a^2}{\delta_{crust}{}^2} \tag{47}$$

where

σ_p	=	the stress at the center of the plate from pressure (MPa)
ΔP	=	pressure differential across the crust (MPa)
ν_P	=	Poisson's ratio (dimensionless)
a	=	plate radius (m)
δ_{crust}	=	plate thickness (m)

Normalizing by the failure strength, σ_f, and setting the normalized TMI-2 stress equal to the normalized experimental stress:

$$\left[\frac{\Delta P\,(1+\nu_P)}{\sigma_f}\,\frac{a^2}{\delta_{crust}{}^2}\right]_{TMI} = \left[\frac{\Delta P\,(1+\nu_P)}{\sigma_f}\,\frac{a^2}{\delta_{crust}{}^2}\right]_{exp} \tag{48}$$

If the TMI-2 and experiment histories of the average through-thickness crust temperatures and crust thicknesses are known, the properties, σ_f and ν_P, can be determined for a given time. This gives a relationship between the pressure differentials and the crust radii.

Before implementing scaling based on pressure differential, crust impermeability should be established. If the crust is found to be gas impermeable, separate effects tests using inert gas as a coolant can be performed to determine the role of system pressure in crust failure. Scaling should also include the effects of porosity using risk of failure analyses, similar to that presented in the previous section.

4.2.2 Gaps

This analysis examines the two competing deformation processes of thermal contraction and high temperature creep. Quantitative scaling is not performed because creep is temperature history-dependent, as well as stress (and therefore, thickness) history-dependent. However, qualitative results which confirm intuitive behavior are discussed.

Upon cooling, the debris bed reduces in volume relative to the molten state. Depending on how long the molten debris contacts the vessel before cooling, the vessel may also expand with heating and contract with cooling. Debris cooling will tend to create a gap, whereas vessel cooling will tend to close a gap. If cooling is slow enough to allow creep deformation, the crust will deform under load closing a gap, whereas vessel creep will tend to cause sagging, which would open a gap.

The difference between debris and vessel total strains, $\Delta\varepsilon_{total}$, determines whether a gap forms.

$$[\varepsilon_{total}]_{debris} = [\varepsilon_{elastic} + \varepsilon_{plastic} + \varepsilon_{creep} - \varepsilon_{thermal}]_{debris} \tag{49}$$

$$[\varepsilon_{total}]_{vessel} = [\varepsilon_{elastic} + \varepsilon_{plastic} + \varepsilon_{creep} - \varepsilon_{thermal}]_{vessel} \tag{50}$$

$$\Delta\varepsilon_{total} = [\varepsilon_{elastic} + \varepsilon_{plastic} + \varepsilon_{creep} - \varepsilon_{thermal}]_{debris} - [\varepsilon_{elastic} + \varepsilon_{plastic} + \varepsilon_{creep} - \varepsilon_{thermal}]_{vessel} \tag{51}$$

where ε is absolute strain. The signs of the strains are assigned so that contraction is negative and expansion is positive. If $\Delta\varepsilon_{total}$ is less than zero a gap exists.

Consider each of the strain terms and compare test conditions to TMI-2. The elastic, plastic and creep strains in the experimental debris are expected to be less than in TMI-2, because the applied load (pressure head from molten debris) is lower. This assumes crust temperature and thickness are approximately the same between TMI-2 and experiment, such as during the early stages of cooling. The thermal strains should be approximately equal, so long as the initial experimental debris temperature matches TMI-2 and the final experimental debris temperature matches TMI-2. This assumes that thermal coefficient of expansion is the same between TMI-2 debris and

experimental debris. So, the experimental debris is predicted to expand less than TMI-2 debris. This tends to enhance gap formation in the experiment.

The elastic, plastic and creep strains in the experimental vessel are expected to be negligible because of the experimental vessel design and the lack of loads (primarily system pressure). If TMI-2 elastic/plastic/creep vessel deformation is significant, then the TMI-2 vessel will tend to sag and enhance gap formation, whereas the experimental vessel will not. However, thermal contraction in the TMI-2 vessel will likely be greater than the experiment because the experimental vessel will be kept cooler. So, vessel deformation due to loads may be greater in TMI-2, tending enhance gap formation, but thermal contraction may also be greater for TMI-2, tending to close the gap.

Clearly, the relative values of all these strains must be determined for the experiment and TMI-2 to perform a scaling analysis for the gap mechanism. In order to do this, the temperature history of the debris must be known, particularly for the creep strains. However, prior to obtaining the temperature history, data are needed to identify what cooling mechanisms are present.

4.3 Material Property Considerations

The chemical compatibility of material to contain debris at temperatures up to 3000 K is an important consideration in the proposed debris coolability experiments. Ideally, the melt pot materials would not chemically interact with the debris to cause either changes in the material properties of the debris or structural failure of the melt pot. In this section, the results of calculations of the thermodynamic stability of the $(U,Zr)O_2$ debris relative to the stainless steel-clad vessel in the TMI-2 accident on the one hand, and tungsten, proposed to be used for the melt pot in the experiment, on the other hand, are presented. The calculations are of thermodynamic equilibrium. In practice, kinetic limitations may prevent achievement of thermodynamic equilibrium. The calculations were performed using HSC Chemistry,[61] a commercially available software package based on SOLGASMIX,[62] which is a program that minimizes the Gibbs free energy of an input chemical system.

4.3.1 Steel (Iron) Debris Analysis Results

The first thermodynamic equilibrium analysis was performed, in part, to gain confidence in the methodology. Thus, the results from this analysis were compared with measurements taken on debris samples from the TMI-2 accident. The TMI-2 conditions were not precisely modeled so the results can only be qualitatively compared with measurements. The Fe-U-Zr-O system was analyzed as a function of temperature and Fe input mass. The input masses for U, Zr, and O were 10, 5, and 30 moles, respectively - modeling 10 moles of UO_2 and 5 moles of ZrO_2. The input mass for Fe was varied between 0.015 and 15 moles and the temperature was varied between 270 and 2800 K. These input values were chosen to be similar to those used in the tungsten melt pot compatibility analysis discussed in Section 4.3.2. The calculation for 1.5 moles of Fe is shown in Figure 37, where the equilibrium masses of UO_2, ZrO_2, and Fe are compared with the combined mass of all iron oxides (representing a total of seven different iron oxides). At low temperatures, there is no significant oxidation of the iron. However, as the temperature increases, the iron becomes increasingly oxidized, though the total iron oxide mass never exceeds a few percent of the total mass of the mix. The temperatures of the reactor vessel lower head during the TMI-2 accident were cool enough that these reactions were minimal, resulting in no measurable chemical attack of the lower head. Steel and Inconel instrument penetrations and guide tubes were observed to have been melted by the debris in the lower plenum of the TMI-2 reactor, but mea-

surements of the composition of samples of the debris revealed only a small concentration of iron, chromium, and nickel (<1.5 wt.%).[1] Although the amounts of these materials in the TMI-2 debris were small, in agreement with the results shown in Figure 37, they were found as eutectic mixtures of oxides primarily in grain boundaries of the $(U,Zr)O_2$ that could have a solidus temperature as low as 1600 K.[63] The influence of this eutectic material on the properties of the debris is not well known, but it could cause the debris to act as a slurry until the eutectic material in the grain boundaries freezes.[63] The impact of this possible behavior on the nature of the crust that forms around the molten debris is of interest for coolability. These considerations suggest that small amounts of iron, chromium, and nickel oxides should be included in the Phase I test debris.

Figure 37. Stainless steel analysis results

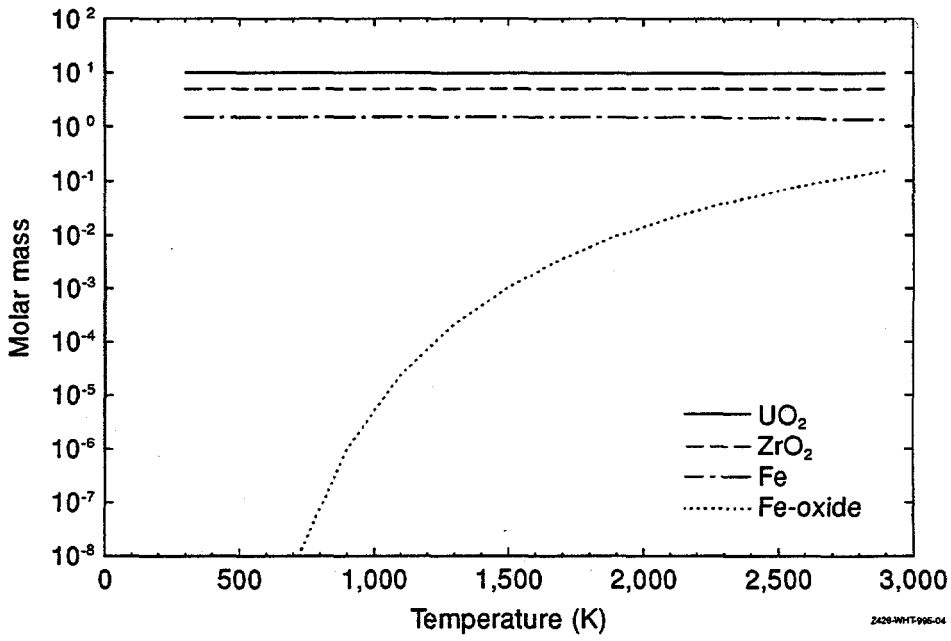

4.3.2 Tungsten/Debris Analysis Results

It is currently proposed to use tungsten as the material for the melt pot for heating the debris because of tungsten's high strength at high temperatures. To be qualified for this application, the melt pot material must also be chemically compatible with the molten debris to avoid adverse effects on the experiment. A chemical equilibrium analysis was performed to determine whether and to what extent: the proximity of tungsten to the melt would change the melt chemistry; and tungsten would oxidize, deteriorating its high temperature characteristics. In this analysis, it was assumed that 10 moles of UO_2 were mixed with 5 moles of ZrO_2 in the tungsten melt pot. A parametric analysis was performed where the mix temperature was varied between 270 and 2900 K and the amount of tungsten available for interaction was varied between 0.015 and 15 moles. The results from one set of calculations (for a tungsten input mass of 1.5 moles) are shown in Figure 38, which includes the molar masses of UO_2, ZrO_2, W, and tungsten oxides (representing the molar sum of 14 different tungsten oxide phases). As shown in this figure, the principle chemical form for tungsten is elemental metal (less than 0.2% of the tungsten was calculated to oxidize throughout the temperature range for this case). The maximum fraction of tungsten that was calculated to oxidize for any analysis was 17%, for the case of 0.015 moles tungsten input

mass. In addition to this analytical evidence, there is experimental evidence that the tungsten integrity should not be significantly affected. Hofmann and Politis performed an experiment wherein they measured the diffusion of oxygen from UO_2 into zircaloy cladding under Power Cooling Mismatch conditions.[64] To provide a positive mark as to the original Zr-UO_2 boundary, they inserted tungsten (either a wire or a grid) as a fiducial. Although tungsten behavior was not explicitly discussed in the paper, based on published microphotographs, it is evident that after 60 minutes at 1500 K, there was no significant oxidation of the tungsten, indicating that the material remained in an elemental form under these test conditions. Based on the current analytical results, the chemical forms for U and Zr are the original oxides, with no significant chemical change due to inclusion of tungsten. Based on this analysis, it is judged that tungsten should not affect the chemistry of the mix nor should the melt pot lose its structural integrity during the test

Figure 38. Tungsten analysis results

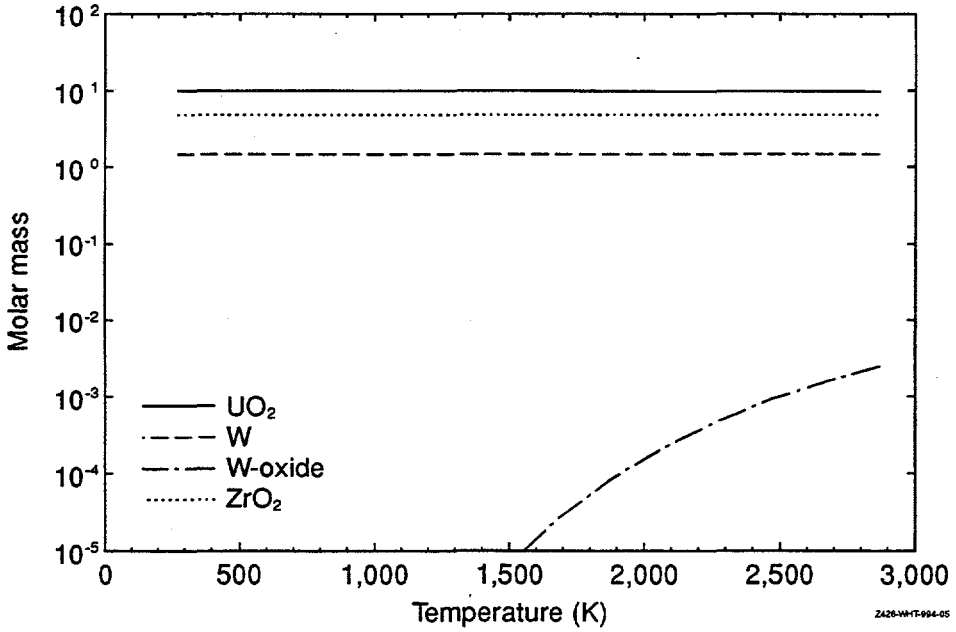

4.4 Suggested Test Conditions for Initial Integral Test

As discussed in this report, if the mechanisms responsible for debris cooling were known, tests would be scaled considering both thermal and stress conditions. However, it is not currently known what mechanisms cause enhanced debris cooling, and several postulated cooling mechanisms yield different stress and thermal scaling relationships. Therefore, scoping calculations were used to gain insights about Phase I test parameters using thermal-hydraulic data from the TMI-2 accident that suggests enhanced debris cooling occurred. This decision allows the debris in the tests to experience thermal conditions equivalent to the TMI-2 thermal conditions, the best source of data for identifying what mechanisms are responsible for debris cooling. However, these tests may not be properly scaled to simulate the stress states experienced by the TMI-2 debris. Therefore, calculations were also performed to gain insights about Phase I test parameters needed to simulate TMI-2 debris stress states.

Based on the thermal analyses discussed in Section 4.1, several important insights have been gained about Phase I tests:

- Debris decay heat can be omitted from the tests if initial pool superheats are greater than 185 K above the melt liquidus.
- Upward heat fluxes from the debris in these tests will range from 0.4 to 1.2 MW/m^2.
- Downward heat fluxes should be less than one tenth the magnitude of the upward heat fluxes.
- For initial tests, the ratio of the debris height to the quenching crucible radius, which will be matched to values estimated for relocated debris in the TMI-2 accident, will be approximately 0.2.
- The ratio of the debris height to the debris upper surface area radius, which will be matched to values estimated for relocated debris in the TMI-2 accident, will be 0.32.
- If it is desired to match initial crust growth rates experienced during the TMI-2 event, tests should be conducted at a pressure of at least 5 MPa (from 0.4 to 9 mm/s).
- The debris may be heated in a tungsten melt pot.
- Low concentrations of metallic species should be included in the simulant debris.

Scaling relationships obtained from stress analyses can be used to identify ranges of parameters for sensitivity studies in the Phase I test facility. For example, if it is desired to run tests to simulate equivalent stress states for cracking, Equations (35), (36), and (45) can be combined to obtain

$$\left[\frac{(a^2\delta_{crust})_{TMI}}{(a^2\delta_{crust})_{exp}}\right] = \left[\frac{(q''\delta_{crust})_{exp}}{(q''\delta_{crust})_{TMI}}\right]^m \tag{52}$$

Using $m = 7$ (a typical value for ceramics, see Section 4.2.1), the above equation reduces to

$$q''_{exp} = q''_{TMI}\left(\frac{a^2_{TMI}}{a^2_{exp}}\right)^{1/7}\left(\frac{\delta_{crust_{TMI}}}{\delta_{crust_{exp}}}\right)^{8/7} \tag{53}$$

Crust thicknesses will not necessarily be preserved. However, the crust thickness ratio to the power of 1.14 can be assumed to be near unity at initial time periods and this term can be neglected. Using an upper surface TMI-2 debris radius of 1.3 m and a test debris upper surface radius of 0.16 m, Equation (53) indicates that debris in the Phase I tests may experience up to the test facility should be designed to accommodate 80% higher heat fluxes (i.e., up to 2.2 MW/m^2).

5. Proposed Experimental Program

As discussed in Section 3, data will be obtained in each of the three major elements of this program, the Phase I Integral Tests, the separate effects tests, and the Phase II Integral Tests. This section provides preliminary information about the types of tests required and the test facilities required to perform these tests. Because of uncertainties about what mechanisms are responsible for debris cooling, this effort has focussed on defining the Phase I Integral Tests. However, preliminary information is also provided about the material property tests that may be required to support the separate effects tests and Phase II Integral Tests.

5.1 Phase I Integral Tests

As discussed in Section 1, the objective of this program is to obtain data and develop models that predict the coolability of debris that relocates to a water-filled lower plenum. Although this cooling may occur in either low or high pressure accident scenarios, the only source of severe accident data indicating its presence is TMI-2 data. Hence, scoping calculations in Section 4 were based on thermal-hydraulic data from the TMI-2 accident in order to estimate test parameters that allow the debris to experience conditions equivalent to the TMI-2 thermal conditions. Results from these analyses yielded the insights and recommendations summarized in Table 9.

Table 9: Summary of recommendations for Phase I Tests

Test Parameter	Recommendation
Configuration	The quenching crucible radius should be 0.3 m, assuming that a scaled TMI-2 mass of 20 kg is sufficient.
	The nominal ratio of the debris height to the debris upper surface area radius should be approximately 0.32.
	The nominal ratio of the debris height to the quenching crucible radius should be approximately 0.2.
Melt Composition	Nominal debris compositions should consist of 78% wt.% UO_2; 17 wt.% ZrO_2, and small amounts (<1.5 wt.%) of iron, chromium, and nickel oxides.
Initial Melt Temperature	Debris decay heat may be omitted from the tests if initial pool superheats are greater than 185 K above the melt liquidus.
Estimated Initial Debris Heat Transfer Conditions	Nominal values for the initial upward heat fluxes from the debris should range from 0.4 to 1.2 MW/m^2.
	In order to perform sensitivity tests simulating equivalent stress states to values predicted for the TMI-2 debris, initial upward heat fluxes as high as 2.2 MW/m^2 should be tested.
	Nominal values for the initial downward heat fluxes should be less than one tenth the magnitude of the upward heat fluxes.
	The debris should initially cool at approximately 0.1 K/s (quench rate will be verified by examining debris microstructure after initial Phase I tests).
Test Facility Pressure	In order to match initial crust growth rates with values expected during initial stages after melt relocation during the TMI-2 accident (between 0.4 and 9 mm/s), tests should be conducted at pressures of 5 MPa or higher.
Melt Pot Material Composition	Tests may be conducted by heating the debris in a tungsten melt pot.
Initial Test Atmosphere	Air should be removed from the vessel to minimize oxidation of the tungsten melt pot.

These recommendations suggest that tests should be conducted at high pressure in a large scale facility that it is able to withstand high pressures. However, debris cooling questions are of interest in both high and low pressure accident scenarios. In fact, recent analyses supporting the direct containment heating resolution issue suggest that without operator intervention, high pres-

sure accidents in CE and Westinghouse plants are unlikely.[4,5] In addition, improvements in operator training since the TMI-2 accident have decreased the likelihood for operator intervention which leads to high pressure scenarios. This information, in conjunction with cost considerations, have yielded a three element approach for this research program. Namely, that exploratory integral tests, Phase I tests, be conducted consistent with all of the Table 9 recommendations except the suggestion for facility pressure; that separate effects tests be conducted to obtain data necessary for model development for a range of possible severe accident conditions; and that larger scale integral tests, Phase II tests, be conducted to validate models for the range of possible severe accident conditions.

In Section 5.1.1, the design of the test facility in which Phase I tests will be conducted is described. A preliminary Phase I test matrix is discussed in Section 5.1.2, and a typical test procedure is outlined in Section 5.1.3. Manufacture of the simulant debris for the proposed tests is discussed in Section 5.1.4. Instrumentation and measurements for these tests are discussed in Section 5.1.5.

5.1.1 Facility Description

A diagram depicting the Phase I test facility is shown in Figure 39. As discussed in Section 5.1.2, a series of tests is planned for this facility. In general, these tests will be conducted by first purging the vessel with an inert gas and then melting simulant debris in the tungsten melt pot. Once the debris is heated to the desired amount of superheat, it will be poured into a prewetted stainless steel clad carbon steel crucible and quench water will be injected on top of the melt. Key facility components are described below.

Pressure Vessel

The vessel will be fabricated from stainless steel to ASME Section VIII pressure vessel standards. The vessel design pressure will be 1.4 MPa, and the vessel peak operating pressure will be 1.0 MPa. The vessel diameter is 1.3 m and its overall length, excluding the elliptical end caps, is 3 m. The vessel's volume is adjustable to accommodate various pressure increases corresponding to different masses of molten test debris. Using only the lower volume, quenching a 20 kg melt mass will yield a peak pressure of approximately 1.0 MPa. Similarly, the larger volume will accommodate 40 kg with a peak pressure of 1.0 MPa. For smaller masses, the pressure will be lower. For larger masses, the pressure relief valve will cycle and the expended steam will be condensed and weighed. This variable volume is accomplished by inserting flanged sections of different lengths into the vessel. Both the top and bottom vessel heads are flanged to allow for easy disassembly and decontamination. Because the experiment will generate uranium vapor, it is expected that the vessel will be slightly contaminated after testing. Effluents will also be contaminated and will be treated as low level radioactive wastes.

Figure 39. Block diagram for Phase I test facility

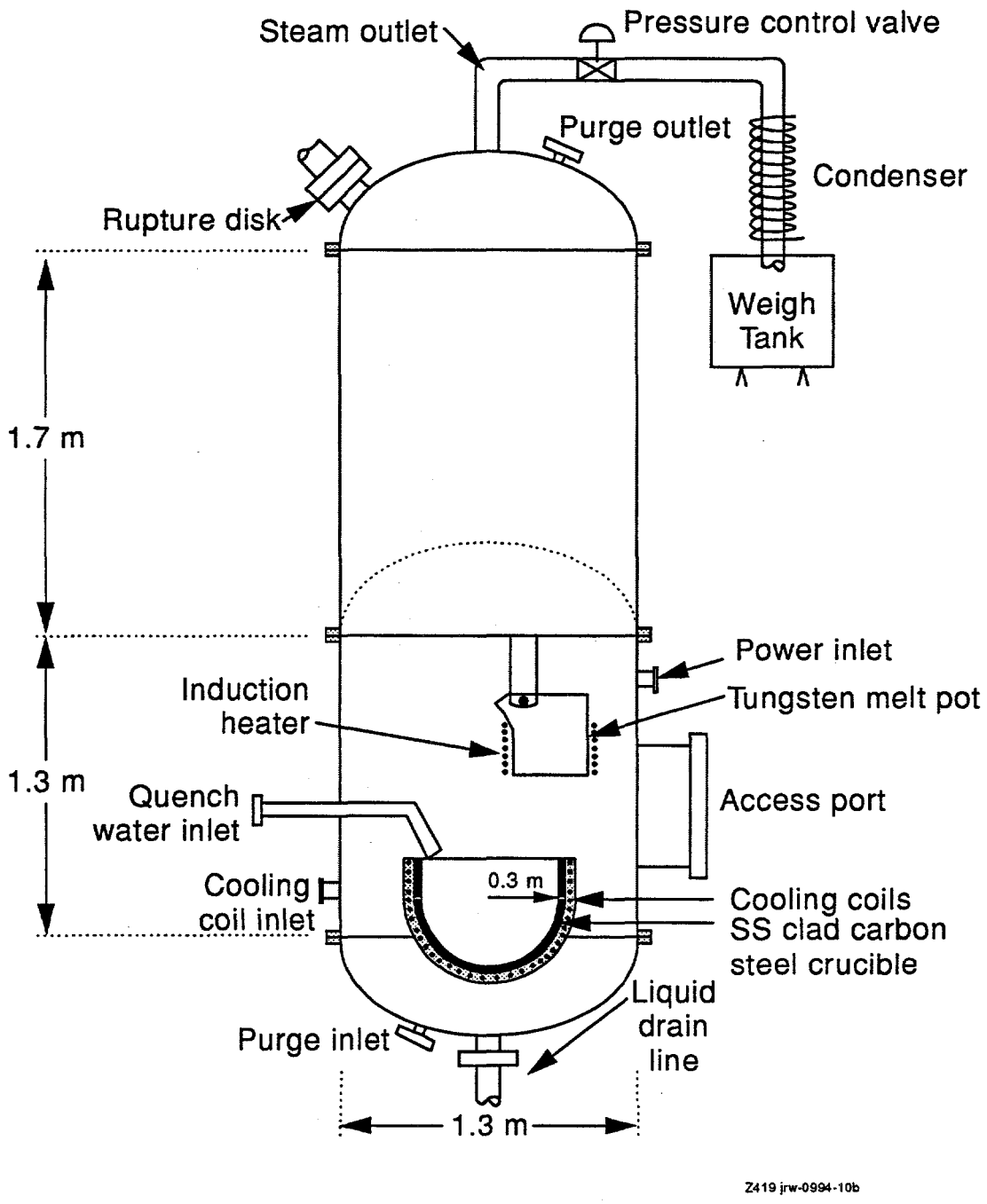

Several ports and penetrations are included in the design to accommodate instrumentation, electrical, gas, and water connections. A large port is located near the bottom of the vessel to provide access for experiment setup without having to remove the top or bottom end caps. Quench water will enter the vessel through a spray port located above the quenching crucible. Liquid

overflow from the crucible or condensate from the vessel walls later in the cooldown will accumulate at the bottom of the vessel and be transported to a weigh tank through the liquid drain line. At the start of each test, the vessel must be inerted to minimize oxidation of the tungsten melt pot. An inert gas, most likely Argon, will be introduced through the gas purge inlet line and will exit through the gas purge outlet line. The vessel pressure during heating will be controlled to within ± 0.01 MPa of 0.1 MPa by using a regulatory on the gas purge outlet line. At the top of the vessel is a steam removal line and pressure control valve. In some tests, steam generated during debris quenching will exit the vessel through this line where it will be condensed and weighed. System pressure will be controlled using a flow control valve in this line.

Except for the largest test debris mass (see Test Series 4 in Section 5.1.2), the vessel pressure will be allowed to rise unchecked during debris quench. The vessel will be protected from overpressurization by a rupture disk set at 1 MPa. Effluents from the rupture disk system will be collected in a catch tank system designed to handle mildly contaminated water.

The outside of the pressure vessel will be insulated to reduce environmental heat losses, although heat losses will be measured.

Carbon Steel Quenching Crucible

It is proposed that the melt would be quenched in the Phase I tests after it is poured into a prewetted crucible. Scoping calculations in Section 4 suggest that initial Phase I tests should pour the melt into a hemispherical crucible with an inner diameter of 0.6 m. This size provides the debris height to upper surface radius ratio corresponding to TMI-2 debris dimensions for the 20 kg mass planned in the Series 1 tests and accommodates the maximum debris mass of 75 kg that is planned for the Phase I Series 4 tests (see Section 5.1.2). The surface of the crucible will be wetted before melt addition. The amount of water required to wet the crucible surface will be minimized to avoid any unwanted debris/coolant interactions.

The crucible will made of carbon steel and consist of a hemispherical lower head below a cylindrical segment. The initial crucible will be clad with stainless steel to simulate PWR lower head designs, although subsequent tests may be clad with Inconel or contain penetrations to simulate other LWR lower head designs. The cylindrical volume above the hemispherical head will allow a level of quench water to be contained above the melt. The thickness of the crucible will be determined after a thermal and stress analysis has been completed.

The outside of the hemispherical portion of the crucible will be wrapped with tubing to allow the circulation of water coolant. The heat flux from the debris to the crucible will be directly measured using thermocouples. In addition, the heat transfer from the bottom of the melt during cool down will be calculated by measuring the temperature and flow rate of the coolant. The energy removal rate through the crucible is determined by measuring the inlet and outlet temperatures and flowrate of the coolant. ZrO_2 insulation will cover the entire outside surface of the crucible and the cooling tubes to reduce heat transfer to the pressure vessel.

Tungsten Melt Pot

The simulant debris will be melted inductively in a tungsten melt pot. A spout is located on the side of the melt pot so that melt can be poured into the carbon steel quenching crucible. This method eliminates potential clogging and release timing problems associated with other possible methods for introducing melt into the carbon steel crucible.

The volume of the melt pot will be selected based on the test melt mass. When quench water is introduced into the vessel, it is anticipated that the tungsten melt pot may experience some oxidation. Hence, different melt pots may also be required for different tests with the same mass. However, replacing the melt pot will not significantly impact either the cost or schedule for performing Phase I tests, because the melt pot is relatively inexpensive and easily replaced.

5.1.2 Proposed Phase I Test Matrix

As discussed in Section 3, Phase I tests will be conducted to determine what debris cooling mechanisms are present when a continuous mass of debris relocates to a water-filled lower plenum. In addition, this data will be used to determine interactions between mechanisms after the debris cooling models are developed from separate effects tests. Therefore, a sufficient number of tests must be performed so that the mechanisms can be identified for a sufficient range of conditions to allow a preliminary evaluation of the manner in which debris cooling characteristic parameters vary with selected test conditions. If more than one debris cooling mechanism is identified, Phase I test data will be used to assess interactions between mechanisms and modify models developed from separate effect tests to incorporate mechanism interactions.

Table 10 lists the seven series of tests planned for Phase I. Each series varies a parameter that may impact the occurrence and characteristic parameters associated with postulated debris cooling mechanisms. The Series 1 tests investigate the impact of the presence of an initial wetted surface and of cooling water addition on debris cooling. The Series 2 tests investigate the effects of pressure and coolant subcooling on debris cooling. Series 3 tests investigate the impact of the initial cooling water height on cooling. Series 4 tests assess the impact of debris height on cooling. Melt mass (and associated height) will be varied in these tests to determine their effect on characteristic parameters associated with debris cooling mechanisms, such as crack length, crack density, and gap size. The Series 5 tests investigate the impact of melt composition on debris cooling. Because scoping analyses indicate that material properties play an important role in postulated debris cooling mechanisms, a range of melt compositions will be tested to quantify variations in characteristic cooling mechanism parameters (crack size, crack length, gap size, etc.) and in the relative importance of various cooling mechanisms. The Series 6 tests will include penetrations in the quenching crucible. These tests are included to assess the potential for penetrations in the melt to enhance debris coolability. The Series 7 tests are included to evaluate the effects of varying the melt's initial superheat. Post-test examinations will be performed on debris from all of the above tests to identify any differences in composition, porosity, and grain size between the test debris and the TMI-2 debris.

This list of tests in Table 10 is preliminary, and some modifications to this matrix may occur as results from certain tests are obtained. For example, results from tests investigating the effects of initial water height in the Series 3 tests may impact the initial water height selected for the remaining test series. In addition, tests may be added to this matrix that investigate mechanism interactions after the separate effects tests are completed.

Table 10: Proposed matrix for Phase I tests

Test ID	Description	Maximum Pressure, MPa	Initial Water Height, m	Quench Water Temperature, K	Melt Mass, kg	Melt Composition
1/1	Scaled TMI-2 melt mass and composition; low pressure, varying introduction of initial water and quench water	1.0	No initial water	90 K subcooled	20	78 wt% UO_2; 17 wt% ZrO_2; < 5 wt% metal oxides
1/2			0.05	No water addition		
1/3			0.05	90 K subcooled		
2/1	Scaled TMI-2 melt mass and composition; varying pressure and quench water subcooling	0.5	0.05	90 K subcooled	20	78 wt% UO_2; 17 wt% ZrO_2; < 5 wt% metal oxides
2/2		1.0	0.05	50 K subcooled		
3/1	Scaled TMI-2 melt mass and composition; varying height of initial water	1.0	0.03	90 K subcooled	20	78 wt% UO_2; 17 wt% ZrO_2; < 5 wt% metal oxides
3/2			0.10			
4/1	Scaled TMI-2 melt composition; varying melt mass	1.0	0.04	90 K subcooled	8	78 wt% UO_2; 17 wt% ZrO_2; < 5 wt% metal oxides
4/2			0.07		40	
4/3			0.09		75	
5/1	Scaled TMI-2 melt mass; varying melt composition	1.0	0.05	90 K subcooled	20	80 wt% UO_2; 20 wt% ZrO_2
5/2						Mixed oxide with metal
6	Scaled TMI-2 melt mass and composition; maximum pressure; various penetrations	1.0	0.05	90 K subcooled	20	78 wt% UO_2; 17 wt% ZrO_2; < 5 wt% metal oxides
7	Scaled TMI-2 melt mass and composition; maximum pressure; varying melt initial superheat	1.0	0.05	90 K subcooled	20	78 wt% UO_2; 17 wt% ZrO_2; < 5 wt% metal oxides

5.1.3 Typical Phase I Test Procedure

As discussed above, specific parameters will be varied in each of the Phase I tests. However, the general procedure for each test is similar. This section outlines steps required to complete each of the Phase I tests.

First, constituents of the simulated debris are mixed together in powder form using glove boxes and mixing apparatus existing at the INEL. Once the composition of the debris powder has been verified, it is placed in the tungsten melt pot and the vessel is sealed.

Second, air inside the vessel is purged and replaced with an inert gas, such as argon, to protect the tungsten heaters and crucible from excessive oxidation.

Third, the heating circuits are energized and the simulant debris is melted to the desired superheat. The vessel pressure is maintained at 0.1 MPa by venting through the purge outlet line.

Fourth, water is added to the carbon steel quenching crucible to wet its inner surface. As discussed above, the water required to wet the surface will be minimized to reduce the potential for unwanted debris/water interactions.

Fifth, the melt pot is tipped to allow melt to relocate to the carbon steel quenching crucible.

Sixth, water is added to the quenching crucible to quench the debris, and the crucible cooling flow is initiated. A test is ended when the debris has cooled to ambient temperature.

5.1.4 Simulant Debris Fabrication

Phase I, Phase II, and some separate effects tests will use simulated debris consisting of $(U,Zr)O_2$. Depleted uranium will be used as the source of uranium. The debris will be fabricated in a manner so that its physical, thermal, and structural properties are representative of that found during a severe accident in which molten debris relocates to the lower head.

The simulant will be in powder form at the start of each test. As the test progresses, the powder will become molten and this molten material will be quenched. At the conclusion of each Phase I test, measurements will be made on the test debris to determine the composition, porosity, and grain size and comparisons will be made with the properties of the debris removed from the TMI-2 vessel. These measurements will insure that the simulated debris has a uniform composition and verify that the quench rates estimated in Section 4 produce debris similar in porosity and microstructure to the TMI-2 debris.

The measurements on the simulated debris will be performed using the INEL scanning electron microscope (SEM). This device has the capability of performing measurements on radioactive samples and could be used for the required verification measurements using TMI-2 lower head debris stored at the INEL. However, rather than performing new SEM examinations on TMI-2 debris, it is proposed to first examine and use all relevant existing data obtained from previous programs at INEL and from programs in other countries. For example, the Department of Fuel Safety Research at JAERI has an active research program to develop physical and material properties of the TMI-2 core debris that was sent to them by INEL in 1991.[65] JAERI has developed a simulant debris similar to what is being proposed here and is also performing microstructure and metallurgical examinations on TMI-2 debris to verify properties of their simulant debris.

5.1.5 Instrumentation and Measurements

Measurements will be performed during and after the tests to obtain required data. Sufficient data must be obtained during the tests to determine when the debris is sufficiently superheated for testing and verify that the debris loses heat more rapidly than possible by conduction through the debris (i.e., comparisons must show that Phase I test debris temperatures are decreasing more rapidly than temperatures predicted by current severe accident code models). Post-test measurements will be performed to verify that the microstructure (i.e., the composition, uniformity, porosity, and grain size) of the simulant and that the TMI-2 debris are similar and to identify

the presence of, and characteristic dimensions associated with, configurations responsible for enhanced debris cooling.

In general, all measurements will be made using standard state of the art instrumentation that has been applied successfully in previous INEL experimental programs. Little, if any, instrumentation development is needed. This section identifies specific measurements required for these tests and the instrumentation needed to obtain these measurements.

Debris temperature during melting

As discussed in Section 4.4, the debris must be superheated more than 185 K above its liquidus in order to obtain representative results. During melting, the debris temperature will be directly measured using two methods: melt wires and two-color optical pyrometers.

The time-dependent change in debris temperature will be confirmed by applying the following energy balance to the debris in the melt pot

$$M_d\left[L_{f_d} + c_{p_{d_s}}(T_{d_{sol}} - T_{d_1}) + c_{p_{d_m}}(T_{d_2} - T_{d_{sol}})\right] =$$

$$\left[\dot{Q}_h - M_{mp}c_{p_{mp}}\Delta T_{mp} - \varepsilon_d\sigma_{SB}(T^4{}_{d_2} - T^4{}_a)A_u\right](\Delta t_h) \qquad (54)$$

where

M_d	=	Debris mass, kg
M_{mp}	=	Melt pot mass, kg
L_{f_d}	=	Debris latent heat of fusion, J/kg
c_{p_d}	=	Debris specific heat, J/kg-K
$c_{p_{mp}}$	=	Melt pot specific heat, J/kg-K
Q_h	=	Power input from heaters, W
σ_{SB}	=	Stefan Boltzmann constant (5.672 x 10-8 W/m^2K^4)
ε_d	=	Debris emissivity
T_d	=	Debris temperature; may be further designated with the subscript 1 for initial state or 2 for melt final temperature (at least 185 K superheated), K
T_{mp}	=	Average melt pot temperature, K
T_a	=	Average vessel atmospheric temperature, K
Δt_h	=	Debris heating time, s

In Equation (54), all of the parameters will be directly measured with the exception of the time-dependent debris temperature during the heating phase of this experiment. Thermocouples will be placed in the body of the melt pot to measure melt pot temperatures.

Debris temperature during quenching

As discussed above, a major objective of the Phase I tests is to verify that heat losses from the debris are greater than those possible by conduction. This will be done by first applying current severe accident code models, such as SCDAP/RELAP5, to predict test debris temperatures

during quench. These temperature predictions will be compared to the Phase I test debris cooling rates. Because of the high temperatures involved, ultrasonic thermometers (UTs) will be used to measure the simulant debris temperatures. UTs have the capability of operating at temperatures in the range of 3300 K in locations that are inaccessible to optical techniques. The UTs to be used in the debris coolability experiments will have a thoriated tungsten sensor that is protected by a rhenium refractory metal sheath. Location-dependent debris temperature will be determined by multiple UTs of different lengths placed through the melt. Although UTs have been used successfully to measure such high temperatures, it is desirable to know the minimum UT sensor length and separation needed for temperature resolution. There are also questions about the integrity of UT sheath materials in an oxidizing environment. To answer these questions, INEL is sponsoring a project at the start of FY-95 to address these questions. In addition, this FY-95 INEL-sponsored project will identify other technologies that can reasonably be developed to obtain surface temperature measurements at ~3000 K through water and saturated steam.

Hafnium sheathed tungsten/rhenium thermocouples will also be used to measure debris temperatures. Although these thermocouples are not expected to survive for long time periods when exposed to the superheated melts anticipated for some of these tests, the recently completed MP-2 tests at SNL indicate that these thermocouples can perform for short time periods before failing. A two color optical pyrometer will also be used as a backup to the UTs to measure the surface temperature of the molten pool. However, the large quantities of steam generated during the debris quench may obscure the molten surface and preclude an accurate measurement. A video camera port will be placed in a location so that it has a view of the crucible during the melting and quench phase of the experiment.

For tests with debris masses of 40 kg or smaller, the vessel's pressure is allowed to rise unchecked and time-dependent debris temperature during quench will be confirmed by applying the following energy balance to the pressure vessel for time periods after quench is initiated

$$M_d\left[L_{f_d} + c_{p_{d_s}}(T_{d_{sol}} - T_{d_1}) + c_{p_{d_m}}(T_{d_2} - T_{d_{sol}})\right] = M_{c_2}u_{c_2} - M_{c_1}u_{c_1} + \dot{m}_{in}h_{in}\Delta t_q - [\Delta\dot{E}_c + \Delta\dot{E}_a + \Delta\dot{E}_s]\ (\Delta t_q) \quad (55)$$

where

M_c = Mass of coolant in the vessel; may be further designated with the subscript 1 for initial state or 2 for melt final temperature, kg

u_c = Internal energy of coolant in the vessel; may be further designated with the subscript 1 for initial state or 2 for melt final temperature, J/kg

Δt_q = Debris quench time, s

$\dot{m}_{in}$ = Quench water flowrate, kg/s

h_{in} = Enthalpy of quenching water, J/kg

$\Delta\dot{E}_c$ = Crucible energy removal rate, W

$\Delta\dot{E}_a$ = Vessel energy loss rate, W

$\Delta\dot{E}_s$ = Test facility structural energy storage term, W

For tests with debris masses greater than 40 kg, steam is released to maintain the vessel's pressure at 1.0 MPa and the time-dependent debris temperature during quench will be confirmed

by applying the following energy balance to the pressure vessel for time periods after quench is initiated

$$M_d\left[L_{f_d} + c_{p_{d_s}}(T_{d_{sol}} - T_{d_1}) + c_{p_{d_m}}(T_{d_2} - T_{d_{sol}})\right] = M_{c_2}u_{c_2} - M_{c_1}u_{c_1} + \dot{m}_{in}h_{in}\Delta t_q -$$

$$[\Delta\dot{E}_c + \dot{m}_{steam}h_{steam} + \dot{m}_{drain}h_f + \Delta\dot{E}_a + \Delta\dot{E}_s]\ (\Delta t_q) \tag{56}$$

where

$\dot{m}_{steam}$ = Flowrate of steam exiting the vessel, kg/s
h_{steam} = Enthalpy of steam exiting the vessel, J/kg
$\dot{m}_{drain}$ = Flowrate of fluid draining from the vessel, kg/s
h_f = Enthalpy of liquid draining from the vessel, J/kg

In Equations (56) and (56), the decrease in debris temperature is estimated by using known parameters, easily measured parameters, or relationships using easily measured parameters. For example, the loss of energy associated with heat losses from the vessel will be measured using heat flux sensors along the vessel. Commercially available heat flux sensors will be installed on the outside of the pressure vessel.

Equation (56) differs from Equation (56) because of the addition of terms associated with coolant exiting the vessel. For Series 4 tests with more than 40 kg debris masses, the energy associated with steam leaving the vessel will be quantified by condensing the steam and then directing the condensate into a weight tank placed on a load cell. The steam enthalpy will be determined by measuring the steam temperature and pressure. Similarly, a weigh tank will be used to quantify the energy associated with fluid draining from the test vessel.

Thermocouples placed in the body of the quenching crucible provide data for an inverse heat transfer calculation to verify that instrumentation readings for crucible coolant mass flowrates and cooling temperatures are correct. This check will be performed using the following relationship

$$q''_d A_d = \sum_{n_d} n\dot{m}_n c_{p_w} \Delta T_{w_n} \tag{57}$$

where

q''_b = Downward heat flux, W/m^2
A_b = Downward surface area, m^2

To verify that the magnitude of the upward heat flux is similar to values estimated for the TMI-2 debris, the following energy balance will be applied to the debris

$$M_d[L_{f_d} + c_{p_d}(T_{d_2} - T_{d_1})] = \sum_{n_d} n\dot{m}_n c_{p_w} + q''_u A_u \tag{58}$$

This equation introduces no new parameters except

q''_u = Upward heat flux, W/m^2

A_u = Upward surface area, m^2

Thus, the initial upward heat flux is estimated by using geometrical relationships to quantify the initial upward heat transfer surface area.

Adequate instrumentation is critical to the success of the debris coolability experiments. Instruments required for completion of the Phase I experiments are all standard state of the art instruments. Temperatures for the quench water, crucible cooling water, steam condenser inlet/outlet, and vessel drain effluent will be measured using stainless steel sheathed type k thermocouple. Steam temperatures in the vessel will be measured using a standard, commercially available, shielded temperature probe. Vessel pressure will be measured using fast reacting piezoelectric or strain gauge pressure transducers. Heat losses from the vessel will be measured using heat flux sensors. Crucible coolant flowrates will be measured using appropriate mass flow meters. Any liquid levels in the vessel will be measured by differential pressure cells. Experimental measurements will be recorded on existing INEL data acquisition systems. It is anticipated that no new instrument development will be performed to obtain data required for interpreting Phase I test results.

Post-test Debris Examinations

After each Phase I test has been completed, visual examinations will first be conducted to identify characteristics associated with cooling mechanisms, such as cracks, gaps, or upward surface concavity. The solidified debris will then be removed and taken to a metallurgical laboratory for examination. There, the debris will be sectioned and examined to measure characteristics of any cracks or other enhanced cooling mechanisms present.

5.2 Material Property Tests

As discussed in Section 3, material property data are needed for each element of this program. However, as discussed below in Section 5.2.1, it is not anticipated that any new material property data will be required to complete the first element (Phase I) of this program. Section 5.2.2 provides preliminary information about the material property data needed to complete the second two elements of this program (Separate effects tests and model development and Phase II).

5.2.1 Simulated Debris Material Properties for Phase I Tests

At this time, material property tests to support Phase I tests are not anticipated. As discussed in Section 4, only thermal properties, such as thermal diffusivity, thermal conductivity, thermal expansion, density, heat capacity, melting point, and latent heat of fusion, are needed to perform Phase I scoping calculations and conduct Phase I tests. Preliminary review indicates that adequate values for the Phase I effort are available in published literature, such as MATPRO,[14] and from other sources, such as the JAERI program to examine TMI-2 and simulated debris.[65]

5.2.2 Thermal and Structural Properties to Support Separate Effects and Phase II tests.

Results from the Phase I tests will be used to identify and characterize enhanced cooling mechanisms and to determine debris cooling rates. The Phase I results will also be used to indi-

cate the nature of the separate effects which will provide the detailed model development data. At this point in the program, it is quite possible that using existing material property data, as was done in the Phase I effort, will introduce an unacceptable level of uncertainty into the enhanced cooling models which have been developed. If this is the case, it will be necessary to perform specific material property tests at the INEL to reduce the model uncertainties to an acceptable level. Because of the costs involved in determining material properties as a function of temperature, a cost benefit analysis will be performed prior to initiating such material property tests.

If key thermal property tests are performed at the INEL on the simulated debris and/or the TMI-2 debris, several different techniques will be utilized to obtain the required data:

- Composition - Scanning electron microscope WDX dot maps, bulk elemental analysis.
- Density - Sample immersion (room temperature), Change in moment of inertia (liquid).
- Porosity - Optical methods on polished metallographic specimens.
- Latent Heat of Fusion - High temperature calorimetry
- Melting Point - Melting temperature determined by black body temperature determined using a spectro-photometer.
- Heat Capacity - Based on INEL experience in developing MATPRO, it is felt that values for heat capacity can be accurately interpolated as a function of temperature from existing data based on mole fractions. No INEL experiments to determine heat capacity are planned.

High temperature structural properties for actual and simulated debris are very limited, if at all available. Specific properties required to complete scaling analyses for separate effects tests will be determined by the cooling mechanisms identified from Phase I tests. Once the required properties are known, published data will be collected, any additional data needed will be specified, and the most cost efficient means of obtaining these properties will be determined. Some of the possible structural properties required include elastic modulus, fracture strength, and creep properties. Thermal coefficient of expansion can be obtained from temperature dependent density discussed above.

6. References

1. J. R. Wolf and J. L. Rempe, *TMI-2 Vessel Investigation Project Integration Report*, TMI V(93) EG10, October 1993.

2. R. Benz, et al., "Melt-Water Interactions in Tank Geometry: Experimental and Theoretical Results," *Proceedings of the Fourth CSNI Specialist Meeting on Fuel-Coolant Interaction in Nuclear Reactor Safety Bounemouth, England*, April 205, 1979, CSNI Report No. 37, Volume 2, p. 363.

3. B. W. Spencer et al., *Hydrodynamic and Heat Transfer Aspects of Corium-Water Interactions*, EPRI NP-5127, Electric Power Research Institute, March 1987.

4. D. L. Knudson and C. A. Dobbe, *Assessment of the Potential for High-Pressure Melt Ejection Resulting from a Surry Station Blackout Transient*, NUREG/CR-5949, EGG-2689, November 1993.

5. D. L. Knudson, et al., *A SCDAP/RELAP5 Analysis supporting DCH Issue Resolution for the Zion PWR*, Appendix to be included in supplement to NUREG/CR-6075, to be issued.

6. C. M. Allison, et. al., *SCDAP/RELAP5/MOD3.1 Code Manual*, NUREG/CR-5273, EGG-2555, 1993.

7. L. A. Stickler, et al., *Calculations to Estimate the Margin to Failure in the TMI-2 Vessel*, TMI V(93) EG01, OECD-NEA-TMI-2 Vessel Investigation Project, October 1993.

8. D. W. Akers, S.M. Jensen, and B. K. Schuetz, *Examination of Relocated Fuel Debris Adjacent to the Lower Head of the TMI-2 Reactor Vessel*, NUREG/CR-6195, March 1994. (Also issued as TMI V(92)EG10, OECD-NEA-TMI-2 Vessel Investigation Project, EG&G Idaho Report EGG-2732, July 1992).

9. G. E. Korth, *Metallographic and Hardness Examinations of TMI-2 Lower Pressure Vessel Head Samples*, TMIV (92)EG01, January 1992.

10. H. Björnsson, S. Björnsson, And Th. Sigurgeirsson, "Penetration of Water into Hot Rock Boundaries of Magma at Grimsövtn," *Nature*, Volume 295, February 198, 1982, p 580.

11. Fauske and Associates, Inc. *Technical Support for the Debris Coolability Requirements for Advanced Light Water Reactors in the Utility /EPRI Light Water Reactor Requirements Document*, DOE/ID-10278, June 1990.

12. B. W. Spencer, et al., *Fragmentation and Quench Behavior of Corium Melt Streams in Water*, NUREG/CR-6133, ANL-93/32, February 1994.

13. B. W. Spencer, personal conversation, June 6, 1994.

14. J. K. Hohorst, *SCDAP/RELAP5/MOD2 Code Manual, Volume 4: MATPRO - A Library of Materials Properties for Light-Water-Reactor Accident Analysis*, NUREG/CR-5273, EGG-2555, February 1990.

15. J. K. Hartwell, et. al., *Fission Product Behavior During the PBF Severe Fuel Damage Test 1-1*, NUREG/CR-4925, (EGG-2462), May 1987.

16. W. W. Tarbell, D. R. Bradley, R. E. Blose, J. W. Ross, and D. W. Gilbert, *Sustained Concrete Attack by Low-Temperature, Fragmented Core Debris*, NUREG/CR-3024, SAND82-2476, July 1987.

17. R. E. Blose, et al., *SWISS: Sustained Heated Metallic Melt/Concrete Interactions with Overlying Water Pools*, NUREG/CR-4727, SAND85-1546, Sandia National Laboratories, July 1987.

18. M. Merilo, EPRI, personal conversation with J. L. Rempe, INEL, July 1994.

19. E. R. Copus, R. E. Blose, J. E. Brockmann, R. B. Simpson, and D. A. Lucero, *"Core-Concrete Interactions with Overlying Water Pool, WETCOR-1*, NUREG/CR-5907, SAND92-1563, April 1992.

20. B. W. Spencer, ANL, personal conversation with J. L. Rempe, INEL, Aug. 1994.

21. B. W. Spencer, M.T. Farmer, and Mati Merilo, *Status of the Melt Attack and Coolability Experiments (MACE)*, presentation at the 1993 CSARP Review Meeting, May 3-7, 1993.

22. Engelstad, R. and Z. Feng, "Mechanical and Structural Analysis of Corium Crusts," SMIRT, 1992?

23. Nuclear Safety Analysis Center, *Interpretation of TMI-2 Instrument Data*, NSAC/28, Electric Power Research Institute, Palo Alto, CA, May 1982.

24. W. Elenbass, "The Dissipation of Heat by Free Convection: The Inner Surface of Vertical Tubes of Different Shapes of Cross-Section," *Physical, IX*, No. 8, 1942, pp. 865-874.

25. J. R. Dyer, "Natural Convection Flow through a Vertical Duct with Restricted Entry," International Journal of Heat and Mass Transfer, 211, 1978, pp. 1341-1354.

26. W. M. Rohsenow, J.P. Harnett, and E. N. Ganic, *Handbook of Heat Transfer Fundamentals*, Second Edition, New York: McGraw-Hill Book Company, 1985.

27. N. E. Todreas and M. S. Kazimi, *Nuclear Systems I, Thermal Hydraulic Fundamentals*, New York: Hemisphere Publishing Corporation, 1990.

28. J. G. Collier, *Convective Boiling and Condensation*, Second Edition, New York: McGraw-Hill International Book Company, 1972.

29. F. W. Dittus, and L. M. K. Boelter, "Heat Transfer in Automobile Radiators of the Tubular Type," *University of California Publications in Engineering* 2, No. 3, 1930, pp. 443-461.

30. R. Henry, FAI, personal conversation with J. Rempe, INEL, Aug. 1994.

31. J. R. Welty, C. E. Wicks, and R. E. Wilson, *Fundamentals of Momentum, Heat, and Mass Transfer*, Second Edition, New York: John Wiley & sons, 1976.

32. G. D. Raithby and K. G. T. Hollands, "A General Method for Obtaining Approximate Solutions to Laminar and Turbulent Free Convection Problems," in *Advances in Heat Transfer, 11*, edited by T. F. Irvine and J. P. Hartnett, p. 266-315, New York: Academic, 1975.

33. G. D. Raithby, et al, "Free Convection Heat Transfer from Spheroids," *Journal of Heat Transfer*, 98, 1976, pp. 452-458.

34. E. R. G. Eckert and T. W. Jackson, *Analytical Investigation of Flow and Heat Transfer in Coolant Passages of Free Convection Liquid Cooled Turbines*, NACA RM, E50D25, July 1950.

35. B. Boyack, et. al, *An Integrated Structure and Scaling Methodology for Severe Accident Technical Issue Resolution,* NUREG/CR-5809, November 1991.

36. R. D. McCormick, *TMI-2 Data Summary Report*, EGG-TMI-7843, September 1987.

37. Nuclear Safety Analysis Center, *Analysis of Three Mile Island-Unit 2 Accident*, NSAC-80-1, March 1980.

38. J. L. Anderson, *Recommended HPI Rates for the TMI-2 Analysis Exercise (0-300 Minutes)*, EGG-TMI-7833, September 1987.

39. P. Kuan and E. L. Tolman, *Electromatic Relief Valve Flow and Primary System Hydrogen Storage during the TMI-2 Accident*, EGG-TMI-7703, May 1987.

40. Y. Nomura, *PORV Discharge Flow during the TMI-2 Accident*, EGG-TMI-7825, July 1987.

41. R. E. Henry and H. F. Fauske, The Two-Phase Critical Flow of One-Component Mixtures in Nozzles, Orifices, and Short Tubes, *Journal of Heat Transfer*, May 1971, pp. 179-187.

42. K.H. Sun, et al., "The Prediction of Two-Phase Mixture Level and Hydrodynamically-Controlled Dryout under Low Flow Conditions," *International Journal of Multiphase Flow, 7*, No. 5, 19981, pp. 521-543.

43. J. H. Keenan, et al., *Steam Tables-Thermodynamic Properties of Water Including Vapor, Liquid, and Solid Phases*, New York: John Wiley & Sons, 1978.

44. R. R. Hobbins, et al., "Fission Product Release as a Function of Chemistry and Fuel Morphology," *Fission Product Transport Processes in Reactor Accidents*, New York: Hemisphere, 1990, pp. 215-224.

45. B. G. Schnitzler, *Fission Product Decay Heat Modeling for Disrupted Fuel Regions (FDECAY)*, EGG-PHYS-5688, December 1981.

46. D. W. Akers, S. M. Jensen, B. K. Schuetz, *Examination of Relocated Fuel Debris Adjacent to the Lower Head of the TMI-2 Reactor Vessel*, NUREG/CR-6195, TMI V(92)EG10, EGG-2732.

47. J. L. Rempe, et al., *Light Water Reactor Lower Head Failure Analysis*, NUREG/CR-5642, October 1993.

48. O. Kymalainen, H. Tuomisto, O. Hongisto, and T. G. Theofanous, "Heat Flux Distribution from a Volumetrically Heated Pool with High Rayleigh Number," Presented at NURETH-6, Grenoble, France, October 1993.

49. "Compendium of Post Accident Heat Removal Models for Liquid Metal Cooled Fast Breeder Reactors," Edited by B. D. Turland and J. Morgan, European Applied Research Reports, Vol. 6, No. 5, April 1985.

50. Stickler, L. et. al., *Calculations to Estimate the Margin to Failure in the TMI-2 Vessel*, TMI V(93)EG01, October 1993.

51. D. R. Bradley, et. al., *CORCON/MOD3: An Integrated Computer Model for Analysis of Molten Core-Concrete Interactions*, SAND 80-2415 Sandia National Laboratories, 1981.

52. J. G. Collier, *Convective Boiling and Condensation*, Second Edition, New York: McGraw-Hill International Book Company, 1972.

53. A. Mendelson and S. S. Manson, *Approximate Solutions to Thermal-Shock Problems in Plates, Hollow Spheres, and Cylinders with Heat Transfer at Two Surfaces*, Transactions of the ASME, 78, 1956, pp. 545-553.

54. S. Timoshenko and S. Woinowsky-Krieger, Theory of Plates and Shells (McGraw-Hill, New York 1959).

55. W. D. Kingery, Factors Affecting Thermal Stress Resistance of Ceramic Materials, Journal of the American Ceramic Society, 38, 1, 1955, pp. 3-15.

56. R. L. Coble and W. D. Kingery, *Effect of Porosity on Thermal Stress Fracture*, Journal of the American Ceramic Society, 38, 1, 1955, pp 33-37.

57. T. Tachibana, K. Ohuchi, H. Furuya, M. Koizumi, Fracture Strength of UO_2 Tokai Works Semi-Annual Progress Report, PNCT 831-76-01, September 1976.

58. H. L. Ewalds, R. J. H. Wanhill, Fracture Mechanics, (Co-published by Edward Arnold and Delftse Uitgevers Maatschappij) 1984, p. 18.

59. G.G. Trantina, Statistical Fracture Analysis of Brittle Materials in Thermally Stressed Components, Thermal Stresses in Severe Environments, Proceedings of the International Conference on Thermal Stresses in Materials and Structures in Severe Environments, Virginia Polytechnical Institute and State University, Blacksburg, March 19-21 1980, (Plenum Press, New York and London) 1980, pp. 229-244.

60. W. Weibull, "A Statistical Distribution Function of Wide Applicability," Journal of Applied Mechanics, 18, pp. 293-297.

61. *HSC Chemistry for Windows*, Outokumpu Research, A. Roine, Finland, 1993.

62. Erikson, G., *Thermodynamic Studies of High Temperature Equilibria, XII., Solgasmix, a computer program for calculation of equilibrium compositions in multiphase systems.* Chem Scripta 8(1975), pp. 100-103.

63. Strain, R. V., L. A. Neimark, and J. E. Sanecki, "Fuel Relocation Mechanisms Based on Microstructures of Debris," *Nucl. Technol.* **87**, 1987.

64. P. Hofmann and C. Politis, "The Kinetics of the Uranium Dioxide - Zircaloy Reactions at High Temperatures," *Journal of Nuclear Materials* Vol. 87, pp 375, 1979

65. Uetsuka, H. and F. Nagase, *Companion Sample Examination and Related Study at JAERI*, proceedings of an open forum sponsored by the OECD Nuclear Energy Agency and the US NRC, Boston, October 1993.